Deposition of Au/Pt on Co/SiO_2 for Fischer-Tropsch synthesis

by

Martin Patrick de Beer

BSc. Chemical Engineering (1st Class Honours), University of Cape Town, South Africa

Thesis presented to the University of Cape Town in partial fulfilment of the requirements for the degree of

Master of Science in Engineering

Supervisors:

Professor E. van Steen

Professor M. Claeys

Plagiarism Declaration

I, Martin de Beer, declare that this submission is my own, unaided work, except for the information obtained from literature sources and my prescribed supervisors. All sources or information have been adequately acknowledged and referenced. I have not received assistance from any other source in completing this submission.

Signature: ……. Date: …….

M. P. de Beer

Acknowledgements

"The root of all goodness lie in the soil of appreciation of goodness" – Dalai Lama

First and foremost I would like to thank Prof Eric van Steen. Words can't express the appreciation for the critical supervision, guidance and support he has given me over the past two years. There are very few academics that will spend time on their Friday evening quickly editing a paper to save a student a weekend of work and there are even fewer who do it as well as he does. Working with him has been an honour and a pleasure.

To my partners in crime Malebelo Maphuta and Avela Kunene, thanks for those Saturday mornings in the labs discussing politics and doing "science".

Thanks to my friends (Matthew Burke in particular) for the adventures, insurance claims and turning my Masters into a two year ordeal with those (often) two hour lunch breaks.

To everyone in the Centre for Catalysis Research, thanks for the fun environment – I cannot think of a better group of people to enjoy donuts with after a very unproductive Friday.

Synopsis

Cobalt Fischer-Tropsch catalysts, which are used when the desired products are long chain, linear waxes and diesel [1], are promoted with noble metals [2]. This is to primarily increase the reducibility of the cobalt oxide (Co_3O_4) phase present in the supported catalyst during preparation but also has also been seen to effect the Co_3O_4 crystallite size (i.e. dispersion) and intrinsic activity of these catalysts [3]. These promoted catalysts are typically prepared by co-impregnation [4] or sequential impregnation [5, 6] with a noble metal precursor.

This study investigates the preparation of cobalt Fischer-Tropsch catalysts. The effect of using mixed cobalt precursors (i.e. cobalt nitrate and cobalt acetate) in the preparation of unpromoted 10 wt% Co/SiO_2 catalysts is investigated. The incorporation of higher amounts of cobalt nitrate is found to result in larger Co_3O_4 particles with higher reducibility and higher metallic Co^0 surface area after reduction. The formation of large amounts of hardly-reducible cobalt species (possibly cobalt silicates) are suspected from the reduction behaviour of catalysts prepared with higher amounts of cobalt acetate. The use of some cobalt acetate, however, in the promoted catalyst (which is expected to have an increased reducibility) may derive greater benefit than the catalyst prepared from pure cobalt nitrate by enhancement of the reduction of these hardly-reducible cobalt species.

The promotion of the calcined cobalt acetate-cobalt nitrate catalyst with platinum and gold by strong electrostatic adsorption (SEA) is investigated. The promotion with these catalysts with platinum and gold by this method is achievable however subsequent calcination results in extensive sintering of gold particles (this was not observed in the platinum case). The pH during SEA is found to have an effect on the adsorption of platinum and gold species with the adsorption of platinum decreasing and that of gold increasing with increasing pH. This is possibly explained by different adsorption mechanisms for the $AuCl_4^-$ and $PtCl_6^{2-}$ species.

The physical characteristics of these promoted catalysts are investigated. Promotion with platinum results in a significant enhancement of the degree of reduction and a decrease in the reduction temperatures of the processes associated with Co_3O_4 reduction as well as the hardly-reducible species present on these catalysts. These catalysts show a higher metallic Co^0 surface area than the unpromoted case. The pH of the SEA solution seems to have a significant effect on the reaction performance of these catalysts. The Pt promoted catalysts promoted at low pH and high pH both demonstrated significantly higher mass specific activity than the unpromoted catalyst with the

catalyst promoted at low pH having the highest activity. These catalysts showed comparable methane selectivities and chain growth probabilities to the unpromoted catalyst.

The promotion with gold is, unfortunately, much less promising. Promotion by SEA (and subsequent calcination) results in very large gold particles. The presence of these particles on the catalyst has some effect on the reduction of the catalyst, but it unlikely any positive effect on the degree of reduction is derived from this effect as the degree of reduction in fact decreases in these catalysts. These catalysts have a marginally higher or slightly lower metallic Co^0 surface depending on the pH of the SEA solution. The gold promoted catalyst prepared at low pH had a slightly higher mass specific activity than the unpromoted catalyst however the catalyst promoted at high pH in fact had a decrease in activity. The gold-promoted catalysts generally had higher methane selectivity and lower chain growth probabilities than the unpromoted catalysts.

The hypothesis of this work was: *"The pH of the solution in which Co_3O_4/SiO_2 is promoted by SEA has an effect on the position at which the noble metal complex adsorbs and will thus ultimately have an effect on the properties of the promoted catalyst"*
It is difficult to state conclusively whether the pH of the SEA solution had an effect on the position of the noble metal but it is apparent that the pH has a significant effect on the catalytic performance of both the platinum- and gold-promoted catalysts.

Table of Contents

List of Figures

List of Tables

Nomenclature

FTS	Fischer-Tropsch Synthesis
HTFT	High Temperature Fischer-Tropsch
LTFT	Low Temperature Fischer-Tropsch
PZC / IEP	Point of Zero Charge / Iso-Electric Point
EDL	Electric Double Layer
TEM	Transmission Electron Microscopy
XRD	X-Ray Diffraction
TPR	Temperature Programmed Reduction
TGA	Thermal-Gravimetric Analysis
GC-TCD	Gas Chromatogram with a Thermal Conductivity Detector
GC-FID	Gas Chromatogram with a Flame Ionisation Detector
TOPAS	Total Pattern Analysis Solution
NTP	Normal Temperature and Pressure
EDX	Energy Dispersive X-Ray Spectroscopy
ICP-OES	Inductively Coupled Plasma Optical Emission Spectroscopy
AAS	Atomic Adsorption Spectroscopy

1. Literature Review

1.1 Fischer-Tropsch Synthesis (FTS)

The catalytic conversion of synthesis gas (a mixture of CO and H_2) to predominantly linear paraffins and olefins was first discovered by Fischer and Tropsch at the Kaiser Wilhelm Institute around 1925 [7]. The Fischer-Tropsch (FT) reaction allows the conversion of coal or natural gas and other carbon sources, such as biomass, to liquid fuels, i.e. gasoline, kerosene and diesel. The exothermic conversion of synthesis gas in the FT process results in the formation of a wide product spectrum of hydrocarbons and oxygenates according to the following stoichiometric equation:

Formation of olefins: $2nH_2+nCO \rightarrow C_nH_{2n}+nH_2O$ $-\Delta_{rxn}H(230℃)=110\text{-}150 kJ/mol_{CO}$

Formation of paraffins: $(2n+1)H_2+nCO \rightarrow C_nH_{2n+2}+nH_2O$ $-\Delta_{rxn}H(230℃)=210\text{-}160 kJ/mol_{CO}$

The heat of reaction values expressed here are for the C_1-C_{10} range; the heat of reaction per mol of CO converted varies due to the decrease in the thermodynamic stability of hydrocarbons with increasing chain length of the product. The heat of reaction for the formation of low molecular mass olefins is lower than that of the corresponding paraffin of the same carbon number and as the chain length increases the heat of reaction asymptotically approaches that of a paraffin (see Appendix A).

Industrially there are currently two different modes of operation for Fischer-Tropsch synthesis; the distinction between the two operating modes is based on the desired product and product distribution required. The two operating modes are high temperature Fischer-Tropsch (HTFT) and low temperature Fischer-Tropsch (LTFT). The HTFT is typically operated at around 340°C uses an iron-based catalyst and targets the production of gasoline and low molecular mass olefins in the C_2-C_{15} range [8–10] . The LTFT, however is operated at around 230°C and can use either an iron-based catalyst or a supported cobalt catalyst. In this process the production of high molecular linear waxes is targeted, which can be converted into high quality diesel with a low sulphur content [1].

Despite major scientific advancement, interest in Fischer-Tropsch synthesis globally has never been intensified as the process fails to be economically competitive with conventional crude oil refining. With the rising price of crude oil, depleting oil reserves, an ever-increasing global demand for liquid fuels, and the increase demand for renewable liquid fuels, the Fischer-Tropsch synthesis is seeing renewed interest as a possible, economically viable option for the production of liquid fuels to aid in meeting the demand for fuels.

1.2 Mechanism for Fischer-Tropsch Product Formation

The FT reaction is a polymerisation reaction and as such will contain three different reaction steps namely the generation of a chain initiator, chain growth and termination of chain growth [11]. Various mechanisms have been proposed but currently the most widely accepted mechanism for chain growth in the Fischer-Tropsch synthesis is known as the 'alkyl' mechanism and is shown schematically in Figure 1.1.

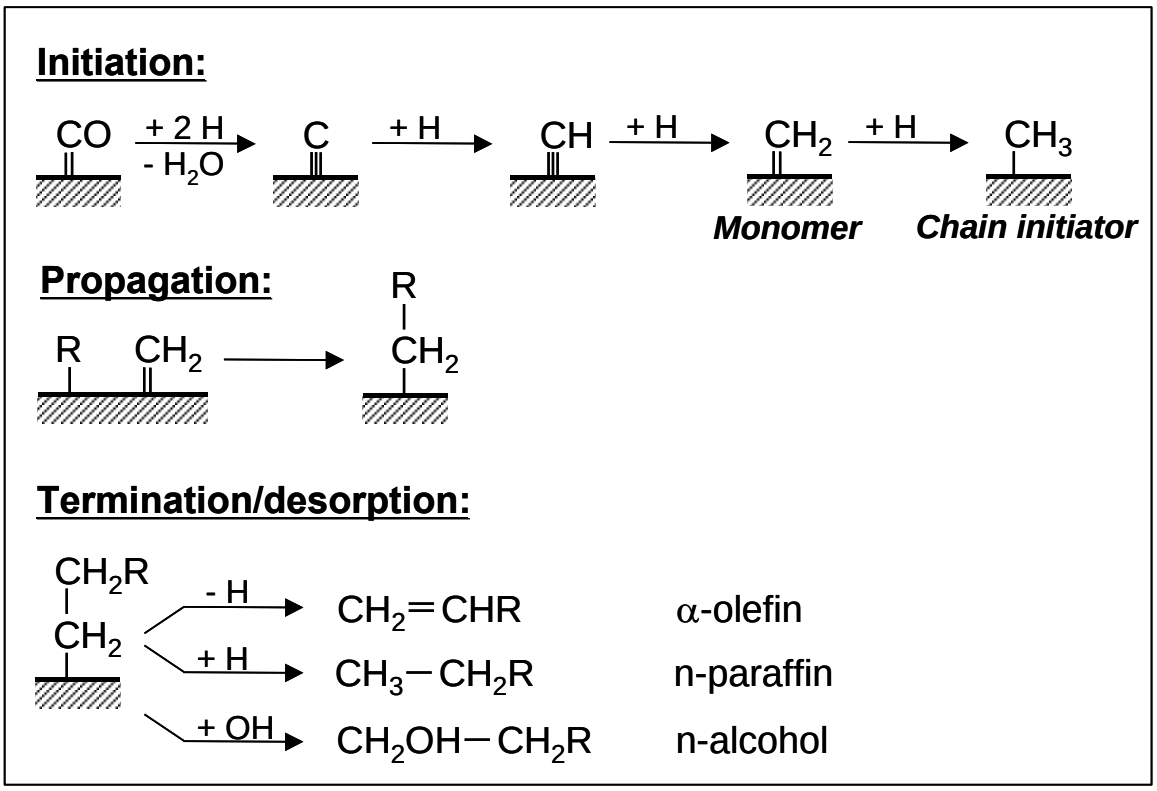

Figure 1.1: Reaction steps in the Fischer-Tropsch Synthesis based on the 'alkyl' mechanism ($R=C_nH_{2n+1}$). (from Claeys and van Steen [15])

Chain initiation may occur by dissociative adsorption of CO, resulting in surface carbon and surface oxygen species. The surface carbon species undergo successive hydrogenation to give rise to surface CH_2 and CH_3 species. There is currently significant debate suggesting these species can be generated via hydrogen-dissociation of adsorbed CO and that this is, in fact, the preferred mechanism on cobalt [12–14]. The surface CH_3 species is generally regarded as the chain starter and the CH_2 species as the monomer in this reaction scheme. Chain propagation is believed to occur by successive incorporation of a monomer, e.g. the CH_2 species. The chain growth is terminated by either β-hydrogen abstraction or hydrogen addition to result in α-olefins and n-paraffins as primary products [15]. The main reaction pathway for the alkyl mechanism fails to demonstrate the formation of branched molecules, it has been suggested that branched molecules are formed in part by re-

adsorption of olefins (such as propene) [16]. An alternative reaction pathway for the formation of branched compounds has been proposed by Schulz *et al*. [17] (Figure 1.2). This pathway involves the reaction of an alkylidene surface species with a CH_2 species analogous to that of the alkyl-mechanism.

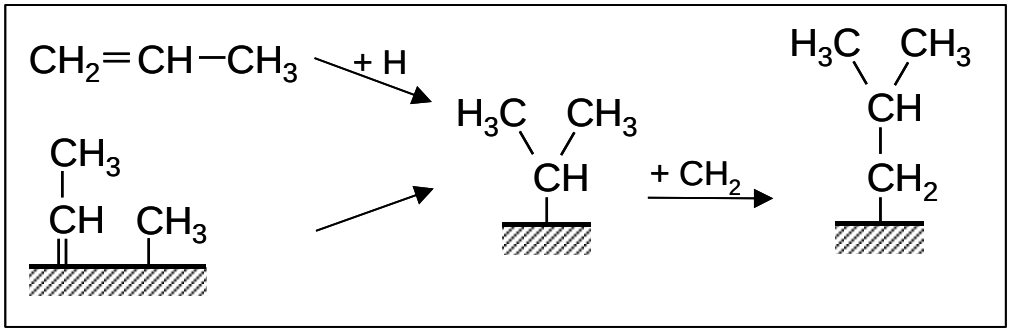

Figure 1.2: Reaction pathway proposed by Schulz *et al*. [17] for the formation of branched compounds in the Fischer-Tropsch synthesis (Taken from Claeys & van Steen [15])

The formation of oxygenates in the Fischer-Tropsch Synthesis cannot be explained by the 'alkyl'-mechanism [15]. It is possible that the formation of primary alcohols can occur by termination of the growing chain with the addition of a hydroxyl group [18] however there is no experimental evidence for the this route of formation of alcohols [15]. The preferred mechanism, however, for the formation of oxygenates in the Fischer-Tropsch synthesis is the "CO-insertion"-mechanism (Figure 1.3) [15].

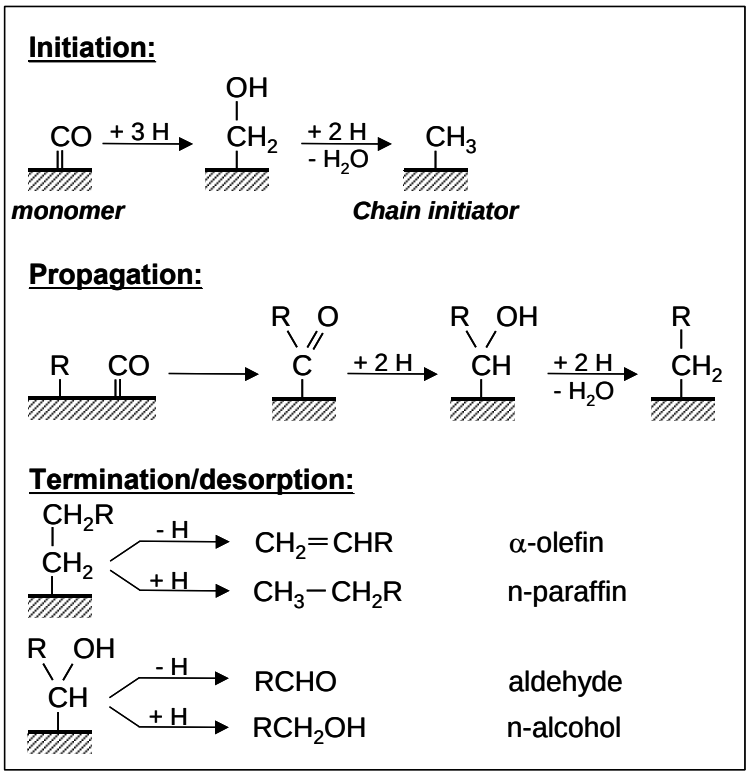

Figure 1.3: CO-insertion mechanism for the formation of Fischer-Tropsch products (taken from Claeys & van Steen [15])

In the CO-insertion mechanism surface CH_3 species initiate chain growth. These are however formed by hydrogenation of adsorbed CO. Undissociated adsorbed CO acts as a monomer by CO-insertion in the metal-alkyl bond of the growing alkyl chain. Termination may occur by hydrogen removal or addition, however this may now involve oxygen-containing species resulting in the formation of oxygenates [15].

1.2 Catalysis for the Fischer-Tropsch Synthesis

A common feature of all catalysts suitable for the Fischer-Tropsch synthesis is their strong interaction with CO and their ability to dissociate adsorbed CO. The interaction between the catalytically active material and CO should be neither too strong nor too weak, since this will lead to the formation of methane and will not promote chain growth [19]. The activity for CO hydrogenation of most of the group VIII elements was investigated by Vannice [20]. The mass specific activity of these metals (supported on silica) for methane formation followed the trend: Co>Ru>Fe>Ni>Rh>Pd>Pt>Ir.

Ru, Fe, Ni and Co are the only metals that show sufficient catalytic activity for commercial application. If one considers the prices of these metals relative to iron (with a value of 1), Ru costs 5850, Ni 50 and Co 80 (as of July 2014). It is interesting to note the significant drop in the relative prices by comparison with the values reported by Dry [8]: Ru 50 000, Ni 250 and Co 1000. A more complete historical comparison of the metal prices is given in Appendix B along with the sources of this data. The use of Ru as a catalyst for the Fischer-Tropsch process has historically been economically unfeasible however the drop in the price relative to Fe over the past 15 years may warrant investigation into Ru as a possible alternative catalyst. Nickel catalysts, while relatively cheap, will produce too much methane under practical Fischer-Tropsch conditions [9].

As implied by their use in industrial Fischer-Tropsch processes mentioned above, iron and cobalt catalysts are seen as the only commercially viable FT catalysts. Table 1.1 offers a comparison between cobalt and iron catalysts. Cobalt FT catalysts are favoured over iron for the production of long-chain hydrocarbons in the LTFT process because of their stability, higher per pass conversion [21] due to higher productivity at high conversion [1, 9] and low water gas activity [22].

Table 1.1: Comparison of cobalt and iron as catalysts for the FT reaction [9]

Parameter	Cobalt Catalysts	Iron Catalysts
Cost	More expensive (~ 80x)	Less expensive
Deactivation	Deactivation by carbon deposition identified as most serious → reversible by catalyst regeneration	Reoxidation and sintering of metal crystallites by water → not commercially reversible
Activity at low conversion	Comparable	
Productivity at high conversion	Higher, less significant effect of H_2O on the rate of CO conversion	Lower, strong negative effect of H_2O on the rate of CO conversion
CO conversion to CO_2	Not very significant, more noticeable at high conversions	Significant
Tolerable sulphur content	1-2 ppb	1-2 ppm
Flexibility (Temperature and Pressure)	Less flexible, significant influence of temperature and pressure on hydrocarbon selectivity	Flexible, methane selectivity is relatively low even at 613K
H_2/CO ratio	~2	0.5-2.5

1.3 Cobalt-based Fischer-Tropsch Catalysts

Due to the price of cobalt it is desirable to maximise the number of available surface metal sites while minimising the amount of metal used in the catalyst [8]. This is achieved by dispersing the cobalt metal on a high area support material. These support materials are typically stable oxides such as Al_2O_3, SiO_2 or TiO_2 [23] (although other supports such as carbon have been used [92]). In addition to the dispersion of the metallic cobalt phase the support material also acts to provide mechanical strength and thermal stability to the cobalt nanoparticles [24]. The composition of typical patented FT catalysts is given in Figure 1.4; of particular interest to this study is the noble metal promoter (whose role will be discussed in detail later).

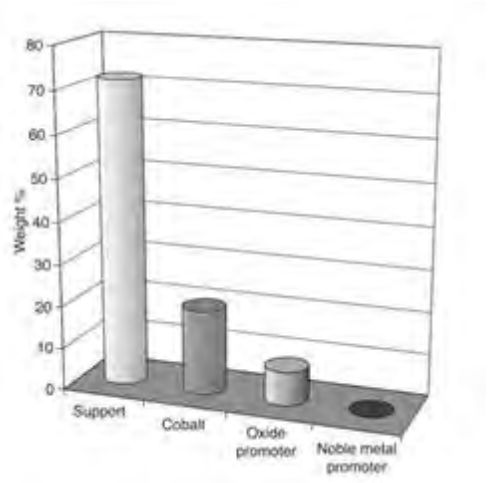

Figure 1.4: Typical composition of conventional patented cobalt Fischer-Tropsch catalysts (from [25])

As the Fischer-Tropsch synthesis is catalysed by the surface of metallic cobalt crystallites present in the catalyst particle [26], the size of the metallic cobalt crystallites is important for the mass specific activity of these catalysts. It is expected that the activity of cobalt FT catalysts will increase with decreasing crystallite size, and hence increasing dispersion. However it has been observed that the intrinsic catalytic activity (i.e. the activity per unit surface area or per 'active site', turn-over frequency) decreases with decreasing average crystallite size of the cobalt crystallite for crystallites less than 6-10nm [27–30]. The combined effect of decreasing dispersion and increasing intrinsic activity as a function of the crystallite size leads to the mass specific activity as a function of crystallite size passing through a maximal value [31] (see Figure 1.5).

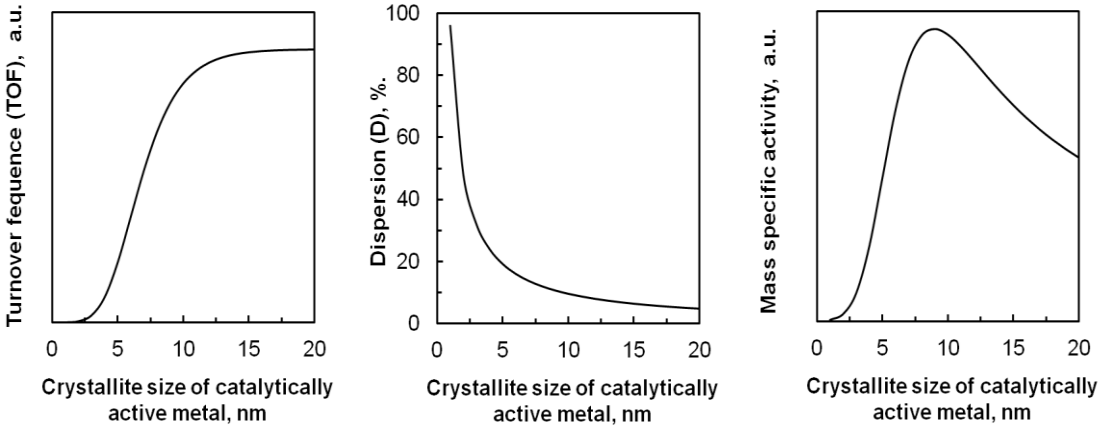

Figure 1.5: Schematic dependency of the observed catalytic activity per surface atom in the working cobalt-based Fischer-Tropsch synthesis [27–30] (left), the dispersion (middle) and corresponding mass specific activity (right) as a function of the cobalt metal crystallite size.

Cobalt-based catalysts are typically prepared via impregnation of the oxidic carrier using a cobalt precursor (most commonly cobalt nitrate) [32]. After calcination of the catalyst precursor in oxygen, cobalt is present on the catalyst as Co_3O_4 [33] , which must subsequently be reduced to metallic Co^0 prior to reaction. This step is typically done in hydrogen (although it can be done in other reducing gases e.g. CO and CO/H_2 [34]) This reduction process was studied by Jacobs *et al*. [25] and verified to occur via the following two-step reduction process:

$$Co_3O_4 + H_2 \leftrightarrow 3CoO + H_2O$$

$$3CoO + 3H_2 \leftrightarrow 3Co^0 + 3H_2O$$

The extent of the conversion of Co_3O_4 to Co^0 in cobalt-based Fischer-Tropsch catalysts is known as the degree of reduction. The degree of reduction is a critical parameter in the preparation of highly active cobalt FT catalysts. The use of oxidic supports in cobalt FT catalysis affects the ease of

transformation of Co_3O_4 to Co^0 [19]. This is observed by the presence of a number of additional H_2 consumption peaks when using temperature programmed reduction (TPR) where the sample is reduced in a hydrogen-containing gas (typically 5% H_2 in an inert gas such as Ar) whilst linearly increasing the temperature. Typical TPR profiles of unsupported Co_3O_4 and Co_3O_4 supported on various oxides are given in Figure 1.6. The appearance of additional higher temperature reduction peaks are indicative of cobalt which is strongly interacting with the surface. Cobalt silicates [35], aluminates [36] or titanates [37] (which may have been formed during calcination) are reduced in the range 800-1000°C [19].

Due to the hardly-reducible species resulting from interaction between the cobalt and the support, higher reduction temperatures are needed to achieve reasonable degrees of reduction. Using higher temperatures during reduction however typically results in the formation larger metallic crystallites due to sintering [19] (the migration of small particles below their melting point to form larger particles). This will result in a lower metal surface area and hence a less active catalyst (see Figure 1.7). It is therefore desirable to reduce the reduction temperature while still obtaining a high degree of reduction.

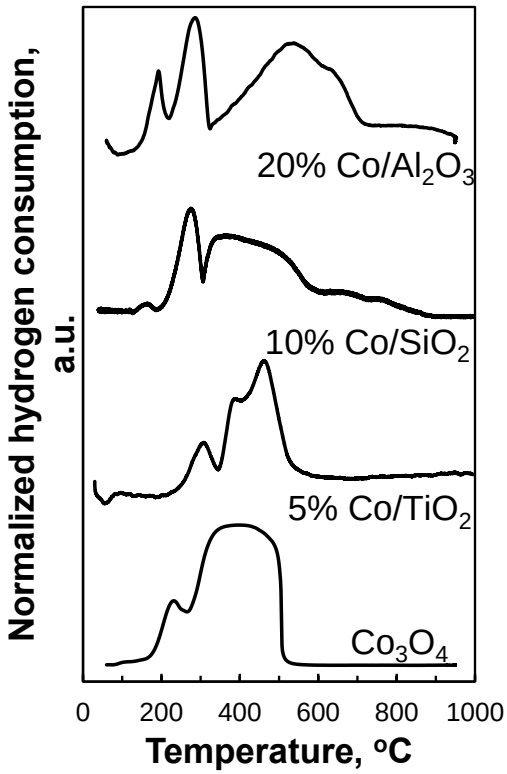

Figure 1.6: Normalized hydrogen consumption during temperature programmed reduction (TPR) of Co_3O_4 and supported cobalt catalysts (heating rate 10 °C/min) [19]

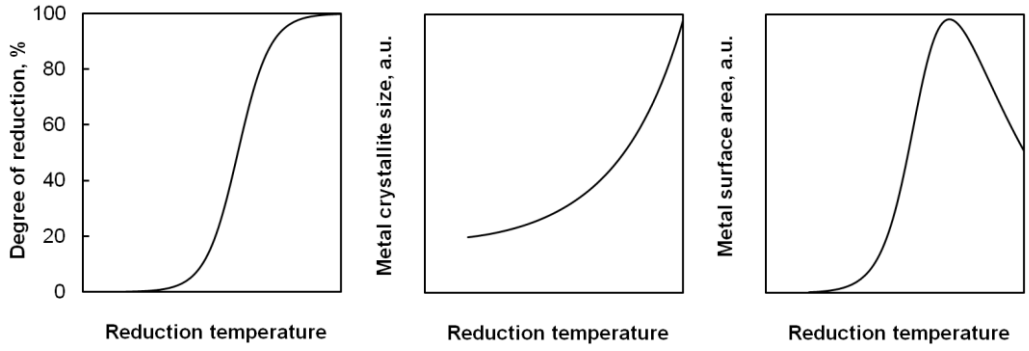

Figure 1.7: Schematic representations of trends observed in the: degree of reduction (left), metal crystallite size (centre) and resulting metal surface area (right) as a function of the reduction temperature.

1.5 Promotion of cobalt Fischer-Tropsch catalysts with noble metals

The addition of small quantities of noble metals, such as Pt, Ru, Au or Re, as a promoter in Co FTS is observed to have several effects on the catalytically active phase:

Cobalt Reducibility: It has been shown that promotion of cobalt FT catalysts with these noble metals results in an enhancement of the cobalt reducibility [3], [37–39] .

Cobalt Dispersion: The presence of noble metal particles can affect the size of both the cobalt oxide and metallic phase. It has been suggested that on weakly interacting supports such as silica a reduction in the size of cobalt oxide particles may occur [2].

Enhancement of Catalytic Performance: Promotion with noble metals results in a considerable increase in the CO conversion at steady state. The extent of the enhancement depends on the type of support used, the reaction conditions and noble metal [2].

Of particular interest to this study is the promotional effect of platinum and gold, which are discussed in detail in the following section.

1.5.1 Platinum and Gold as Promoters for Cobalt Fischer-Tropsch Catalysts

Promotion of cobalt-based Fischer-Tropsch catalysts with platinum has an effect on the reduction temperature of both stages of the reduction of Co_3O_4 phase supported on an oxide. Increases in the degree of reduction and decreases in the reduction temperature of unsupported Co_3O_4 [40] as well as Co_3O_4/SiO_2 i.e. cobalt oxide supported on silica when promoted with platinum have been reported in literature (see Table 1.3).

Jalama *et al*. [41] studied the promotion of Co/SiO_2 with 1.5% gold and found an increase in the degree of reduction from 20.1 to 42.7%. In addition, a number of authors have investigated the promotion of Co/TiO_2 and Co/Al_2O_3 with gold. These results will give insight into the promotional effect of gold and can hopefully be extended to Co/SiO_2. Jacobs *et al.* [6] showed that gold promotion of Co/Al_2O_3 with various amounts of Au resulted in an enhanced Co reducibility and increased the dispersion at all loadings (Table 1.2). Other work done by Jalama *et al.* [42] suggests that promotion with Au on Co/TiO_2 has no significant effect on the reducibility of Co_3O_4/TiO_2 but does increase the cobalt dispersion. Jacobs *et al.* [6] also noted an increase in the dispersion when promoting Co/Al_2O_3 with gold.

Table 1.2: Cobalt reduction and dispersion for 15 wt.-% Co/Al_2O_3 promoted with Au as a function of gold loading [6]

Gold Loading, wt.-%	0	0.1	1.51	5.05
Reduction of Cobalt (%)	49.8	58.9	94.1	81.5
Dispersion (%)	11.4	12.6	15.3	16

The effect of the presence of the noble metal in the catalyst on the degree of reduction and the required reduction temperature are attributed to the presence of noble metals in their metallic state at a low temperature and, in their metallic state, facilitating the dissociation and spillover of hydrogen to enhance the cobalt reduction process at lower temperatures as well [25].

Mechanism for enhanced reduction by noble metal promotion

The hydrogen spillover mechanism is generally postulated to be responsible for the enhanced reducibility observed upon addition of noble metals (such as platinum and gold) to supported cobalt FT catalysts [2, 33, 43]. Hydrogen spillover is the process whereby gaseous H_2 is chemisorbed on a metal surface to form adsorbed hydrogen species which subsequently migrates along the surface.

It has been observed that promotion of Co/SiO_2 with Pt has the effect of increasing the dispersion [5, 37, 44] (Table 1.3). The increase in the dispersion is attributed to a larger number of nucleation sites for the adsorption of hydrogen [2] as a larger number of nucleation sites will result in a larger number of crystallites and hence, at constant loading, a higher dispersion. Furthermore, Diehl and Khodakov [2] suggested that the reduction of smaller cobalt oxide particles is enabled in the presence of Pt. It is important to note that an increase in dispersion (while increasing the active metal area) may not in fact result in an increase in catalytic activity as the turn-over frequency also depends on the dispersion (See Figure 1.5).

Table 1.3: Effect of promotion with platinum on the characteristics of Co/SiO_2 FT Catalysts

		Schanke *et al.* [37]	Tsubaki *et al*. [44]	Jacobs *et al*. [5]
Catalyst system		0.4Pt/8.7Co/SiO_2	0.2Pt/10Co/SiO_2	3.8Pt/15Co/SiO_2
Co_3O_4 reduction	Degree of reduction	90 → 92%	50 → 56%	64 → 72%
	$T_R(Co_3O_4 \rightarrow CoO)$[1]	600K → ~ 420 – 450K	640K →o 473K	570K → ~ 410K
	$T_R(CoO \rightarrow Co^0)$[2]	from 670K to 630K		640 → 570 K
Dispersion		7,5% → 9.6%	8.63% → 22.67%	2.1% → 2.77%
Catalyst performance	CO consumption rate	7.2 → 21.0 μmol/g_{Co}.s	X_{CO}: 33.5 → 49.5 %	X_{CO}: 64.3 → 76 %
	CH_4-selectivity	62 → 68%	8.89 → 13.78 %	
Reactor conditions		1 bar, H_2/CO = 7.3, 483 K, fixed-bed reactor	10 bar, H_2/CO = 2, 513 K, slurry-phase reactor	25 bar, H_2/CO = 2, 493 K, CSTR

1. Peak reduction temperature for the reduction of Co_3O_4 to CoO
2. Peak reduction temperature for the reduction of CoO to Co^0

Promotion with platinum has been shown [5, 37, 44] to result in a higher, steady-state conversion of carbon monoxide as well as higher rates of CO conversion. This higher conversion comes at the cost of a slightly higher selectivity to methane production (see Table 1.3). It is suggested that this increase in the rate comes largely as a result of the increase in the dispersion and not from significant electronic promotion from the Pt [37, 45, 46]. Xu *et al.* [39], however, reported an enhanced catalytic activity on a Co/Al_2O_3 system due to a synergistic effect between cobalt and the noble metal which resulted in an increased reactivity of adsorbed CO.

Jacobs *et al.* [6] showed that promotion of 15% Co/Al_2O_3 with small amounts of gold had beneficial effects on the rate of carbon monoxide conversion and methane selectivity. Addition of larger amounts, however, resulted in a decrease in the rate. This was attributed to the gold effectively blocking the active sites on the cobalt metal. This would be expected due to the lower surface energy of gold than cobalt and will thus occupy the surface of the cobalt. The experimental data is shown in Table 1.4.

Table 1.4: Activity and selectivity of Fischer-Tropsch synthesis with Au promoted Co catalysts [6]. CSTR, 220°C, 210 psig, $H_2/CO = 2$, WHSV = 4.2 ($NL/g_{cat}.h$).

Catalyst loading	15% Co/Al_2O_3	1.51%Au/15 $\%Co/Al_2O_3$	1.51%Au/15 $\%Co/Al_2O_3$*	5.05%Au/15 $\%Co/Al_2O_3$	5.05%Au/15 $\%Co/Al_2O_3$*
CO conversion (%)	28.7	50	46.9	9.0	14.1
$-r_{CO}$ ($Nl/g_{cat}.h$)	121.4	210	197.1	37.8	59.1
CH_4 selectivity (%)	9.2	8.0	8.2	15.1	8.6

*Ex situ reduction followed by transferral under H_2 blanket

1.4 Preparation of supported cobalt Fischer-Tropsch catalysts

Khodakov *et al*. [9] reviewed the synthesis of supported cobalt-based catalysts. These catalysts are typically synthesized by impregnation with an aqueous solution (although other solvents can be used as well [35]) of a cobalt salt precursor. This impregnation is termed 'incipient wetness impregnation' (IWI) if the amount of precursor solution is equal to the pore volume of the support [35] and 'wet impregnation' if the volume of solution is larger than the pore volume [47]. The most commonly used cobalt precursor is cobalt nitrate but the use of other precursors has been investigated. Van Steen *et al*. [35] investigated the reduction behaviour of Co/SiO_2 catalysts prepared from cobalt nitrate, cobalt acetate, cobalt chloride and cobalt sulphate with temperature programmed reduction. The reduction of the Co_3O_4/SiO_2 catalysts prepared from cobalt chloride and cobalt acetate was essentially the same as the unsupported Co_3O_4 indicating negligible interaction between the support and the salt. The TPR profiles of those prepared from nitrate and acetate showed a number of broad peaks which indicate the formation of a number of species during catalyst preparation.

Sun *et al*. [48] investigated the use of a mixture of cobalt acetate and nitrate during impregnation and found that the use of more cobalt acetate as a precursor results in smaller Co_3O_4 crystallites and lower degrees of reduction.

Noble metals have typically added to Fischer-Tropsch catalysts by co-impregnation (i.e. addition of a noble metal salt to the cobalt precursor during IWI / WI) [4] or sequential impregnation where the noble metals are added to the cobalt catalyst before calcination [5, 6].

A number of studies have been done on the addition of platinum and gold to oxidic and carbon supports by a method known as strong electrostatic adsorption (SEA) [47, 49–51]. SEA is essentially a wet impregnation however the solution pH is tailored to maximise adsorption. The importance of the pH in this method of preparation will become apparent in the following sections.

1.3 Adsorption on the Co_3O_4/SiO_2 Surface

1.3.1 Surface Charge and ζ-potential

The hydroxyl groups which populate the surface of metal oxides can be either protonated or deprotonated in aqueous media. This process is governed by the specific chemistry of the metal oxide and the pH of the solution [52]. The protonation and deprotonation reactions are generally described as:

$$-OH + H^+ \leftrightarrow -OH_2^+$$

$$-OH \leftrightarrow -O^- + H^+$$

The point at which the protonation and deprotonation are balanced and the surface has no net charge is known as the point of zero charge (PZC). At all pH values below the PZC the surface has an overall positive charge and an overall negative charge at those pH values above the PZC (it should be kept in mind that deprotonated sites, i.e. $–O^-$ can still be present at pH below PZC and protonated sites, $–OH_2^+$ can still be present at a pH higher than PZC).

The surface charge present on metal oxides (and other surfaces) causes an electric field which attracts a layer of oppositely charged ions. This is known as the "electric double layer" or EDL [53]. There are a number of models which describe the EDL. In reality all models can only describe certain aspects of the EDL. In the Stern model (see Figure 1.8) the double layer is divided into two parts, the Stern layer and the Gouy-Chapman or diffuse layer [53]. The Stern Layer consists of the layer of ions which are directly adsorbed to the surface while the diffuse layer consists of mobile ions. The potential at the shear plane – which is located marginally further than where the stationary Stern layer ends - is known as the ζ-potential [54], [55]. The concentration of potential-determining ions (or pH) at which the ζ-potential is zero is called the isoelectric point (IEP) (typically the same numerical value as the PZC). While the ζ-potential is not the actual thermodynamic or surface potential (which is an unobtainable quantity) it is pragmatically accepted to be the effectiveness of a surface's charge in solution. The ζ-potential on a surface can be calculated from the electrophoretic mobility of particles suspended in aqueous solution. It should be mentioned that the ζ-potential is dependent on the thickness of the electric double layer; this thickness (often related to the Debye length) is in turn dependent on the ionic strength of the solution. It is important that care is therefore taken to conduct ζ-potential measurements at constant ionic strength. The ionic strength of the solution does not, however, affect the value of the PZC.

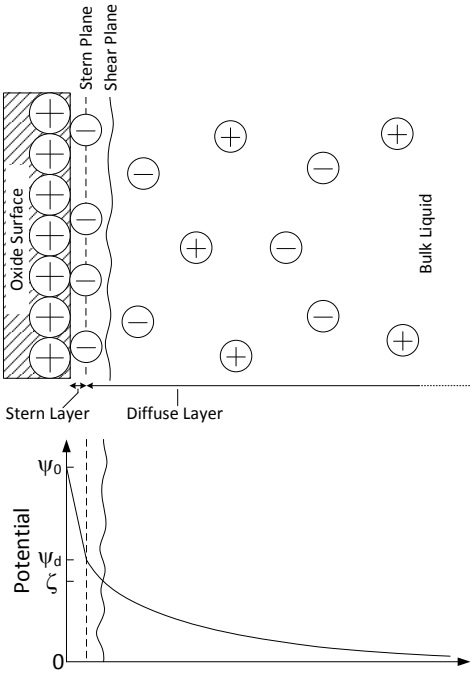

Figure 1.8: Schematic representation of the electric double layer according to Stern's Theory. ψ_0 - surface potential, ψ_d - Stern potential (adapted from Shaw [55])

Brunelle [52] concluded that the pH and isoelectric point are the most important parameter when aqueous metallic complexes adsorb onto metal oxide surfaces and that adsorption is thus Coulombic in nature. It has been widely shown that metal oxide surfaces will only adsorb cations at pH values below their characteristic IEP and anions at pH values above the PZC [50–52], 56, 57]. The adsorption capacity of counter-ions on a particular oxide surface is dependent on the amount of available $–OH_2^+$ / $-O^-$ groups present on the oxide surface and hence the magnitude of the ζ-potential (although the specific surface area will also have a large effect on the number of available sites). It is therefore useful to know, not only the PZC, but also how the ζ-potential develops as a function of pH [52] (as seen for SiO_2 in Figure 1.9). In this investigation SiO_2 and Co_3O_4 are of particular interest, the PZC of these oxides found in literature are given in Table 1.5.

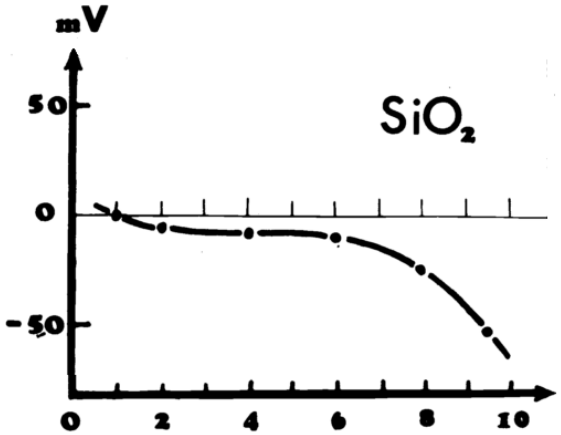

Figure 1.9: ζ-potential curve for SiO_2 (adapted from Brunelle [52])

Table 1.5: Literature values for Co_3O_4 and SiO_2 PZC

PZC Co_3O_4	PZC SiO_2
9.5-10.5 [58]	1.0 [52]
7.3 [59]	4.2 [56]
-	3.0 [51]
-	2.0 [60]
-	1.8-3.4 [53]

The PZC of SiO_2 is lower than that of Co_3O_4, although literature available on the PZC of Co_3O_4 is very sparse. The wide range of PZC observed are a result of different oxide structures, background types and concentrations used when determining the PZC [53]. It is therefore essential to measure the PZC of the oxides present in the system under consideration.

1.3.2 Adsorbing Complexes

When investigating the adsorption characteristics of surfaces (in particular the characteristics over a pH range) it is imperative to consider the adsorbing ions behaviour over this pH range. With the end goal of depositing Pt / Au in close proximity to the Co_3O_4 it would make sense to adsorb Pt and Au complexes which are negatively charged in solution as the Co_3O_4 surface is, according to the PZC value, positively charged across for pH less than 9.5 [53] (although according to [54] this value is 7.3). Hexachloroplatinate $[PtCl_6]^-$ and tetrachloroaurate $[AuCl_4]^-$ anions are thus obvious choices for adsorption onto Co_3O_4. The adsorption system is complicated by the speciation (typically by ligand exchange, aquation or hydrolysis) these complexes undergo in aqueous solutions of varying pH.

1.3.2.1 $AuCl_4^-$ Speciation and Adsorption

It has been shown that aqueous $[AuCl_4]^-$ undergoes successive ligand exchange, whereby the Cl^- is exchanged with OH^-, as the pH of the solution is increased [61]:

$$[AuCl_4]^- \leftrightarrow [AuCl_3OH]^- \leftrightarrow [AuCl_2(OH)_2]^- \leftrightarrow [AuCl(OH)_3]^- \leftrightarrow [Au(OH)_4]^-$$

The kinetics of these ligand exchange reactions are suspected to be slow as aging time and temperature have a noted effect on the speciation [62]. While the speciation does not occur at a distinct pH, the general pH values at which these transformations occur is widely varied in literature (Figure 1.10**Figure**).

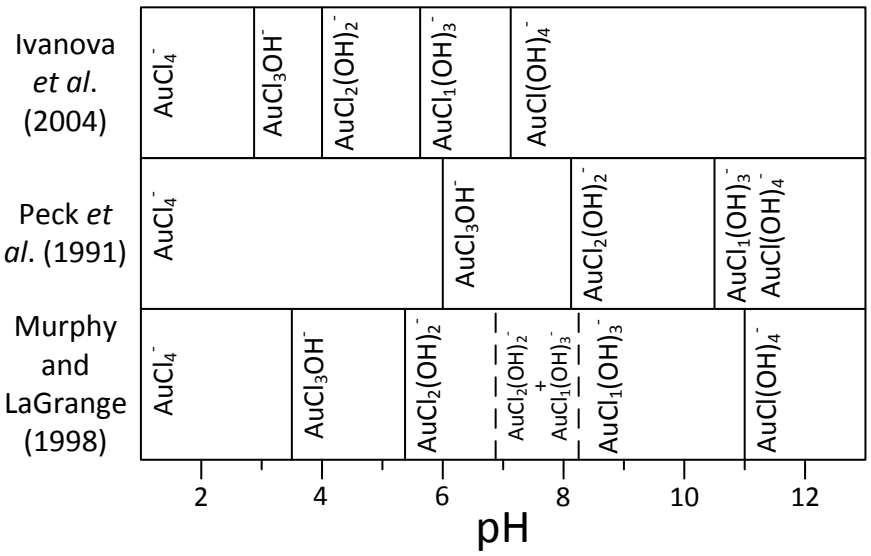

Figure 1.10: Illustration of approximate pH ranges for $[AuCl_4]^-$ speciation. Adapted from Ivanova *et al.* [63] , Murphy and LaGrange[61] and Peck *et al.*[64]

The mechanism for adsorption of certain gold hydroxychloride complexes is suggested to be not exclusively electrostatic in nature [65]. It has been suggested, for the case of TiO_2 [65] and γ-Al_2O_3 [66], that the gold hydroxychloro complexes bond covalently to the oxide surface by reaction with the surface –OH groups; the $[AuCl_2(OH)_2]^-$ and $[AuCl(OH)_3]^-$ species are the most strongly adsorbing complexes [67]. The postulated mechanism of adsorption of gold on the solid, oxidic surface [57] is given in Figure 1.11. The extent gold adsorption onto oxides is thus dependent not only on the oxide surface species but also on which species are present in the liquid phase both of which are dependent on the pH of the solution.

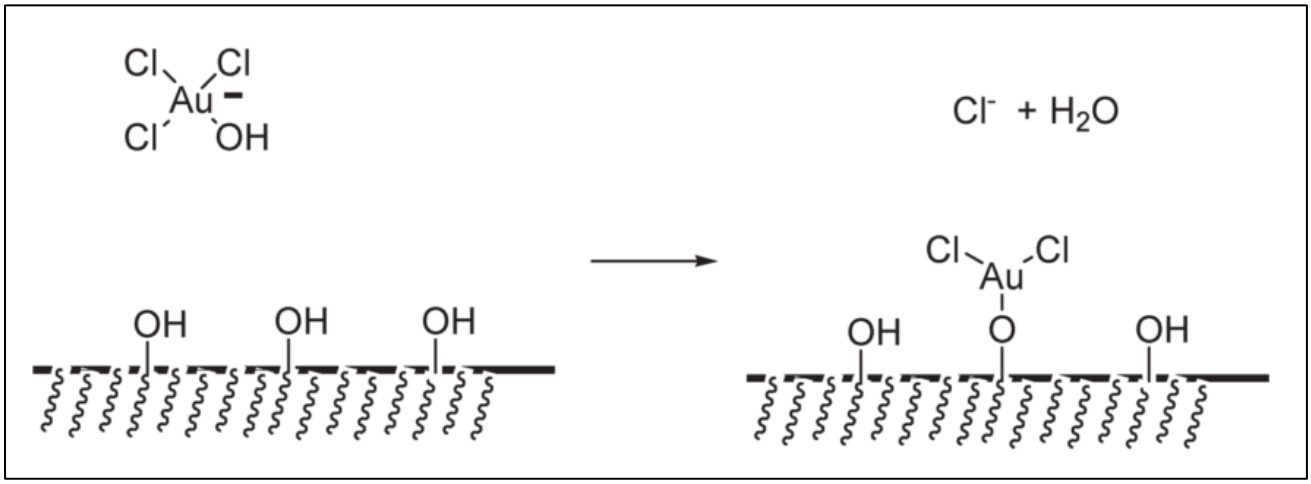

Figure 1.11: Initial step in the adsorption of gold hydroxychloro complexes on oxidic surfaces withthe gold species becoming covalently bonded to the surface [62]

1.3.2.2. $PtCl_6^{2-}$ Speciation and Adsorption

Aqueous $[PtCl_6]^{2-}$ complexes undergo speciation by aquation to form weakly acidic chloroaqua platinum(IV) complexes with increasing pH [68–71]. The mechanism for this speciation consists of two aquation steps:

$$[PtCl_6]^{2-} + H_2O \leftrightarrow [PtCl_5(H_2O)]^- + Cl^- \qquad K_1 = [PtCl_6]^{2-}/[PtCl_5(H_2O)]^-[Cl]^-$$

$$[PtCl_5(H_2O)]^- + H_2O \leftrightarrow [PtCl_4(H_2O)_2]^0 + Cl^- \qquad K_2 = [PtCl_5(H_2O)]^-/[PtCl_4(H_2O)_2]^0[Cl]^-$$

Although further aquation is theoretically possible it is not observed unless under very basic conditions or high temperature [68]. The $[PtCl_5(H_2O)]^-$ and $[PtCl_4(H_2O)]^0$ behave as weak acids and undergo deprotonation with increasing basicity [68]. Spieker *et al*. [70] developed the distribution of Pt species across the pH range 2-10 (see Fig. 1.10) and suggested the formation of more extensively hydrolysed Pt species (e.g. $[PtCl(OH)_5]^{2-}$ and $[Pt(OH)_6]^{2-}$) at high pH values.

The mechanism of adsorption of these Pt species on Al_2O_3 is, for short contact times, mainly electrostatic in nature with the platinic species being held in close vicinity to the surface by "weak, but specific, bonding" (i.e. hydrogen bonding) [68]. This is shown schematically in (Figure 1.12). Mang *et al*. [72], however, suggested thatas the pH is increased towards the PZC some form of ligand exchange reaction becomes increasingly important for the interaction between platinum species and the alumina surface.

It is suggested that all adsorbed species are di-anionic and that the local pH conditions near the surface, which are typically higher than the bulk for pH values below the PZC (where the adsorption of anions will occur), favour the speciation to divalent hydroxy complexes[71]. Interestingly, with the addition of NaOH a slower, less understood, mechanism whereby Pt species are grafted onto the oxide surface is believed to occur at room temperature [68, 71].

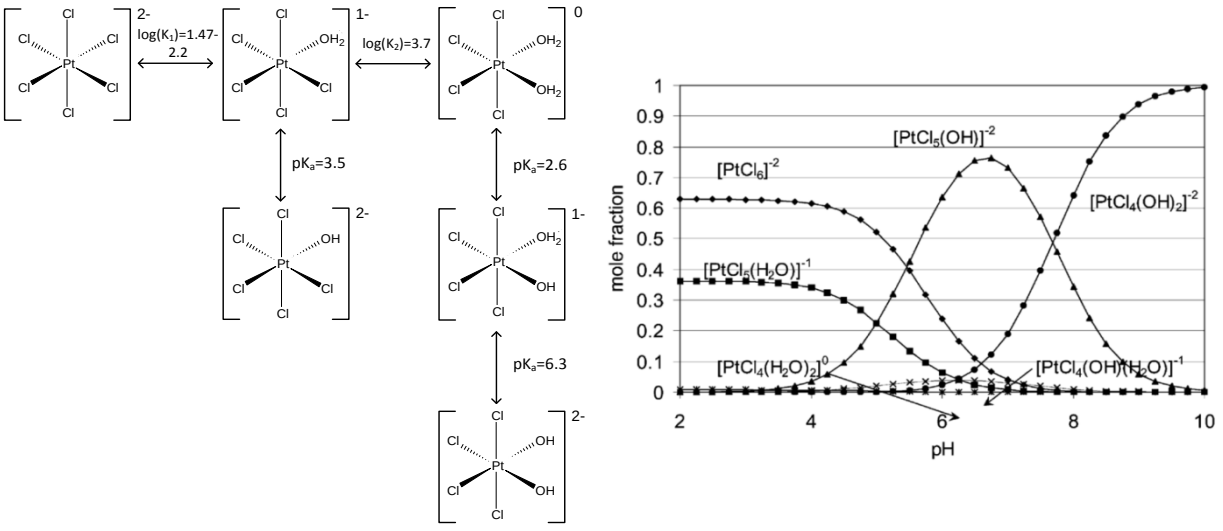

Figure 1.12: Left: $[PtCl_6]^{2-}$ speciation and equilibrium constant values. Adapted from Shelimov *et al*. [68] with K_1 and K_2 values from Kramer and Koch [69]. Right: Pt species distribution from Spieker *et al*. [70] with the constants supplied by Sillen and Martel [90]

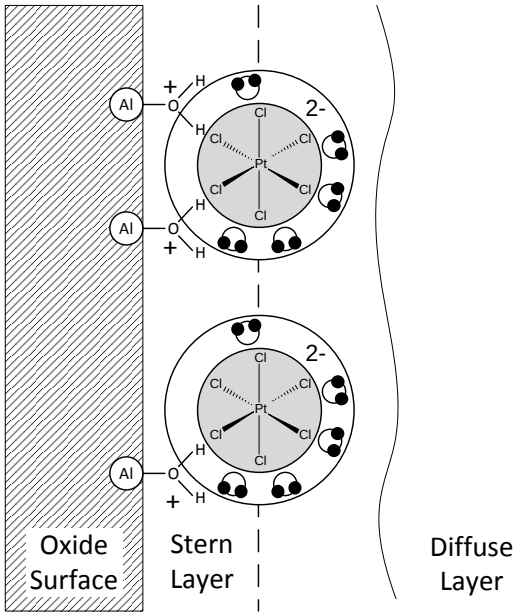

Figure 1.13: Molecular mechanism of the initial adsorption of chloroplatinates on Alumina with two different adsorbed Pt complexes. (Adapted from Shelimov *et al*. [68])

2. Scope of the Study

This investigation is centred on the preparation of cobalt-based Fischer-Tropsch catalysts. It investigates the preparation of cobalt catalysts supported on SiO_2 from mixed cobalt precursors (cobalt nitrate and cobalt acetate) with the goal of identifying the best acetate to nitrate ratio for preparation of Fischer-Tropsch catalysts by characterisation of these catalysts by a number of methods.

It investigates the charges present on the surface of Co_3O_4 and SiO_2 at different pH values (in the form of the ζ-potential) during the promotion of Co_3O_4/SiO_2 with noble metal complexes by strong electrostatic adsorption.

The effect of Pt and Au promotion of Co_3O_4/SiO_2 by SEA at different pH values is investigated by characterisation techniques as well as Fischer-Tropsch reaction tests. The performance of these catalysts will be compared on the basis of mass specific activity as well as selectivity to the various Fischer-Tropsch reaction products.

2.1 Hypotheses

The pH of the solution in which Co_3O_4/SiO_2 is promoted by SEA has an effect on the position at which the noble metal complex adsorbs and will thus ultimately have an effect on the properties of the promoted catalyst

2.2 Key Questions

- How do the ζ-potentials of Co_3O_4 and SiO_2 evolve as a function of pH?
- Does the cobalt acetate to cobalt nitrate ratio have a significant effect on characteristics of cobalt catalysts supported on SiO_2 (in this case Davisil 646)?
- How does the pH of the SEA solution affect the adsorption of $PtCl_6^{2-}$ and $AuCl_4^-$ complexes and hence the properties of the catalysts promoted by this method?

3. Materials and Methods

3.1 Overview of Materials used

Davisil 646 (batch number: 07020BA, 36-60 mesh, d_{pore} = 150Å, pore volume 1.15ml/g, surface area: 300m^2/g) was used as the support in this study. Cobalt (II) acetate tetrahydrate (Sigma Aldrich, batch number MKBF387IV) and cobalt (II) nitrate hexahydrate (Sigma Aldrich, MKBJ6633V) were used as the cobalt source. Solid chloroplatinum hexahydrate (Alfa Aesar, 99.9%) and a 250g/L solution of chloroauric acid (Alfa Aesar, 99.9%) were the platinum and gold sources. NaOH (Kimix, 98%), a 25% NH_3 solution (Kimix) and 10M HCl (Kimix) were used to adjust the pH. KCl (Kimix, batch number 1108060701) was used as a background in the ζ-potential measurements. CO [AFROX, 99.95%], H_2 [Air Liquide, 99.999%], N_2 [Air Liquide, 99.999%] and Ar [Air Liquide, 99.999%] were used in catalyst testing and other operations.

3.2 ζ-potential determination of Co_3O_4 and SiO_2

As mentioned above the surface charge, and hence the ζ-potential, is of utmost importance in the current investigation. Due to the large variation in the PZC of metal oxides, as a result of variations in structure and preparation methods, observed in literature it is necessary to determine the PZC of the system under investigation (i.e. Co_3O_4 and SiO_2). Furthermore, a complete understanding of the variation of the ζ-potential of the species is necessary for any meaningful investigation into the adsorption of metal complexes on oxide surfaces.

Co_3O_4 was prepared by calcination in air of cobalt(II) nitrate hexahydrate at 350°C for 6 hours. This was ground in a mortar and pestle to create fine, easily-suspended particles. The pH of a number of 50ml 0.1M aqueous solutions of KCl was adjusted in the pH range 2 – 10 using 0.2 / 0.02 / 0.002M solutions of HCl and KOH. 0.1g of the crushed sample was then added to the solution and allowed to equilibrate overnight. The equilibrium pH was then recorded. This was repeated for commercially available SiO_2 (Davisil Grade 646).

The suspensions were ultra-sonicated for 2 minutes in a 100W ultrasonic bath prior to ζ-potential measurement. A small arbitrary amount of solution (containing suspended particles) was carefully placed in the capillary of a disposable capillary cell (Figure 3.1). It is important to avoid any bubbles in the capillary during measurement as this will give rise to errors during measurement. The ζ-potential as a function of pH, for both Co_3O_4 and SiO_2, was then measured with a Malvern Zetasizer (which uses electrophoresis). 3 measurements were taken of each suspension for SiO_2 and Co_3O_4. The Smoluchowski approximation was chosen (on the instrument) to relate the electrophoretic

mobility to the ζ-potential. The absorption values used for Co_3O_4 and SiO_2 were 0.9 and 0.05 respectively.

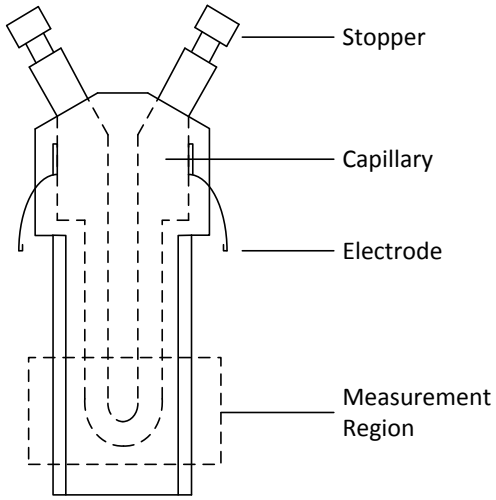

Figure 3.1: Schematic diagram of capillary cell used with the Malvern Zetasizer.

3.3 Catalyst Preparation

To investigate the effect of using various ratios of cobalt nitrate (nitrate) and cobalt acetate (acetate), a number of catalysts with different fractions of nitrate were prepared and characterised.

Determination of pore volume

As these catalysts are to be prepared by wet impregnation (i.e. impregnation of a porous support with a solution whose volume is greater than the pore volume) it is necessary to determine the pore volume of the support being used. A sample of the silica was thinly distributed on a watch glass and dried overnight at 60°C in a static oven. 1g of the dried sample was then placed in a beaker and water was added by titration from a burette while constantly stirring. When the silica no longer maintained its dry appearance, it was known that the pores were filled. The initial and final volumes were recorded to calculate the volume added. This was done in triplicate.

Preparation by wet impregnation

28.4869g of $Co(NO_3)_2.6H_2O$ (Sigma Aldrich, batch number: MKBJ6633V) and 23.2851g of $Co(Ac)_2.4H_2O$ (Sigma Aldrich, batch number: MKBF387IV) were each dissolved in 100ml of deionised water. A concern when using hydrated salts in experimentation is the uncertainty in the stated degree of hydration as these salts are typically very hydrophilic and will absorb moisture from the atmosphere over time. Thus, to quantify precisely the amount of cobalt in the solutions these solutions were diluted (5ml into 1l) and sent, in triplicate, for atomic absorption spectroscopy (AAS)

analysis. The concentration of the $Co(Ac)_2$ and $Co(NO_3)_2$ solutions prepared by mixing 28.4869g of $Co(NO_3)_2.6H_2O$ and 23.2851g of $Co(Ac)_2.4H_2O$ were found to be 0.923 and 0.983mol/L respectively. The results from the AAS were then used to calculate the volumes needed for impregnation (see Appendix E).

3g of silica was placed in a beaker and approximately 6ml of the cobalt-containing solution with varying ratios of cobalt nitrate to cobalt acetate ratios of N:Ac=[0, 0.15, 0.3, 0.45, 0.6, 0.85 1] was added while stirring. These samples were then placed on a watch glass and dried at 60°C overnight. The samples (still spread out on the watch glass) were then calcined in a furnace at 350°C for 6 hours (heating rate ~ 3°C/min).

Platinum and Gold Promotion of Co_3O_4/SiO_2 catalysts by strong electrostatic adsorption (SEA)

For the promotion with Pt and Au a large batch of Co_3O_4/SiO_2 was prepared by the same method using 25g of SiO_2 and 48.8ml of cobalt precursor solution (Ac:N=0.3) as described above however the drying step was different in this preparation. These catalysts were dried in a Rotavap at 60°C for 1 hour and then at 80°C for a further hour at 100mbar rotating at 50rpm.

A 0.00155mol/L solution of H_2PtCl_6 (aq) was prepared by dissolving H_2PtCl_6 (Alfa Aesar) in deionised water. This concentration was calculated to give slightly more than monolayer coverage on the Co_3O_4 crystallites present in the catalyst (see Appendix F). A solution of the same concentration (0.0193mol/L) was prepared by dilution of a 250g/L $HAuCl_4$ (aq) solution.

50ml of this solution was placed in a number of sample vials. The pH of the solution in these vials was then adjusted to various values in the range of approximately 2 – 10 (the pH measurement was done with a Mettler Toledo pH probe). 1.5g of the calcined Co_3O_4/SiO_2 was then introduced to the system and kept in contact with the solution for 1.5 hours under constant stirring from a magnetic stirrer rotating at 30 rpm. The solid catalyst particles were subsequently separated from the solution by filtration using a vacuum filter. The catalyst precursors were then dried overnight in an oven at 60°C and subsequently spread out on a watchglass and calcined at 350°C in an oven for 6 hours.

3.4 *Ex-Situ* Characterisation of catalysts

Various characterisation techniques were used to determine some of the physical and chemical properties of the catalysts in their calcined form *ex-situ*.

3.4.1 Digestion and Inductively Coupled Plasma (ICP) or Atomic Absorption Spectroscopy (AAS)

Solid samples were placed in an Xpress Teflon tube and digested in 10ml of a 60/20/20 volume ratio mixture of concentrated $HCl/HF/HNO_3$. These were digested in a MARS-5 Microwave digester for

15min at 180°C. The resulting liquid was then diluted. Liquid samples were also diluted prior to analysis. The reason for dilution was to not overload the instrument's detector. ICP with a Varian 730 ICP-OES Spectrometer or AAS with a Varian AAS Spectrometer were then used to determine the concentration of the desired species in solution.

3.4.2 Temperature Programmed Reduction (TPR)

Temperature programmed reduction (TPR) in H_2 was conducted to investigate the reduction behaviour of the various catalyst precursors. A small mass of sample, typically 0.1g, was placed on top of a small amount of quartz wool in a quartz U-tube, and inserted into a Micromeritics Autochem HP II 2950. The samples were dried at 100°C in a 20ml(NTP)/min flow of argon. After cooling the sample to 60^{o}C in argon, the temperature was then linearly ramped in a 10ml(NTP)/min flow of 5%H_2 in Ar from 60 - 900°C at 10°C/min. The heating rate was typically 10 K/min, but also varied to determine the activation energy of the reduction process using the Kissinger method [73] (see Appendix G). The sample gas was diverted to a cold trap with an NaCl/ice mixture at ~0°C to condense any volatiles/water before the detector.

3.4.3 X-Ray Diffraction (XRD)

In order to determine the crystallographic structure and a measure, through broadening, of the size of the crystallites present in the catalyst. A small amount of catalyst was placed in an x-ray invisible sample holder and placed in a Bruker AXS D8 Advance X-Ray laboratory diffractometer operated at 40kV and 40mA utilizing a Co source ($\lambda_{Co\text{-}K\alpha 1}$=0.178897nm). The sample was scanned at 2100 points in the range 2θ = [20:80], with each point being scanned for 0.5s.

The average crystallite size of Co_3O_4 in the catalyst precursor was determined in cases with no peak overlap by applying, the –Debye-Scherrer equation on the most intense diffraction peak, (h k l) = (3 1 1):

$$\tau = \frac{K\lambda}{\beta \cos(\theta)}$$

where τ is the crystallite domain size in Å, K is a shape factor typically assumed to be 0.9, λ is the radiation wavelength in Å, β the width of the peak (taken as the full width at half maximum height, FWHM) and θ is the Bragg angle in either degrees or radians.

In cases where there was significant peak overlap a total pattern analysis solution (TOPAS) Rietveld refinement was used to determine the particle size and obtain an estimate of the composition.

3.4.4 H_2 – Chemisorption

H_2-chemisorption was used to determine the available metallic surface area for H_2 adsorption and hence the surface area available for the Fischer-Tropsch reaction. Approximately 0.1g of sample was weighed out into a quartz U-tube and dried in an oven at 60°C overnight. The sample was then re-weighed to determine the dried mass. The analysis was then carried out in a Micromeritics ASAP 2020. The method used for the chemisorption analysis was as follows:

The sample was initially evacuated with He backflow and then heated at 1 atm to 350°C using a heating rate of 10°C/min. H_2 was then flown over the sample at a rate of 10ml(NTP)/min for 12 hours. The sample was then purged with He, evacuated and the temperature reduced to 120°C. H_2 was then dosed to the sample at a number of pressures between 10 and 600mmHg. The volume of H_2-adsorbed at each of these pressures was recorded. The volume adsorbed to form a monolayer could then be calculated. This could then be used to calculate the metallic surface area.

3.4.5 Transmission Electron Microscopy (TEM)

In order to see the morphology of the Co_3O_4 particles and their size distribution on the SiO_2 surface transmission electron microscopy (TEM) was used. The samples were finely ground and suspended in ethanol, ultrasonicated for 10min and subsequently mounted on a copper grid. The samples were viewed using a FEI Tecnai 20 transmission electron microscope (FEI, Eindhoven, Netherlands) operating at 200kV (LaB_6 emitter) and fitted with a Tridiem energy filter and Gatan CCD camera.

3.4.6 Thermal Gravimetric Analysis (TGA)

To determine the degree of reduction of the Co_3O_4 TGA was carried out in a Mettler-Toledo TGA/SDTA851^o fitted with an autosampler. The mass of the alumina crucible was determined and a small amount (typically 5-10mg) of sample was added to the crucible. The sample mass was then determined by subtraction. The sample was heated in N_2 flowing at 10ml(NTP)/min from room temperature to 350°C with a ramp rate of 10°C/min. H_2 was then flowed over the sample at 10ml(NTP)/min for 16 hours. The degree of reduction was calculated from the initial and final masses (see Appendix F).

3.5 Fischer-Tropsch Reaction Test

Experimental Rig Set Up

The performance of selected catalysts was evaluated using a micro scale experimental rig with a fixed-bed reactor (see Figure 3.2).

The flow of Ar, N_2, H_2 and CO into the rig was controlled electronically by four mass flow controllers (MFCs). The pressure behind the H_2 and CO MFCs was maintained at 25bar and that for

N_2 was maintained at 5bar (N_2 is used as a reference gas in the TCD). Argon from the flow controller was not used in this experiment. The flow of H_2 and CO fed into a four way valve which allowed the flow to be directed through the reactor or via a bypass. If the H_2/CO was directed through the reactor then a pressure controlled flow of Ar would flow through the bypass, and vice versa. In this way the pressure of the reactor could be controlled by the Ar backpressure.
The reactor was heated by three separate heating coils each with a thermocouple. This, unfortunately, resulted in uneven heating across the reactor. Thus it was necessary to determine the temperature profile and hence the position of the isothermal zone. This was achieved by moving a separate K-type thermocouple throughout the length of the reactor and recording the temperature and position of the thermocouple. The temperature of each individual heating coil was then fine-tuned to give a reasonably flat temperature profile.

The reactor effluent passes a hot trap (~75ml) which was controlled at a temperature of 200°C and then flows using heated lines controlled to 220°C (to prevent condensation of any products) to a cold trap and an ampoule sampler.
The cold trap is maintained at room temperature to condense all reaction products and only allow for the flow of N_2, H_2, CO and CH_4 to the online gas chromatograph (GC) [Varian 3300] equipped with a thermal conductivity detector (TCD) which is connected to a HP 225E series integrator. The GC-TCD was fitted with a 6-way sample loop which allowed the reactor product to be sampled manually. The TCD is sensitive to all gases with a different thermal conductivity to the carrier gas (argon) and as such is sensitive to H_2, CO, N_2 and CH_4. The TCD response factor for each of these gases was determined from a standard gas mixture ($H_2/N_2/CO/CH_4/CO_2/Ar$ = 45/5/25/5/5/15 vol.%). By adding N_2 at a constant flow rate to the product stream the conversion of CO in the reactor, X_{CO}, can be calculated from the integrator output using the following:

$$X_{CO} = \frac{\frac{A_{CO_B}}{A_{N_2B}} - \frac{A_{CO_{OUT}}}{A_{N_2OUT}}}{\frac{A_{CO_B}}{A_{N_2B}}}$$

where A_{CO_B}/A_{N_2B} is the area of CO relative to N_2 flowing through the reactor bypass and $A_{CO_{OUT}}/A_{N_2OUT}$ is the area of CO relative to N_2 flowing through the reactor.
As the online GC-TCD is not sensitive to organic products from the Fischer-Tropsch reaction it is necessary to take samples to analyse using an off-line GC with a flame ionisation detector (FID) in order to determine the selectivity to various products.

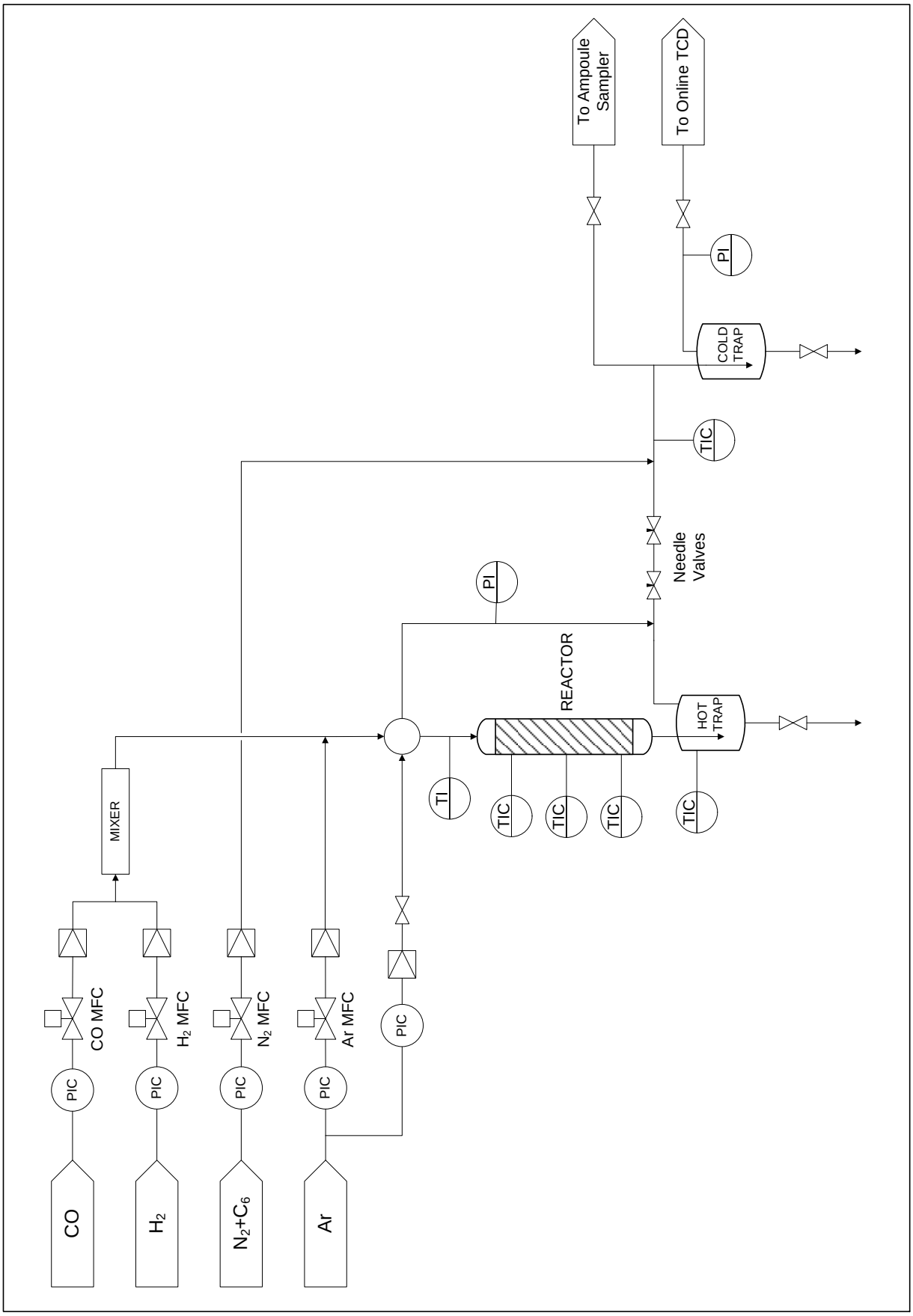

Figure 3.2: Flow diagram of experimental rig used to test Fischer-Tropsch catalysts

Off-line GC Analysis using GC-FID

Ampoules are prepared from drawing, evacuating and sealing Pasteur pipettes and the gas is sampled using an ampoule sampler (see Figure 3.3).

The ampoules are transferred to an offline GC fitted with a flame ionisation-detector (FID) where they are crushed and injected using a pneumatic ampoule breaking device. The conditions and temperature program used in the analysis are shown in Table I.1 in Appendix I.

Not all organic products give the same response in the FID, Kaiser [74] proposed an incremental method for determining the response factor for various oxygenates:

$$f_i = \left(\frac{N_{C,i}}{N_{C(noO)} + 0.55 N_{C(O)}} \right)$$

Where f_i is the response factor for a specific compound i, $N_{C,i}$ is the total number of carbon atoms in the compound i, $N_{C(noO)}$ is the number of carbon atoms without bonds to oxygen and $N_{C(O)}$ is the number of carbon atoms with single bonds to an oxygen atom.

Since the response factor can be determined the inclusion of a known amount of cyclohexane (which is not a product of the Fischer-Tropsch reaction) allows the determination of the selectivities for the formation of the various other hydrocarbons.

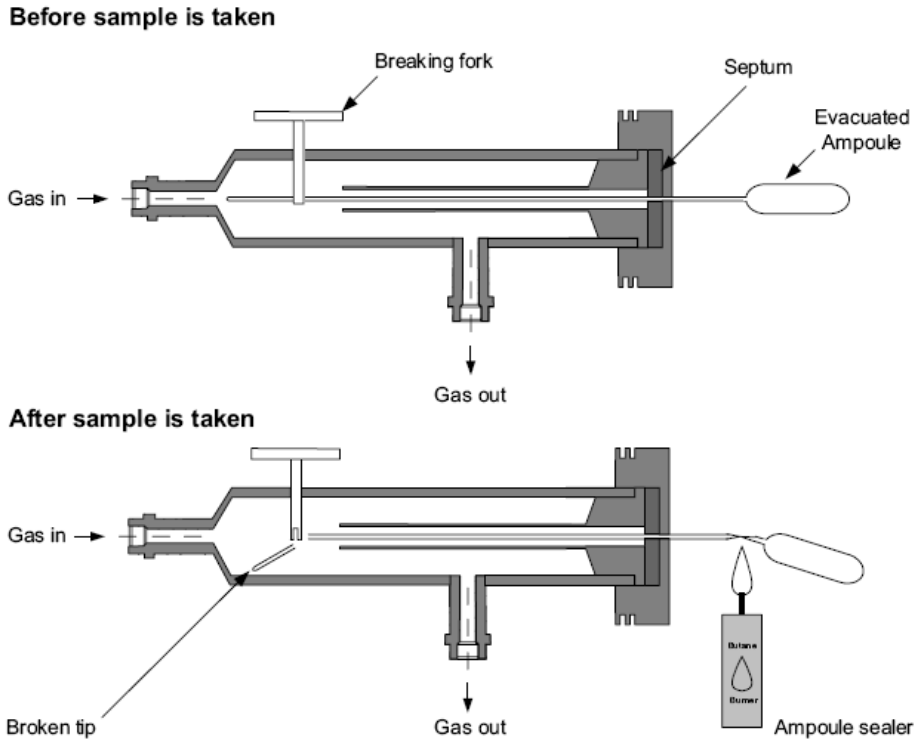

Figure 3.3: Schematic diagram of the ampoule sampler and the ampoule sampling method ([75])

Catalyst Testing

1g of unpromoted catalyst or 0.5g of promoted catalyst was diluted with 500µm SiC (Sigma Aldrich) to a volume of 7.5cm^3 this was done in order to reduce the occurrence of potential hotspots in the catalyst bed. Glass wool was placed into the reactor tube to position the catalyst bed in the isothermal zone of the reactor (note a thermowell is present down the centre of the reactor which houses the thermocouple for the reaction temperature measurement). The catalyst was then placed around the thermowell to fill the isothermal zone (i.e. from 3 to 10cm from the bottom of the reactor) and more glass wool placed on top of the catalyst. The remainder of the reactor was then filled with silicon carbide and the reactor fitted to the rig. This is shown schematically in Figure 3.4.

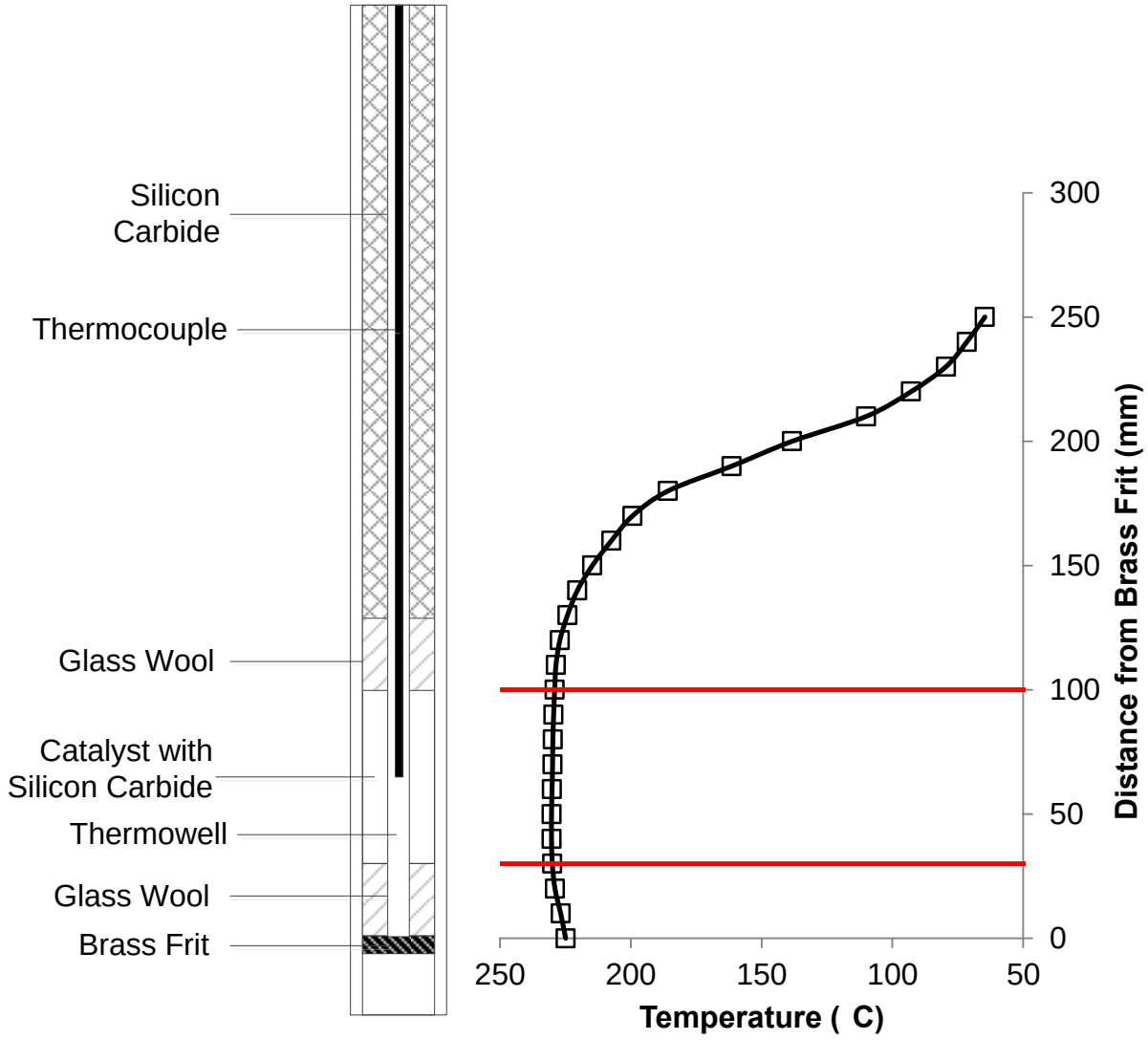

Figure 3.4: Schematic showing reactor filling and temperature profile along the reactor tube

The catalyst was reduced in a flow of 200ml(NTP)/min of H_2 at 350°C for 16 hours. The temperature was then lowered to 220°C and a 2:1 mixture of H_2:CO was fed to the reactor. The total flowrate of these gases was varied to obtain a low syngas conversion (<10%). The pressure in the reactor was maintained at 20bar by the Ar backpressure regulator.

Ampoule samples were taken sporadically from the reactor product stream for testing with the GC-FID over the entire period of the catalyst test (which typically lasted 2-4 days).

4. Results

4.1 ζ-Potential Measurements for Co_3O_4 and SiO_2

The ζ-potential as a function of pH was determined for SiO_2 and for Co_3O_4. The ζ-potential as a function of pH for SiO_2 shows a small positive value in the very acidic region (pH <2) and a PZC in the pH range 2-3. The values are then small and negative until a pH of around 6 where they begin to decrease to larger negative values. The same curve for Co_3O_4 shows higher positive ζ-potential values for pH values below 6 than in the pH range 6-9 with negative ζ-potential values at pH values above approximately 9. The PZC appears to be in the range 9-10. The error at the 95% confidence interval for the measurement of the ζ-potential of SiO_2 is, in general, much larger than for those of Co_3O_4. The reason for this is that the measurement of the ζ-potential is an optical measurement and the SiO_2 has a much lower absorption value than Co_3O_4 effectively making it more difficult for the instrument to detect.

Using the equilibrium equations for the protonation and deprotonation of the oxide surface in aqueous media, an empirical model for the ζ-potential as a function of pH (see Appendix A) was developed:

$$\zeta - potential = \alpha \cdot \frac{\left(K_1 10^{-pH} - \frac{K_2}{10^{-pH}}\right)}{\left(K_1 10^{-pH} + \frac{K_2}{10^{-pH}} + 1\right)}$$

where α is a positive constant which relates the surface charge to the ζ-potential. K_1 and K_2 are the equilibrium constants for the protonation and deprotonation, respectively, of surface –OH groups. The use of a constant to relate the ζ-potential to the surface charge is a simplification. The understanding that the ζ-potential is the potential at the shear plane implies it is a function of the thickness of the Stern Layer (which is in turn function of the charge on the surface). Thus the constant will itself be a function of the pH, and will vary as the surface takes on different charges. The model was fitted with linear least squares fitting to the experimental data obtained by adjusting the α, K_1 and K_2 values (see Figure 4.1).

The model explains the trend observed in the ζ-potential of SiO_2 quite well for pH values less than 8. The model predicts a flattening out of the ζ-potential as a function of pH at a pH larger than 8, which was not observed in this study (more measurements of the ζ-potential at a pH-value of larger than 8 would be required to accept or reject this model; this was not attempted in this study, since it was not of primary interest here)

This type of model fails to explain the "plateau" observed for the Co_3O_4 in the pH range from 6-9. Empirically, it is therefore necessary to have additional terms to describe this trend in the ζ-potential. Thus, it was postulated that since Co_3O_4 is a mixed valence compound (with cobalt present as both Co^{2+} and Co^{3+}in the crystal structure) there will be surface –OH groups in two different electronic environments (i.e. those bonded to Co^{2+} and Co^{3+}). This is, at least in part, justified by the identification of terminations on Co_3O_4 with differing reactivities for water adsorption by Chen and Selloni [76].

The revised model for Co_3O_4 is (see Appendix B):

$$\zeta - potential = \alpha_1 \cdot \frac{\left(K_{1,\alpha_1} 10^{-pH} - \frac{K_{2,\alpha_1}}{10^{-pH}}\right)}{\left(K_{1,\alpha_1} 10^{-pH} + \frac{K_{2,\alpha_1}}{10^{-pH}} + 1\right)} + \alpha_2 \cdot \frac{\left(K_{1,\alpha_2} 10^{-pH} - \frac{K_{2,\alpha_2}}{10^{-pH}}\right)}{\left(K_{1,\alpha_2} 10^{-pH} + \frac{K_{2,\alpha_2}}{10^{-pH}} + 1\right)}$$

α_1 and α_2 are positive constants which relate the surface charge to the ζ-potential. K_{1,α_i} and K_{2,α_i} are the equilibrium constants for protonation and deprotonation for the surface –OH groups belonging to different sites. This was once again fitted by linear least squares to the experimental data by adjusting α_1, α_2, K_{11}, K_{12}, K_{21}, K_{22} (see Figure 4.1). While the model for Co_3O_4 assumes two independent cobalt sites, it does not glean any further information on the identity of these sites i.e. Co^{2+}/Co^{3+}. Furthermore, the ratio of α_1/α_2 can be misunderstood to be some representation of the ratio of Co^{3+}/Co^{2+} sites on the surface of the Co_3O_4 crystal and thus compared with known ratios of these sites present on the surface. This ratio, however, is a convoluted value which represents the activity for preferential proton adsorption in conjunction to the ratio of surface sites.

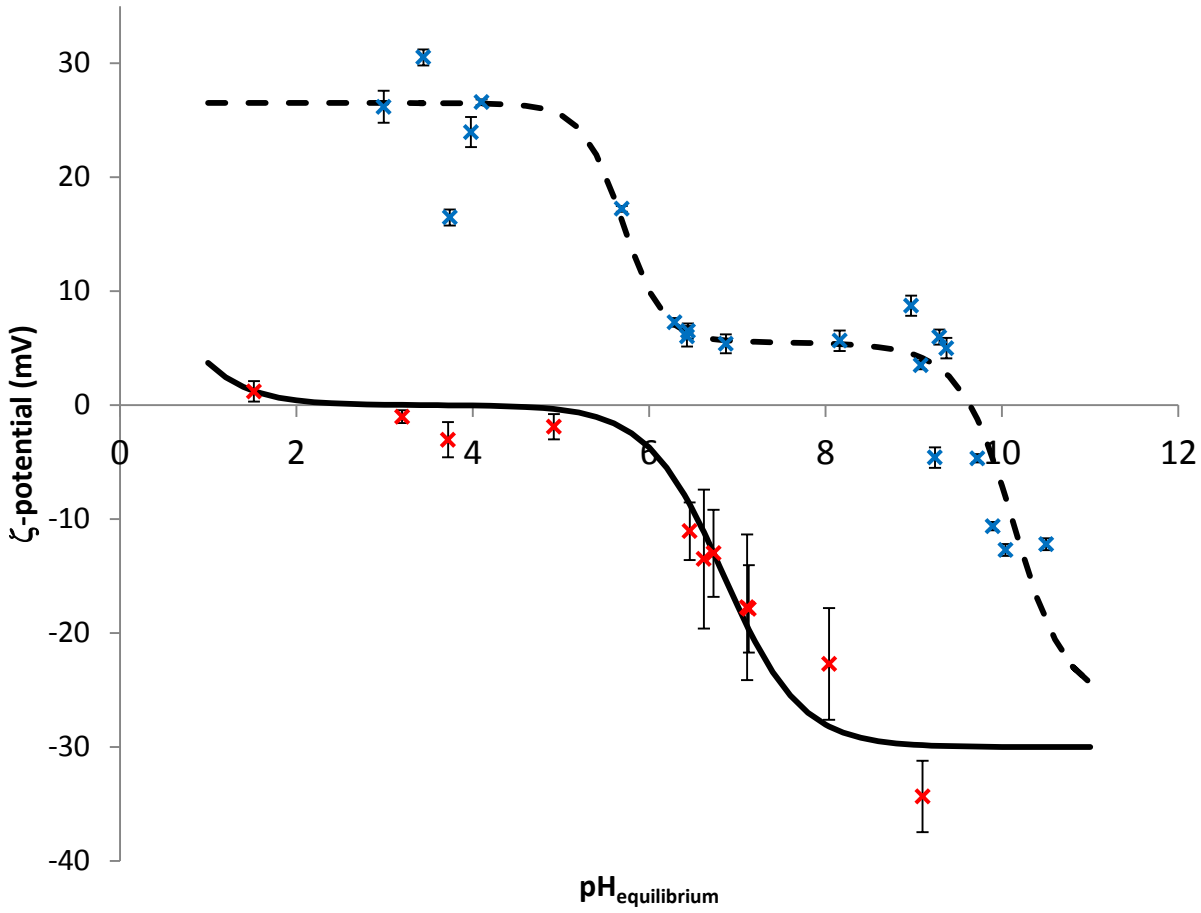

Figure 4.1: ζ-potential as a function of equilibrium pH for Co_3O_4 and SiO_2. × SiO_2, × Co_3O_4, – SiO_2 model, - - - Co_3O_4 model. Error bars at the 95% confidence interval shown

The constants used in the models are given in Table 4.1. The pK_a and pK_b values are calculated as follows: $pK_a = -\log(K_2)$ and $pK_b = -\log(1/K_w K_1)$

Table 4.1: Values determined from fitting empirical z-potential models for SiO_2 and Co_3O_4

Surface		α	K_1	K_2	pK_a	pK_b
SiO_2		30	1.41	1.42×10^{-7}	6.8*	13.9
Co_3O_4	Site 1	16	4.00×10^{6}	1.60×10^{-5}	4.8	7.4
	Site 2	10.5	1.64×10^{10}	8.80×10^{-11}	10.	3.8

From the model curves the PZC of silica can be estimated to be 3.5 and that of Co_3O_4 9.6. These values are in general agreement with the range of values given by various authors [51–53, 56, 58–60] (see Table 1.5). The pK_a value obtained from fitting for SiO_2 is in fair agreement to the value of

7.1±0.5 obtained by IR measurements by Hair and Hertl [77]. There is little literature to compare the other values obtained with. It should be realized that it is assumed in SiO_2 that there is one adsorbing site and in Co_3O_4 there are two. This is a simplification and most certainly not the case; these surfaces may have multiple sites which are able to adsorb protons.

4.2 Co/SiO_2 Catalysts Prepared from Mixed Cobalt Salts

The pore volume of the SiO_2 (Davisil) was determined by wetting the particles with water and was found to be 1.4±0.15cm^3/g. This was higher than that reported by the manufacturer (1.15cm^3/g). This is likely due to the presence of some water being present between the SiO_2 particles which are not directly visible . As we are using a wet impregnation method it is only required that the impregnation volume be larger than that of the pores (chosen arbitrarily to be ~2cm^3/g)

The catalysts prepared by wet impregnation with varying fractions of $Co(Ac)_2$ and $Co(NO_3)_2$ are presented in Table 4.2. The total volume used during impregnation was between 1.92 and 2.04 ml/g_{cat} (i.e. between 5.75 and 6.13 ml per 3g batch), the difference in impregnation volume was necessary, due to the differing concentrations of the $Co(NO_3)_2$ and $Co(Ac)_2$ solutions, to ensure equal amounts of cobalt on the end catalyst. This difference in volume is not significant (~6%) and should not affect the final catalyst performance significantly.

Table 4.2: Catalysts prepared by wet impregnation from various mixtures of cobalt nitrate and cobalt acetate

Catalyst	Fraction $Co(NO_3)_2$	Volume Added (cm^3)*		wt.% Co**
		$Co(NO_3)_2$	$Co(Ac)_2$	
NA1	1	5.75	0.00	10.16
NA2	0.85	4.94	0.87	9.26
NA3	0.7	4.10	1.76	9.51
NA4	0.55	3.25	2.66	9.55
NA5	0.4	2.39	3.58	9.36
NA6	0.15	0.91	5.16	9.34
NA7	0	0.00	6.13	9.56

*Volume added to each 3g batch of SiO_2
**Mass percent of cobalt in calcined catalyst determined by digestion and AAS

The amount of cobalt achieved on the catalysts (determined by AAS) is satisfactory as these catalysts all have weight loadings within 1% of each other. During the impregnation it was troublesome to get all of the impregnating liquid onto the dried catalyst as some inevitably adhered to the glassware. When preparing small amounts of catalysts (i.e. 3g) this small error in the preparation solution volume may result in some deviations in the final loading (as observed here).

X-Ray Diffraction

XRD was done on the calcined Co_3O_4/SiO_2 catalyst precursors (Figure 4.2). The XRD scan shows a broad peak at 2θ = 20-40° as well as a number of sharp peaks. The broad peak is attributed to the SiO_2 present in the sample (the broadness is due to the lack of crystalline structure in SiO_2) while the other sharp peaks are characteristic of the different crystal planes present in Co_3O_4. These XRD spectra showed only the presence of Co_3O_4 and SiO_2.

As the fraction of $Co(NO_3)_2$ in the sample preparation decreased (and hence the fraction of $Co(Ac)_2$ increased) the peaks become less intense and broader. The increase in the broadness is indicative of the formation of smaller Co_3O_4 particles. Furthermore, it can be noted that the area under the diffraction peak representing the (311) plane in Co3O4 becomes less relative to the diffraction peak representing silica. This may be taken as in indication for the formation of XRD-invisible particles. These "invisible" particles may be Co_3O_4 crystallites which are too small for XRD to detect but may also be small cobalt silicates formed during calcination. Jablonski *et al*. [78] confirmed the formation of XRD-invisible Co_2SiO_4 during calcination at lower temperatures. It should be mentioned that the samples prepared with high amounts of $Co(Ac)_2$ (i.e. NA6 and NA7) showed a blue colour after calcination. Jablonski *et al*. [78] also observed the visible colour change in catalysts containing significant amount of cobalt silicates (i.e. a blue hue).

The crystallite domain size was determined using the Debye-Scherrer equation on the most intense Co_3O_4 peak i.e. the [3 1 1] peak. The shifting baseline, due to the SiO_2 peak, was corrected for by subtraction. The results from this analysis (i.e. the Co_3O_4 crystallite size) are shown in Figure 4.3.

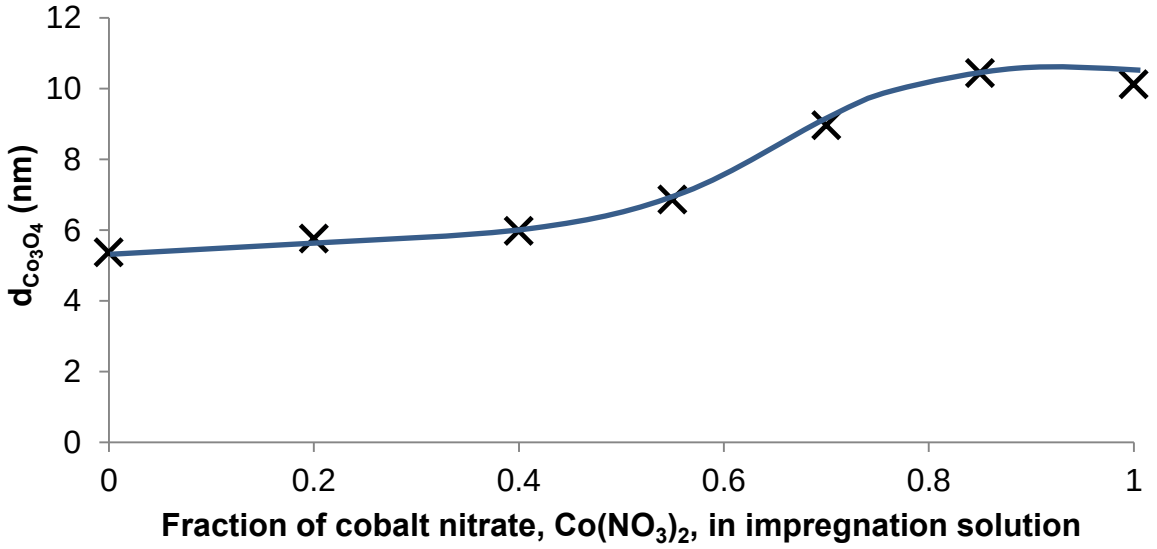

Figure 4.3: Average crystallite size for Co_3O_4 in Co/SiO_2 prepared by wet impregnation using different fractions of $Co(NO_3)_2$ in the impregnation solution.

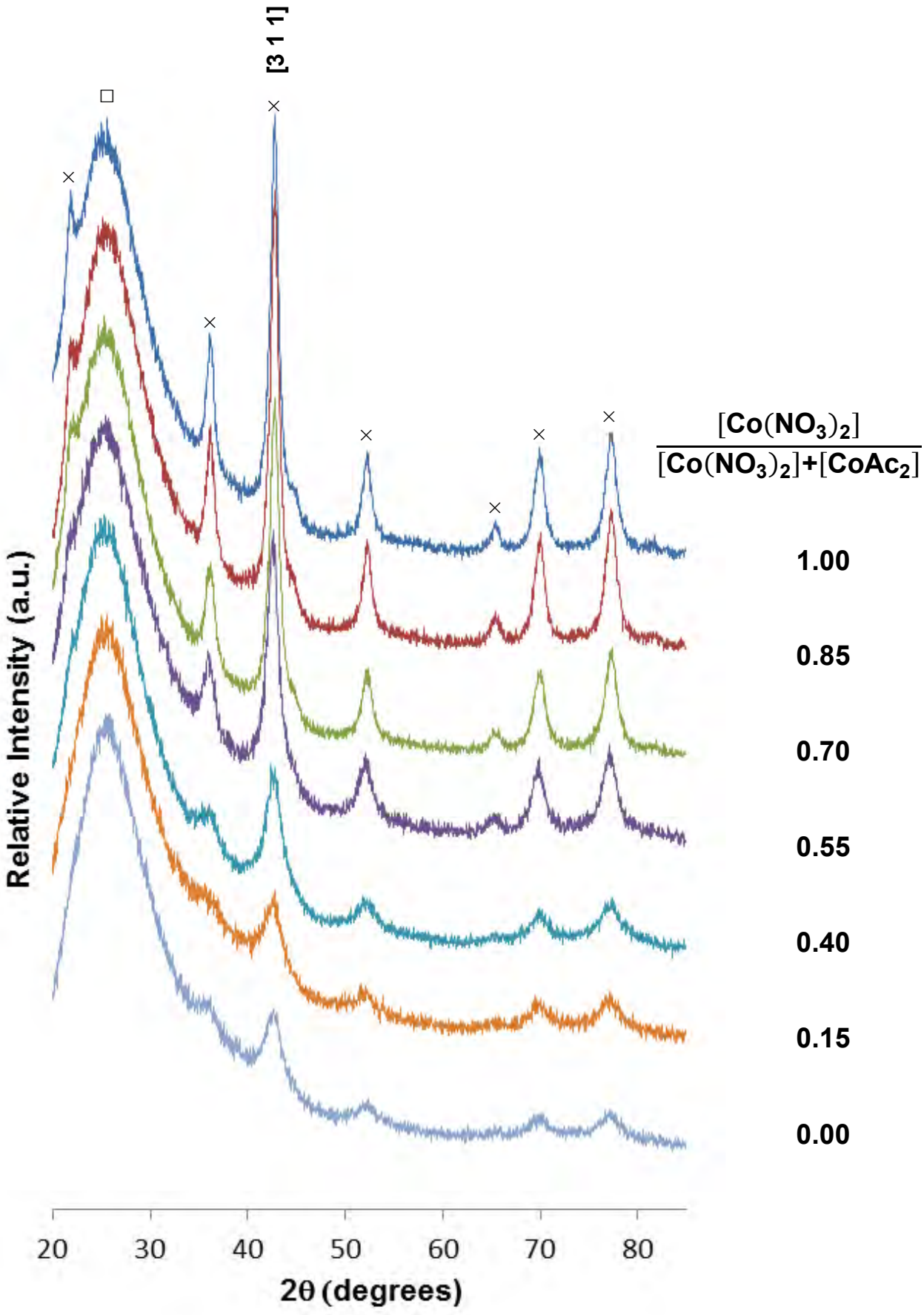

Figure 4.2: XRD scans of various Co_3O_4/SiO_2 catalysts prepared by wet impregnation from different fractions of $Co(NO_3)_2$ and $Co(Ac)_2$. × – Co_3O_4 □ – SiO_2The average Co_3O_4 crystallite size

decreases as the fraction of $Co(NO_3)_2$ in the impregnating solution decreases. The same trend was observed by Sun *et al*. [48], however they reported a XRD average Co^0 particle size of 15.5nm for the $Co(NO_3)_2$ and undetectably small particles for $Co(Ac)_2$. This differs from the values obtained in the current study of 10.4 and 5.4 nm respectively for Co_3O_4 (this would correspond to 7.6 and 4 nm respectively taking $d(Co^0) = 0.75d(Co_3O_4)$ [37]). There are a number of differences in the preparation technique and materials used which could have resulted in this difference. The support used by Sun *et al*. [48] was Fuji Davison ID Gel with specific a surface area of 270 m^2/g and a pore volume of 1.22 cm^3/g. The catalyst was also dried at 120°C for 12 hrs – much harsher drying conditions than the ones used in the present study.

Temperature Programmed Reduction

Temperature programmed reduction was conducted to investigate the reduction behaviour of these catalysts (Figure 4.4). All profiles obtained show a dip in the hydrogen consumption at a temperature of just below 100°C. This is attributable to the evaporation of residual water present in the sample; this dip in the hydrogen consumption disappears when a cold trap with ice water at ~0°C is introduced, and hence condenses water vapour, before the thermal conductivity detector.

The TPR profile for the Co_3O_4/SiO_2 prepared from pure $Co(NO_3)_2$ (i.e. AN1) shows a peak at approximately 280°C and a broad reduction peak which extends over the entire range from 300-900°C. The TPR profile for the Co_3O_4/SiO_2 prepared from pure $Co(Ac)_2$ i.e. AN7 differs significantly from that of AN1. It shows a much smaller peak at 280°C and the appearance of a large peak (which appears to consist two peaks) in the range from 700 to 900°C. As the fraction of $Co(NO_3)_2$ decreases from AN1 to AN7 there is a gradual shift from the one extreme to the other. The TPR profiles for Co_3O_4/SiO_2 prepared from pure cobalt nitrate and pure cobalt acetate are qualitatively very similar to those obtained by van Steen *et al*. [35] and Sun *et al*. [48].

The first hydrogen consumption peak, at 280°C, is generally assigned to the first step of the reduction of Co_3O_4 (i.e. $Co_3O_4 \rightarrow CoO$). The peak temperature for this reduction process agrees well with the value of ~280°C observed by van Steen *et al*. [35] and is slightly lower than the value of ~310°C observed by Sun *et al*. [48]. The temperature of the first reduction peak does not appear to be affected by the precursor (or ratio thereof), this is in line with the observation by van Steen *et al*. [35]. The area below this peak, however, does decrease as the cobalt acetate content increases indicating less Co_3O_4 present on the catalyst (possibly as a result of cobalt being present as divalent cobalt in the form of either CoO or cobalt silicates).

The broad peaks observed above 300°C indicate a number of species with similar reduction temperatures. The appearance of large broad peaks at 700-900°C in the catalysts prepared with high fractions of cobalt acetate (i.e. AN4, AN5, AN6, AN7) further supports the presence of large amounts of hardly reducible cobalt species (tentatively ascribed to cobalt silicates) on these catalysts.

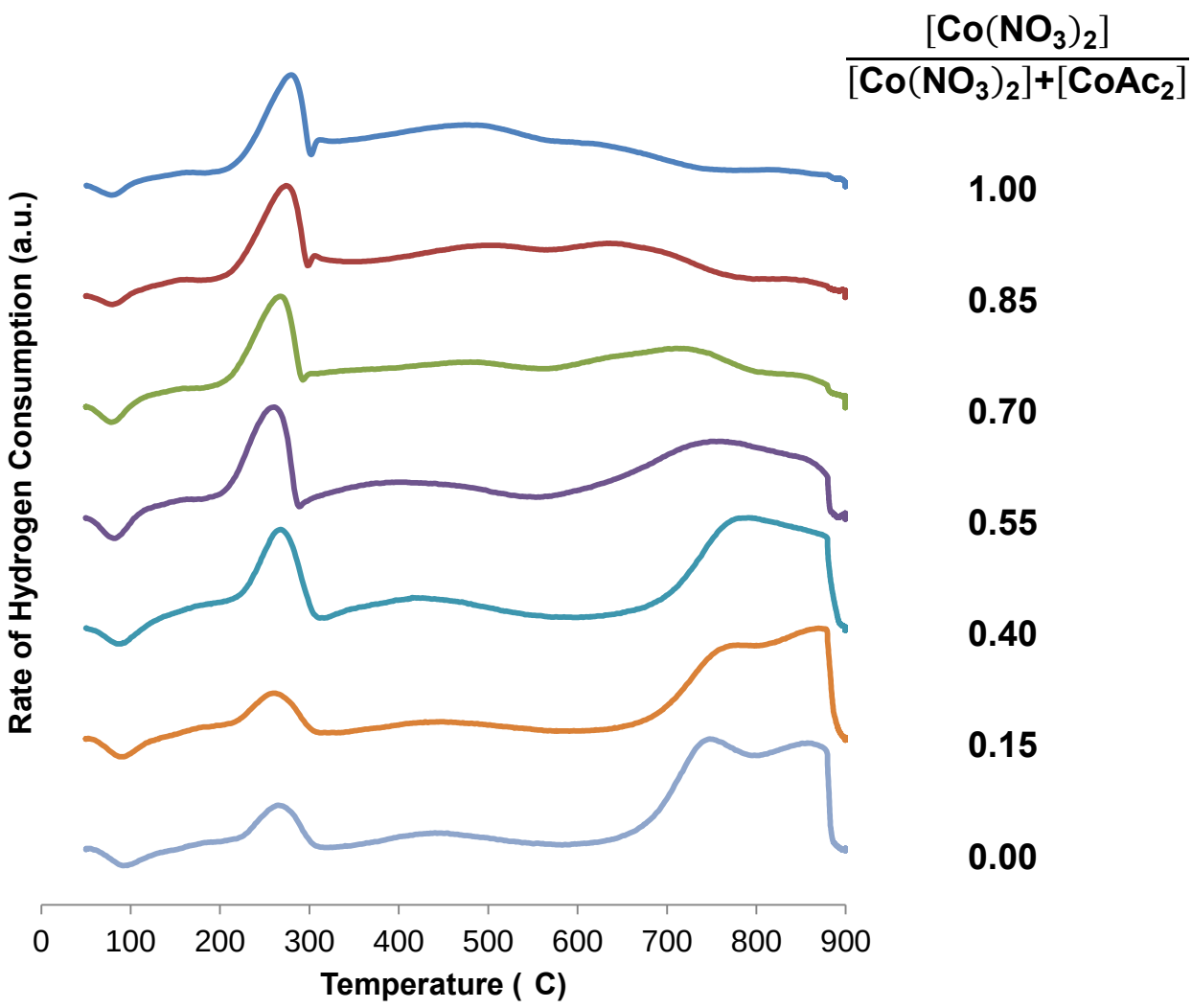

Figure 4.4: TPR profiles for Co_3O_4 prepared by wet impregnation with different fractions of $Co(NO_3)_2$ in the impregnating solution

In order to get an indication of the reducibility of these catalysts, it was decided to calculate the fraction of the total reduction which occurred below 550°C. The temperature of 550°C was chosen, arbitrarily, as at this temperature it is assumed that the reduction of the low temperature peak will be complete and the reduction of the high temperature peaks will not have begun.

This function is defined as:

$$f_R^{550} = \frac{\int_{60}^{550} C_{H_2}(T)\, dT}{\int_{60}^{900} C_{H_2}(T)\, dT}$$

Where f_R^{550} is the fraction of the reduction which occurs below 550°C, $C_{H_2}(T)$ is the hydrogen consumption as a function of temperature. In principle one should integrate over time, however since the temperature is directly proportional to the temperature we may use temperature and time interchangeably. The result of this analysis is shown in Figure 4.5.

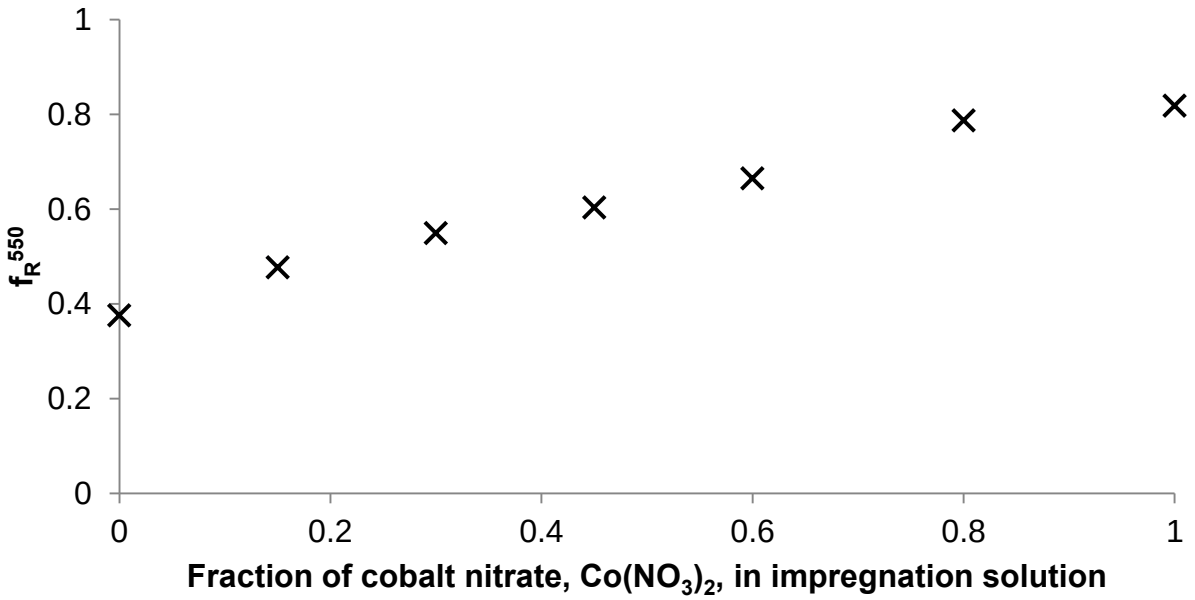

Figure 4.5: Fraction of reduction occurring below 550°C for Co_3O_4/SiO_2 catalysts prepared by wet impregnation from different fractions of $Co(NO_3)_2$

Looking at the hydrogen fraction consumed below 550°C of the various catalysts prepared (Figure 4.5) it is apparent that as the fraction of acetate increases the amount of hydrogen consumed above 550°C increases. It is important to note that there is no physical reason for this plot to be a straight line although it assumes a very linear relationship. This analysis gives an indication of the reducibility of these catalysts. It can therefore be inferred that catalysts produced from cobalt acetate will have a lower reducibility than those produced from cobalt nitrate.

Transmission Electron Microscopy

Transmission electron microscopy was done in order to get another measure of the particle size as well as some idea of the morphology of the Co_3O_4/SiO_2 surface. Selected images for each of the catalysts are given in Figure 4.6.

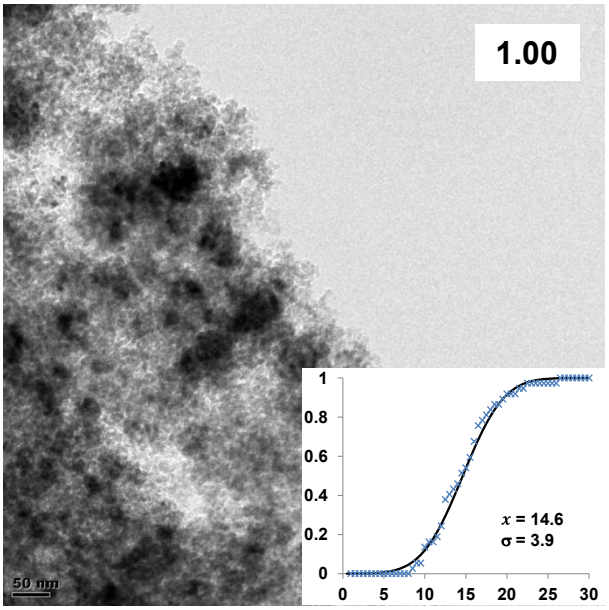
1.00
50 nm
x = 14.6
σ = 3.9

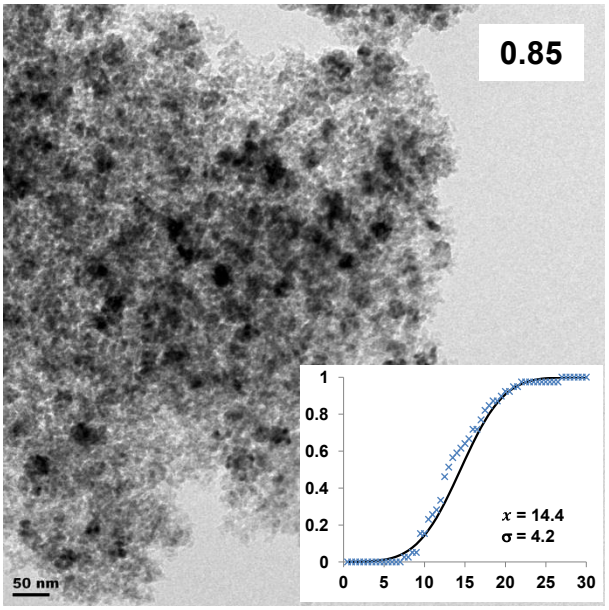
0.85
50 nm
x = 14.4
σ = 4.2

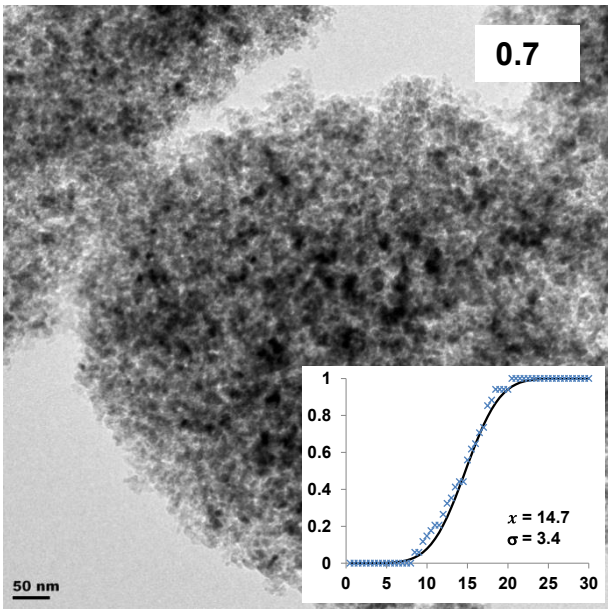
0.7
50 nm
x = 14.7
σ = 3.4

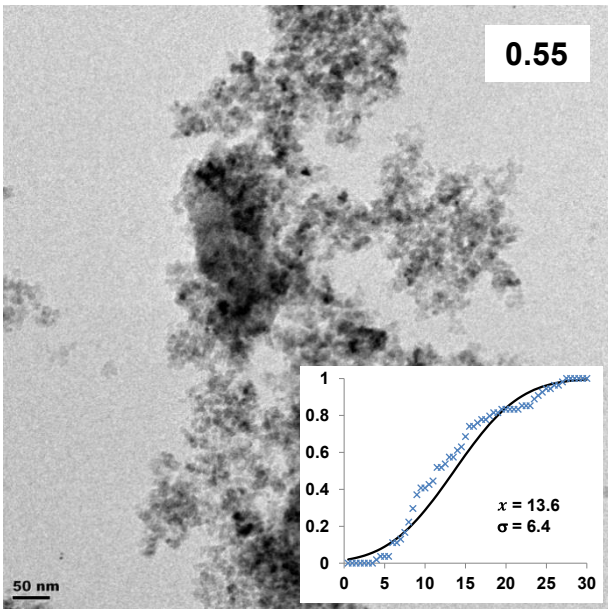
0.55
50 nm
x = 13.6
σ = 6.4

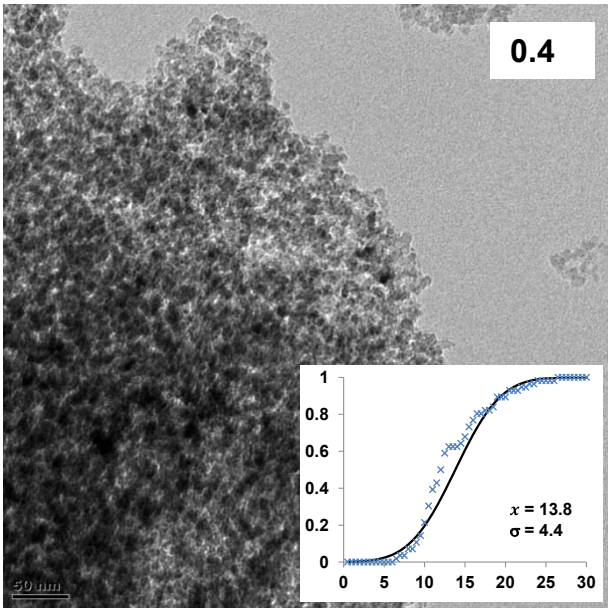
0.4
50 nm
x = 13.8
σ = 4.4

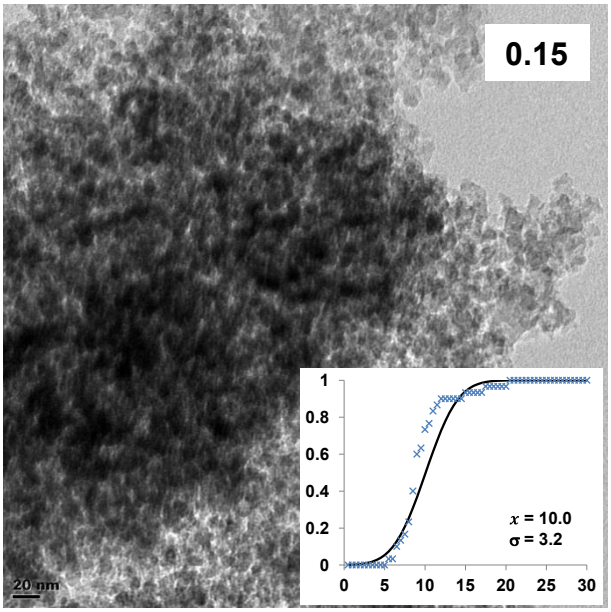
0.15
20 nm
x = 10.0
σ = 3.2

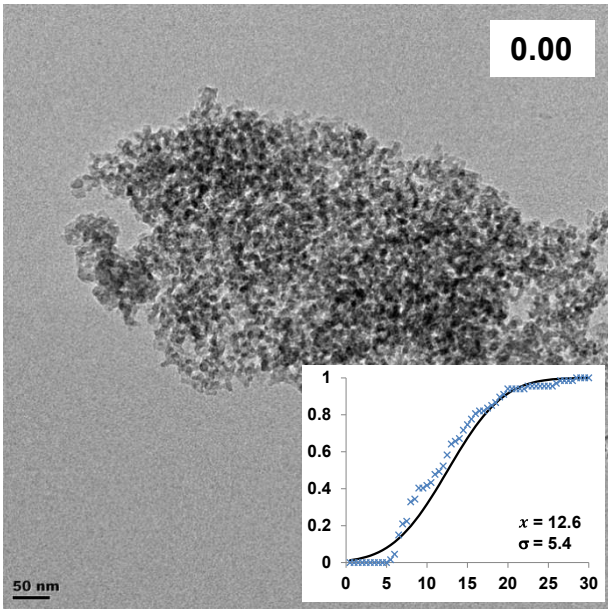

Figure 4.6: TEM micrographs of calcined catalysts prepared with different fractions of cobalt nitrate and cobalt acetate. Fraction of cobalt nitrate is shown in the top right of each image. A plot of the normalised frequency against particle size is given in the bottom right of each image; this has been fitted to a cumulative normal distribution with the mean and standard deviation shown.

It was necessary to focus only on the edge of the Co_3O_4/SiO_2 clusters as the SiO_2 support became too thick in the centre for the electron beam to pass through. There did not appear to be any morphological difference between the catalysts prepared with the different precursors. The Co_3O_4 particles appear to be well dispersed on the SiO_2 support (although one cannot determine whether these particles were on the surface or within the catalyst originally as the catalysts were crushed prior to TEM analysis). The size of a number of Co_3O_4 particles on each catalyst was measured; the averages of these sizes are shown in Table 4.3.

Table 4.3: Particle sizes for different calcined catalysts prepared from different fractions of cobalt nitrate and acetate

Catalyst	$Co(NO_3)_2$ fraction (-)	$Co(NO_3)_2$ fraction in the impregnation solution (-)	Co_3O_4 Particle Size (nm) {number of particles analysed}
NA1	1	1.00	14.8±3.9 {37}
NA2	0.85	0.85	14.4±4.2 {39}
NA3	0.6	0.70	14.7±3.4 {37}
NA4	0.45	0.55	13.6±6.4 {59}
NA5	0.3	0.40	13.8±4.4 {56}
NA6	0.15	0.15	10.0±3.2 {31}
NA7	0	0	12.8±5.4 {69}

From this analysis the particle sizes across the different catalysts are not statistically different from each other. The reason for this may be that the particles observed in the transmission electron microscope images are in fact agglomerates of smaller particles.

H_2 Chemisorption

H_2-chemisorption was conducted in order to investigate the effect on the metallic surface area when preparing catalysts with different fractions of cobalt nitrate. The metallic surface areas of the various catalysts prepared are shown in Figure 4.7. The metallic surface area available for reaction decreases with an increase in the amount of cobalt acetate used in the preparation. Since the Fischer-Tropsch reaction happens on the metallic cobalt surface it would seem that the pure cobalt nitrate catalyst would have the highest mass specific in the Fischer-Tropsch synthesis activity since it has the highest surface area per gram catalyst and the pure cobalt acetate would have the lowest for the same reason. The catalysts prepared by aqueous mixtures of these two salts can be expected to have a per-gram activity between these two extremes although the relationship does not appear to be linear. .

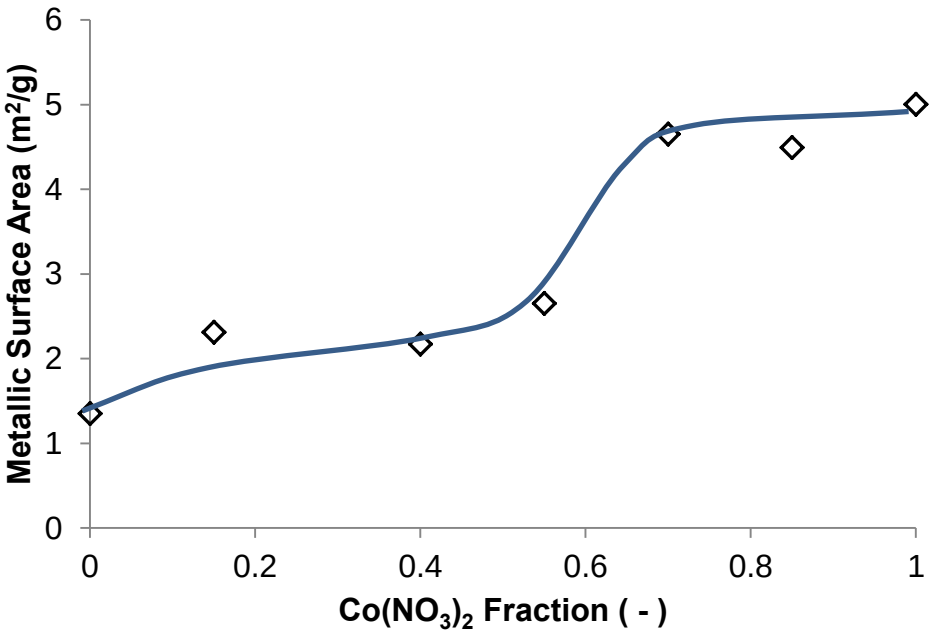

Figure 4.7: Metallic surface area attributable to metallic cobalt for the various catalysts prepared with different fractions of cobalt nitrate and cobalt acetate.

Concluding Remarks

The resulting decrease in the Co_3O_4 particle size upon addition of cobalt acetate to the impregnation solution is desirable. Addition of some cobalt acetate will result in Co_3O_4 crystallites in the range of the optimal particle size. Upon addition of the noble metal promoter (which will be done in the next section) we expect an improvement in the reduction characteristics of these catalysts which may result in a more significant improvement in the metallic surface area on those catalysts with some cobalt acetate in the preparation solution. Thus it is of interest to investigate the promotion of the catalyst prepared with 0.7 cobalt nitrate fraction.

4.3 Pt/Au Promotion of Co_3O_4/SiO_2 by Strong Electrostatic Adsorption (SEA)

4.3.1 Pt Promotion

For each of the catalysts a sample of the supernatant fluid was sent for analysis by ICP-AAS before and after the adsorption of Pt. The expected Pt-loading could then be calculated by the conservation of mass. The platinum loading in the dried and calcined promoted catalyst was determined independently by digestion and ICP (results shown in Table 4.4). The measured loading is then plotted against the expected loading in Figure 4.8.

Table 4.4: Pt-promoted catalysts prepared by SEA

Catalyst	$pH_{initial}$	Pt-loading*
Pt#1	6.8	0.20
Pt#2	5.5	0.22
Pt#3	7.8	0.28
Pt#4	8.8	0.39
Pt#5	9.7	0.28
Pt#6	2.1	0.51
Pt#7	4.3	0.49
Pt#8	3.4	0.42
Pt#9	1.4	0.46

*Determined by digestion and ICP

In principle the expected loading should equal the measured loading and this plot should assume a straight line passing through the origin. This, however, is not what is observed here. This may occur as a result of solution which is trapped in the pores of the support (which will result in Pt being deposited onto the support physically rather than chemically) or simply as a result of an error in the measurment of the Pt-concentration of the liquid samples taken.

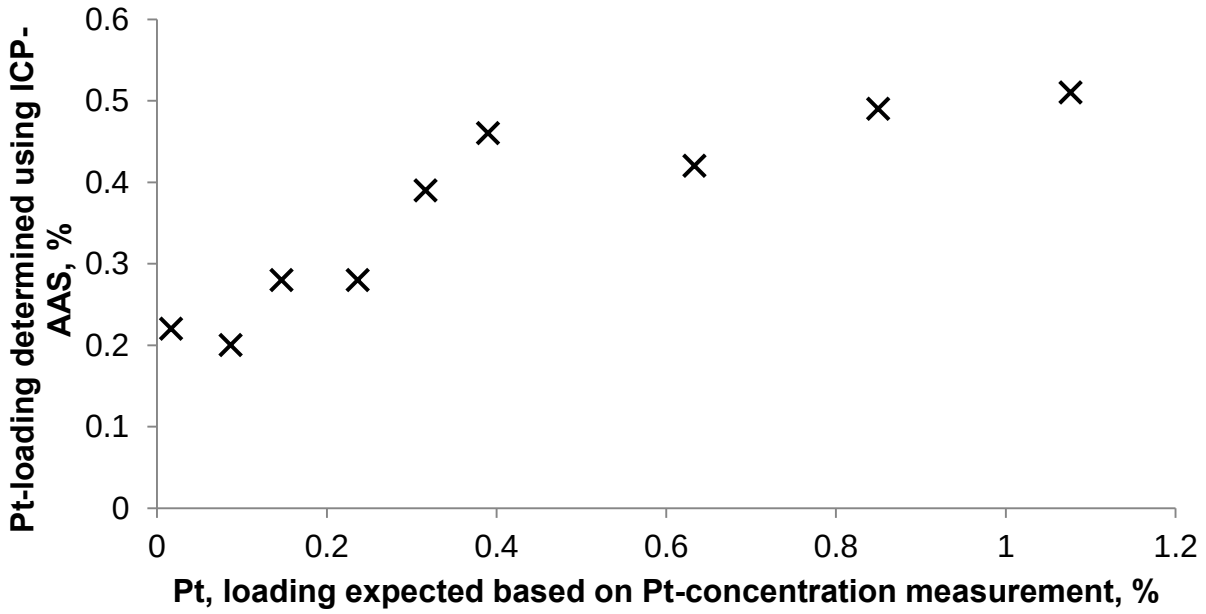

Figure 4.8: Pt-loading determined using ICP-AAS (%) as a function of the expected Pt-loading calculated based on the Pt-concentration measurement (%)

The promotion of the Co_3O_4/SiO_2 at constant pH was made difficult by the fact that the pH of the solution changed as the adsorption proceeded (Figure 4.9). The pH shift which occurs in this system is not fully understood and may occur as a result of a number of simultaneous process occurring. Firstly, when the Co_3O_4/SiO_2 is introduced to the system the –OH groups on the surface of both the SiO_2 and Co_3O_4 establish an equilibrium (see Appendix C & D) with the aqueous phase. The pH shift upon contact of an aqueous medium with an oxide surface is well documented [50, 79, 80] (although the pH shift in the presence of a mixed oxide phase has not been reported). Furthermore, the adsorption reaction of $PtCl_6^{2-}$ (and related species) onto the SiO_2 or Co_3O_4 surface may cause some shift in the pH value. It is therefore important to note that the pH value which the system tends towards, 7.6 (shown by the red line in Figure 4.9), is not the PZC of the oxide (as is calculated by the method of Park and Regalbuto [79])

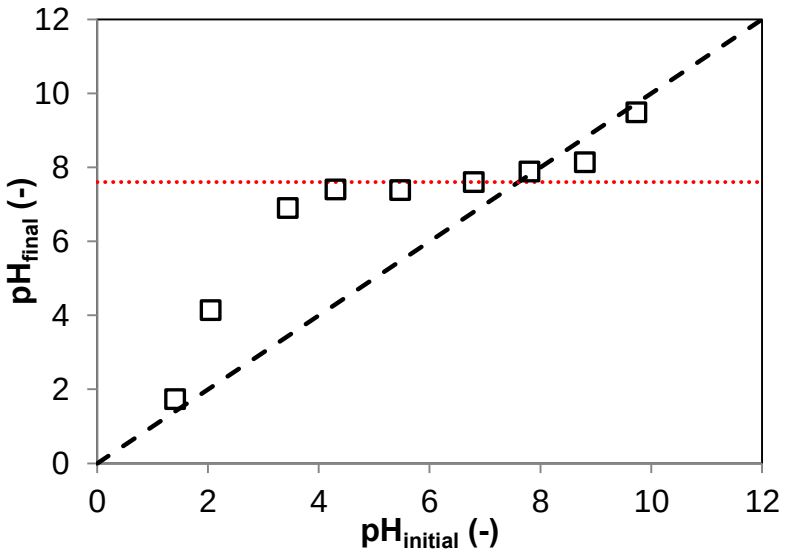

Figure 4.9: Initial and final pH of Pt adsorption solution during SEA. - - $pH_{initial} = pH_{final}$ included for reference.

The initial and final Pt concentrations in the adsorption solution can be used to determine the Pt-adsorption as a percentage:

$$\%Adsorbed = \frac{[Pt]_{initial} - [Pt]_{final}}{[Pt]_{initial}}$$

The platinum loading was determined from digestion and ICP. The %Pt adsorbed and Pt-loading (%) are shown as a function of $pH_{initial}$ (Figure 4.10). The initial pH was chosen as the independent variable as this is more practical experimentally than the final pH value.

The Pt-adsorption vs. $pH_{initial}$ (on the right of Figure 4.10) should be treated with care when analysed as it may be subject to significant error in measurement that may have arisen as a result of the successive dilutions which are necessary to lower the concentration to within the detection limit of the ICP instrument.

The two graphs in Figure 4.10 are not independent (by conservation of mass) and can therefore be considered in conjunction. It appears that, in both graphs, there is more platinum adsorbed at low pH values than at the higher pH values.

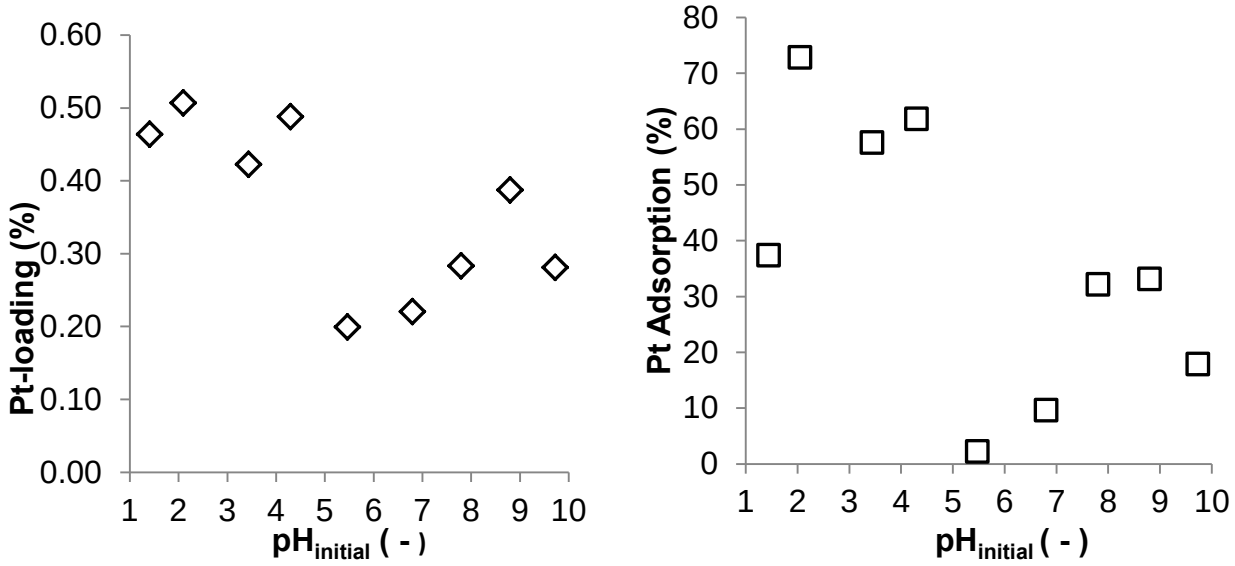

Figure 4.10: Pt-loading on calcined catalyst (left) and % Pt adsorption during SEA (right) as a function of the initial pH of the adsorbing solution.

X-Ray Diffraction

XRD was done to determine whether the promotion of Co_3O_4/SiO_2 with platinum via the applied procedure results in a change in the particle size or crystallite structure of the Co_3O_4 (and also whether platinum is detectable by XRD). The XRD spectra of selected promoted catalysts prepared at various pH values are shown in Figure 4.11.

The XRD scans of the Pt-promoted catalysts contains the same peaks as the unpromoted catalysts i.e. those attributable to Co_3O_4 and SiO_2. There does not appear to be any additional peaks due to the presence of a Pt phase. The absence of Pt peaks on the XRD spectrum is due the small size of the crystalline domains of platinum rendering them XRD-invisible; this may be due the presence of XRD-amorphous platinum or or platinum crystallites which are too small for XRD to detect.

The Debye-Scherrer equation was used on the Co_3O_4 [3 1 1] peak to determine the crystallite size. This data is reported in Figure 4.12. The crystallites prepared at a pH<5 have a crystallite size of approximately 9nm (i.e. similar to that of the unpromoted Co_3O_4), whereas those prepared at pH>5 have a crystallite size of approximately 7nm. The drop in the particle size is unlikely to be due to dissolution of the Co_3O_4 phase as the solubility of Co_3O_4 at pH<5 is far too low to result in a reduction of this magnitude in the size of the Co_3O_4 particles additionally the amount of cobalt present in the promoted catalyst does not suggest significant dissolution. The decrease in the particle size observed in those catalysts prepared at a higher pH, therefore, cannot be explained at this point.

A decrease in the particle size upon promotion with Pt has been observed in literature [37, 44], however those catalysts were prepared by co-impregnation not by the consecutive SEA-process.

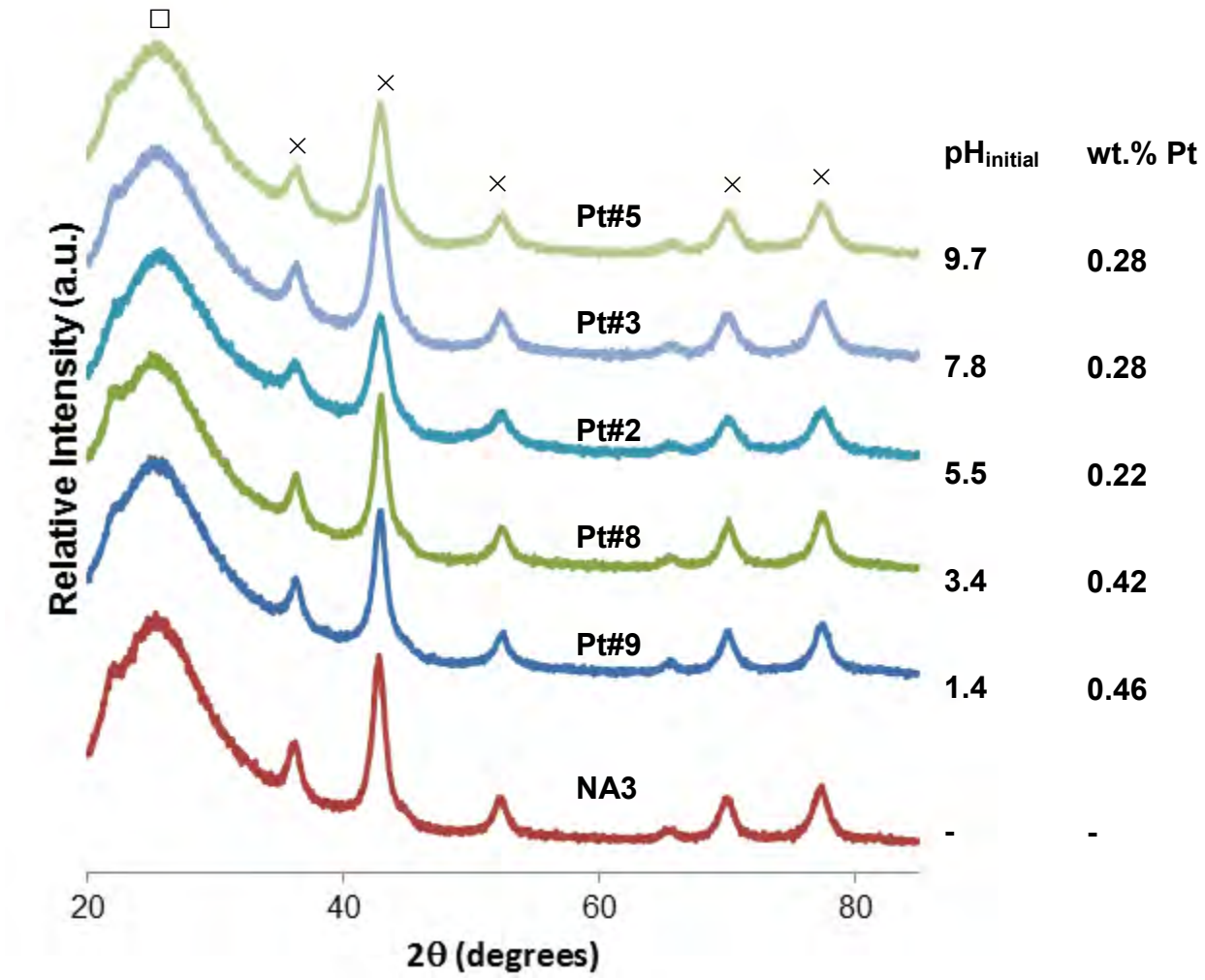

Figure 4.11: XRD spectra of unpromoted Co_3O_4/SiO_2 (NA3) and selected Co_3O_4/SiO_2 promoted with Pt by SEA at different pH values. × - Co_3O_4, □ – SiO_2

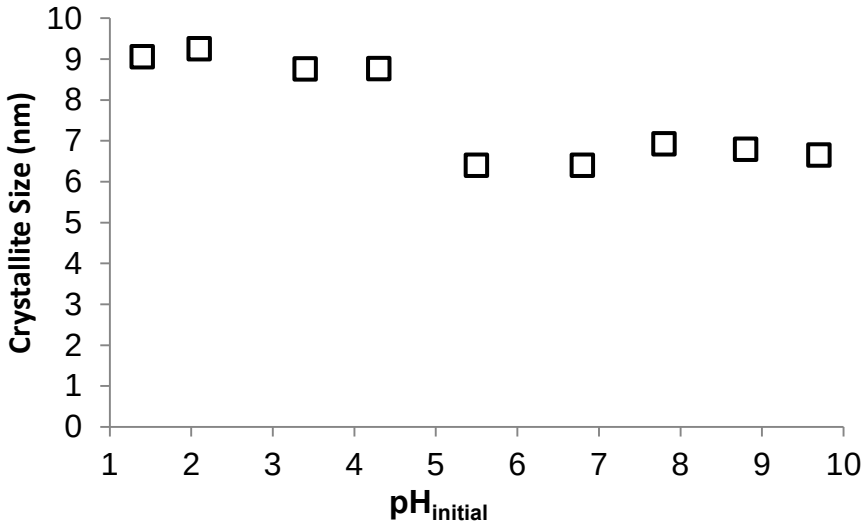

Figure 4.12: Co_3O_4 crystallite size of Pt-promoted catalysts prepared at different pH values

Temperature Programmed Reduction

The effect on the reduction behaviour of Co_3O_4/SiO_2 when promoted with Pt by SEA is of utmost importance to this investigation. TPR was conducted on the promoted and unpromoted catalysts to give insight into the promotional effect on the reduction behaviour. TPR profiles for selected catalysts prepared at different pH values across the pH range are shown in Figure 4.13.

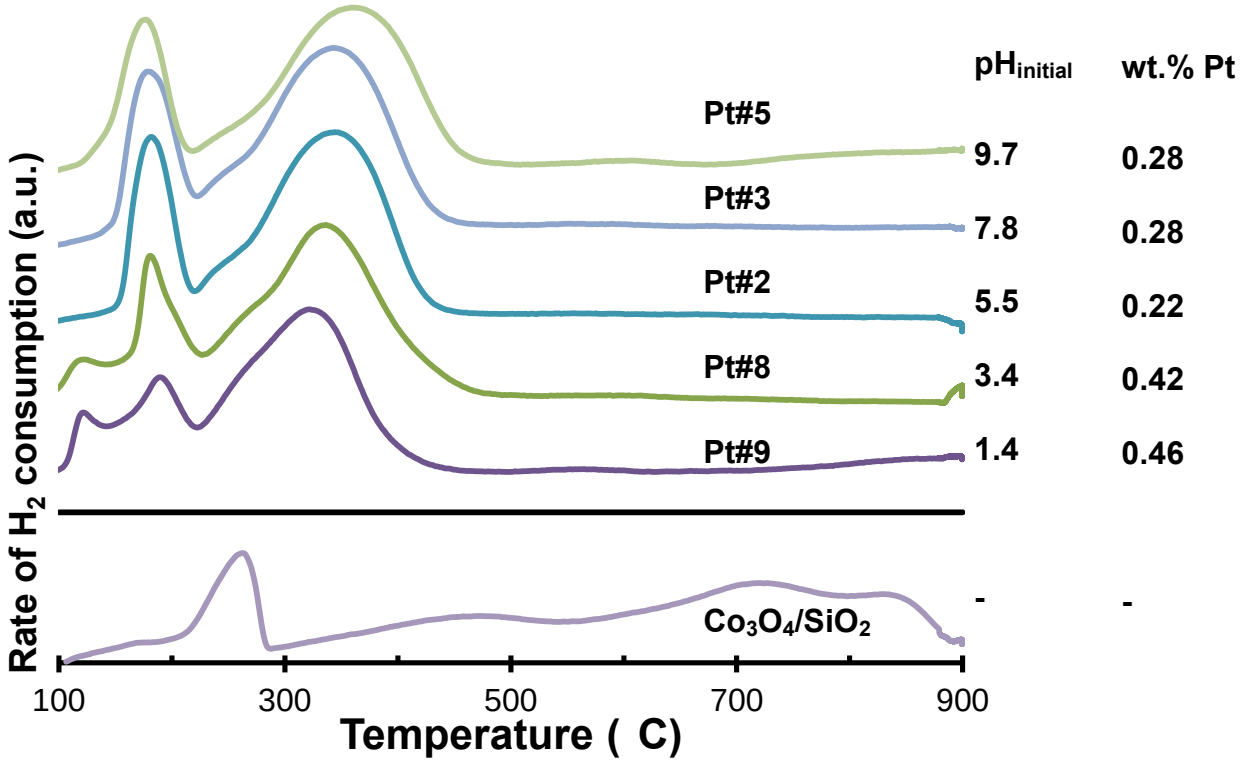

Figure 4.13: TPR profiles for unpromoted Co_3O_4/SiO_2 and various Pt-promoted Co_3O_4/SiO_2 prepared by SEA at different pH values

The TPR profiles for the promoted catalysts all show a dramatic shift in the H_2-consumption peaks towards lower temperatures. The first reduction peak (i.e. $Co_3O_4 \rightarrow CoO$) shifts from 280°C in the unpromoted catalyst to 180°C in the promoted catalyst. The second reduction peak (i.e. $CoO \rightarrow Co^0$) is reduced from a broad, diffuse peak ranging from 300-900°C to a large peak at approximately 320-360°C.

The decrease in the reduction temperature of the Co_3O_4 reduction processes upon Pt-promotion has been reported extensively in literature. The reduction peak temperatures obtained in the present study agree well with those obtained by Schanke *et al*. [37]. They noted a decrease from 330°C to 150-180°C and 400°C to 360°C for the first (i.e. Co_3O_4 to CoO) and second (CoO to Co^0) reduction peaks respectively in a Pt-promoted Co/SiO_2 catalyst. However they differ to those obtained by Tsubaki *et al*. [44] where a decrease from 370°C to 200°C for the first reduction peak and a shift from a broad peak from 420 – 820°C to a single peak at 710°C for the second reduction was observed. Tsubaki *et al*. [44] attribute the reduction peak at 200°C in the promoted catalyst to the reduction of cobalt around noble metals.

There also appears to be a pre-shoulder on the second main reduction peak in the TPR-profiles of the platinum promoted catalysts at ca. 250-270°C. This may be attributable to the reduction of Co_3O_4 which is not influenced by the Pt or may be due to an intermediate phase [37]. One would expect that the reduction of Co_3O_4 not influenced by Pt would yield a high temperature CoO peak (which is also unaffected by Pt). However there is no peak on the TPR profile to support this.

In the cases where the Co_3O_4/SiO_2 is promoted at low pH a new peak appears at 120°C. The area of this peak increases with decreasing pH. The increase in this peak area is associated with a decrease in the area of the peak at 180°C. As the pH at which the Co_3O_4 was promoted increases it appears the temperature of the first reduction peak gradually decreases and the temperature of the second peak gradually increases. This peak disappeared when the gold promoted catalysts were tested after this set of catalysts, indicating that it is unlikely that this is an instrumental error. It is also difficult to attribute this peak to the reduction of $PtCl_6$ on SiO_2 as this has been observed to reduce at temperatures of around 350°C [91]

To investigate the effect of promotion on the activation energy of the reduction processes in the promoted and unpromoted catalysts TPR was conducted at different ramp rates. This allows for the use of the Kissinger equation to determine the activation energy for these processes.

$$\ln\frac{\beta}{T_{max}^2} = -\ln\frac{Ea}{A\cdot R\cdot p_{H_2}^q} - \frac{Ea}{R}\cdot\frac{1}{T_{max}}$$

where β is the heating rate, T_{max} is the peak maximum temperature, E_a is the activation energy of the reduction process, A is the pre-exponential factor for the reduction process, R is the gas constant, $p_{H_2}^q$ is the partial pressure of hydrogen. A semi-logarithmic plot of $\frac{\beta}{T_{max}^2}$ against $\frac{1}{T_{max}}$ should thus yield a straight line with the gradient of $-\frac{E_a}{R}$.

The unpromoted Co_3O_4/SiO_2 and Pt#1 catalysts were chosen for this analysis. These TPR profiles are shown in Figure 4.14 (note that the intensities of these peaks have been normalised with respect to the intensity of the most intense peak). The results from the Kissinger analysis for these catalysts are given in Table 4.5. Interestingly during this analysis the presence of a small peak at 250°C between the two reduction peaks is highlighted.

Table 4.5: Results from Kissinger analysis of unpromoted and Pt-promoted Co_3O_4/SiO_2

Catalyst	Activation Energy (kJ/mol)	
	Co_3O_4 to CoO	CoO to Co^0
Unpromoted Co_3O_4/SiO_2	192±26	185±10*
Promoted Co_3O_4/SiO_2	114**	88**

*The first "peak" of the diffuse peak from 300-900°C was used in calculation.
**This value was determined from a two point analysis and as such the standard error could not be determined.

From the Kissinger analysis we can see that the additional of Pt substantially lowers the activation energy of the reduction of Co_3O_4 on SiO_2, this implies a different reduction pathway by which the reduction can occur. The decrease in the activation energy of the reduction processes implies the reduction is proceeding via a different route (one with a lower activation energy) meaning the Pt present on the catalyst facilitates the reduction of Co_3O_4 (possibly by H_2-spillover).

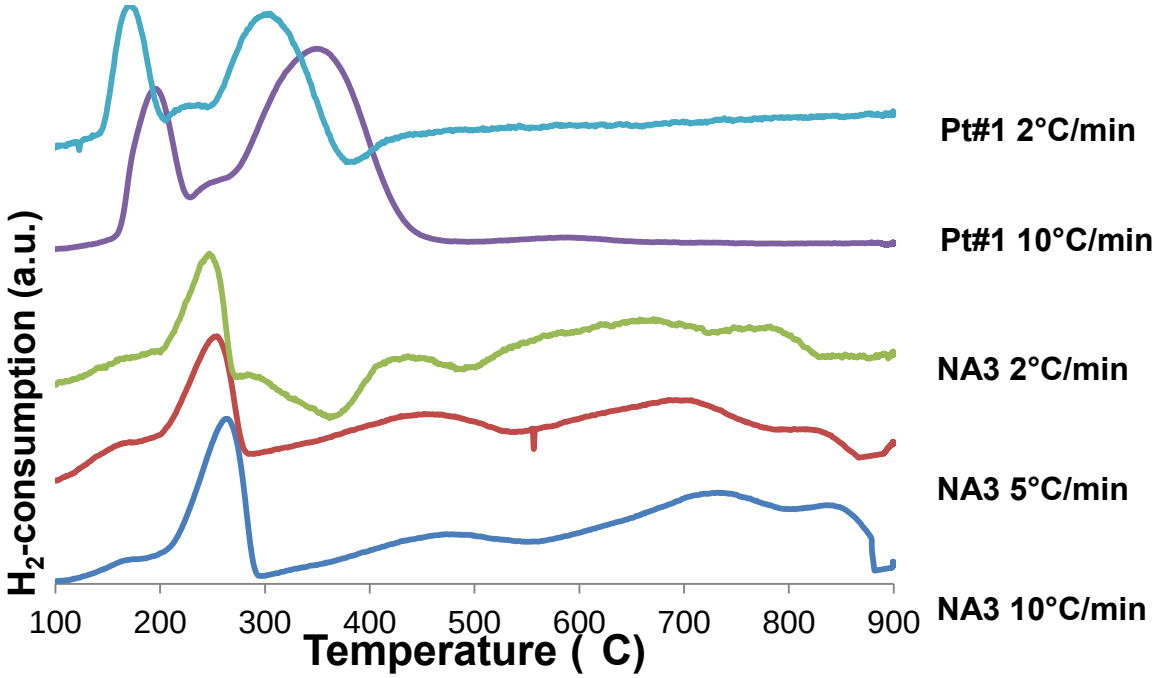

Figure 4.14: TPR profiles for unpromoted (NA3) and promoted (Pt#1) Co_3O_4/SiO_2 at different heating rates for activation energy determination

It is also interesting to note that the activation energy of the unknown process occurring between the two main cobalt reduction peaks (suspected to be reduction of Co_3O_4 unaffected by Pt) is found to be 149 kJ/mol. This is lower than the value for unpromoted Co_3O_4 (192±26kJ/mol) which means that if this was a reduction peak for Co_3O_4 with no interaction with Pt, these particles are still affected at least to some extent by the presence of Pt.

Thermal Gravimetric Analysis

The degree of reduction (DOR) for the Pt-promoted and unpromoted catalysts were determined using thermal gravimetric analysis (TGA). The TGA curves are given in Figure 4.15. The mass of the samples initially decreases due to the removal of water which has been absorbed from the atmosphere. This decrease followed by an increase which is peculiar and can't be explained by density changes associated with increasing temperature of the carrier gas with increasing temperature or some oxidation process as this heating section is carried out under N_2 flow. The mass stabilises prior to the initiation of H_2 flow. As this mass represents the mass of the dried catalyst the mass is normalised with respect to this value for ease of calculation. When the H_2 flow is initiated the mass of the sample begins to decrease as the Co_3O_4 present in the sample is reduced to Co^0 (with the release of H_2O). Assuming that all the cobalt present in these catalysts is present initially as Co_3O_4 we

can calculate the theoretical maximum mass loss that can occur in these catalysts. The fraction of this mass loss which is observed is then the degree of reduction.

This assumption is faulty as we know that cobalt is most likely present on these catalysts in other forms i.e. cobalt silicates and possibly CoO. If cobalt is present as CoO, complete reduction will require a smaller amount of H_2 and hence correspond to a smaller mass loss. This means that the observed degree of reduction will be lower. The assumption that all of the cobalt is present as Co_3O_4 will result in our calculation yielding a smaller degree of reduction.

The mass loss is calculated from the difference in mass from when the H_2 flow is initiated (i.e. a relative mass of 1) and the mass after 12hrs. A sample calculation is provided in Appendix.

To circumvent the uncertainty of the initial oxidation state of the cobalt phase reoxidation in O_2 can be carried out after the reduction. However due to time constraints on the instrument was not possible when analysing the Pt-promoted catalysts.

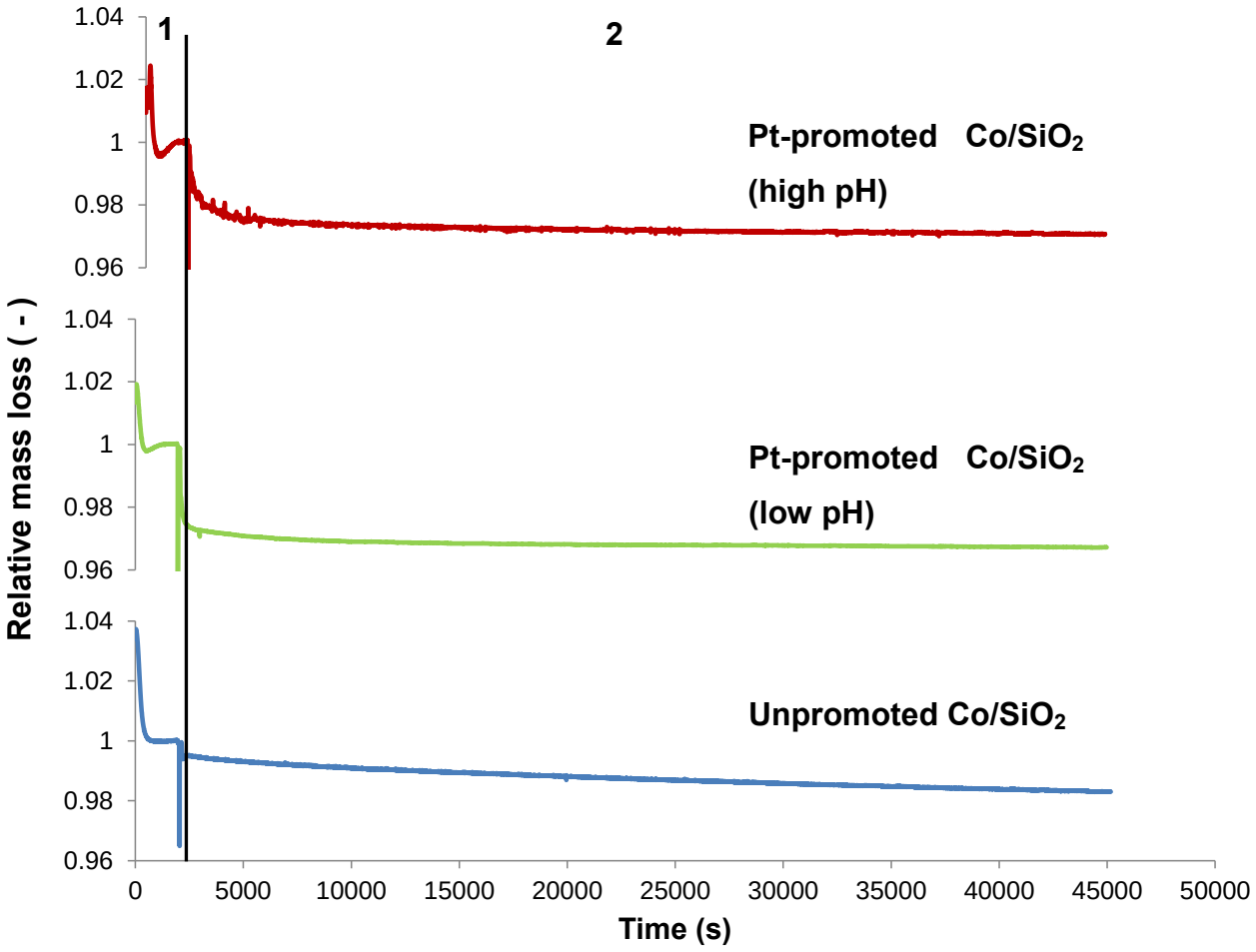

Figure 4.15: TGA curves for unpromoted Co_3O_4/SiO_2 and Co_3O_4 promoted with Pt by SEA at a low and high pH. 1 –temperature ramp in N_2 flow, 2-isothermal reduction in H_2 flow

The degree of reductions obtained for the unpromoted and the Pt-promoted catalysts which were tested in the Fischer-Tropsch reaction are given in Table 4.6.

Table 4.6: Degree of reductions calculated from TGA data

Catalyst	Degree of Reduction (%)
NA3	47
Pt#9 (low pH)	92
Pt#5 (high pH)	81

The degree of reduction is increased significantly upon addition of Pt to the Co_3O_4/SiO_2 catalyst. This increase in the degree of reduction upon addition of Pt has been reported extensively in literature. Schanke *et al*. [37] noted a slight increase in the degree of reduction from 90 to 92% and Tsubaki *et al*. [44] noted an increase from 50 to 56% upon addition to Co/SiO_2 catalysts.

Hydrogen Chemisorption

As the Fischer-Tropsch reaction is a surface reaction catalysed by the cobalt metal surface, the effect on the metal surface area after promotion with Pt is of key importance. Thus H_2-chemisorption was conducted on selected catalysts to investigate the effect of the Pt-promotion as well as the pH of the SEA solution on the metal surface area. The metal surface area of the unpromoted catalyst is shown by the red line. The unpromoted catalyst has a much lower metallic surface area than the same unpromoted catalyst prepared previously (see Figure 4.7). This may be as a result of the different drying conditions (the catalyst in the previous section was dried in an oven on a watch glass at 60°C whereas these were dried in a Rotavap under vacuum at 60°C / 80°C) used in the two distinct catalyst preparations although this is purely speculation.

That being said from Figure 4.16 it is apparent that the addition of Pt to this Co_3O_4/SiO_2 catalyst dramatically increases the metallic surface area on the catalysts. However since Pt atoms will adsorb H_2 during chemisorption it is necessary to take this adsorption into account when analysing the metallic surface area. If we calculate the maximum possible surface area increase due to the addition of Pt (i.e. atomically dispersed Pt) we can determine whether the observed increase in surface area comes only as a result of the addition of Pt. The results from this analysis are shown with a dotted blue line in Figure 4.16. We can therefore say that the increase in surface area can't be explained solely by the increase due to addition of Pt. The presence of Pt must increase the surface area of the Co phase as well i.e. by increasing the degree of reduction and/or increasing the dispersion of the

Co^0 phase. Both of these effects have been observed in literature when cobalt catalysts (on a variety of supports) are promoted with Pt [33, 37, 44, 81].

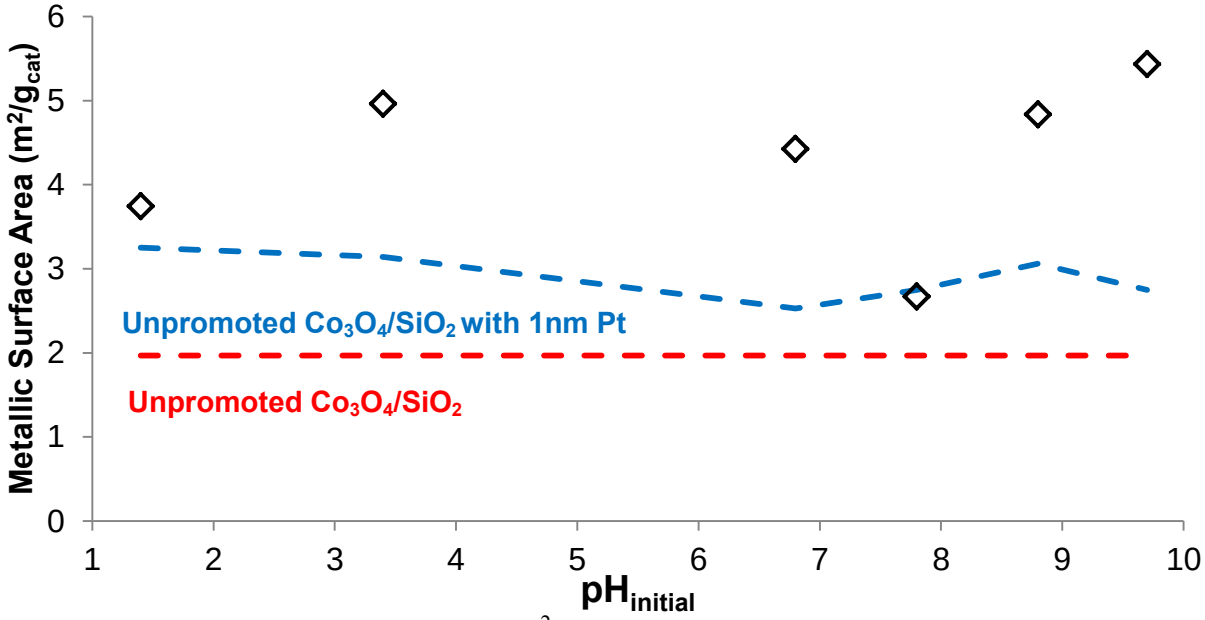

Figure 4.16: Active metal surface area (m^2/g_{cat}) of promoted catalysts prepared by SEA at different pH values. - - - Unpromoted Co_3O_4 (from chemisorption) - - - Unpromoted Co_3O_4 + 0.4wt% atomically dispersed Pt.

It is difficult to state without doubt whether the increase observed here is as a result of increased degree of reduction or an increase in the dispersion as the particle size of the metallic Co^0 phase has not been independently measured. The metallic surface area appears to increase as the pH of the SEA solution increases but it is unclear whether this is strictly a pH effect or one which is related to the Pt loading.

Transmission Electron Microscopy

In order to measure the effect of Pt-promotion on the particle size TEM analysis was done. In addition to this the position and size of the Pt particles is also of particular interest in this study. Due to the time required for analysis TEM was only conducted on selected catalysts across the pH range investigated i.e. Pt#1, Pt#5 and Pt#9.

The morphology observed in the TEM images for these catalysts is not significantly different from those of the unpromoted catalysts (Figure 4.6). However under higher magnification on certain regions of the surface (Figure 4.17: Pt#1b & Pt#9b) there appears to be a large number of very small particles (~2nm). As particles of this size weren't observed in any of the unpromoted catalysts it is possible that these particles are highly dispersed Pt particles. However, an elemental analysis on

these particles to verify their identity (by EDX for example) was not possible due to the limitations of the instrument. One concern, however, is the lack of contrast of these particles as one would expect much darker particles for Pt (due to its significantly higher density).

The average particle size of a number of Co_3O_4 crystallites was determined and is shown in Table 4.7. The Co_3O_4 particle size in the promoted catalysts is not significantly different from those in the unpromoted case.

Table 4.7: Co_3O_4 particle size from TEM analysis in Pt-promoted and unpromoted Co_3O_4/SiO_2 systems

Catalyst	Co_3O_4 Particle Size (nm) {number of particles analysed}
NA3 (unpromoted)	9.2±2.1 {79}
Pt#1	7.7±1.7 {29}
Pt#5	8.6±1.6 {75}
Pt#9	9.0±2.8 {22}

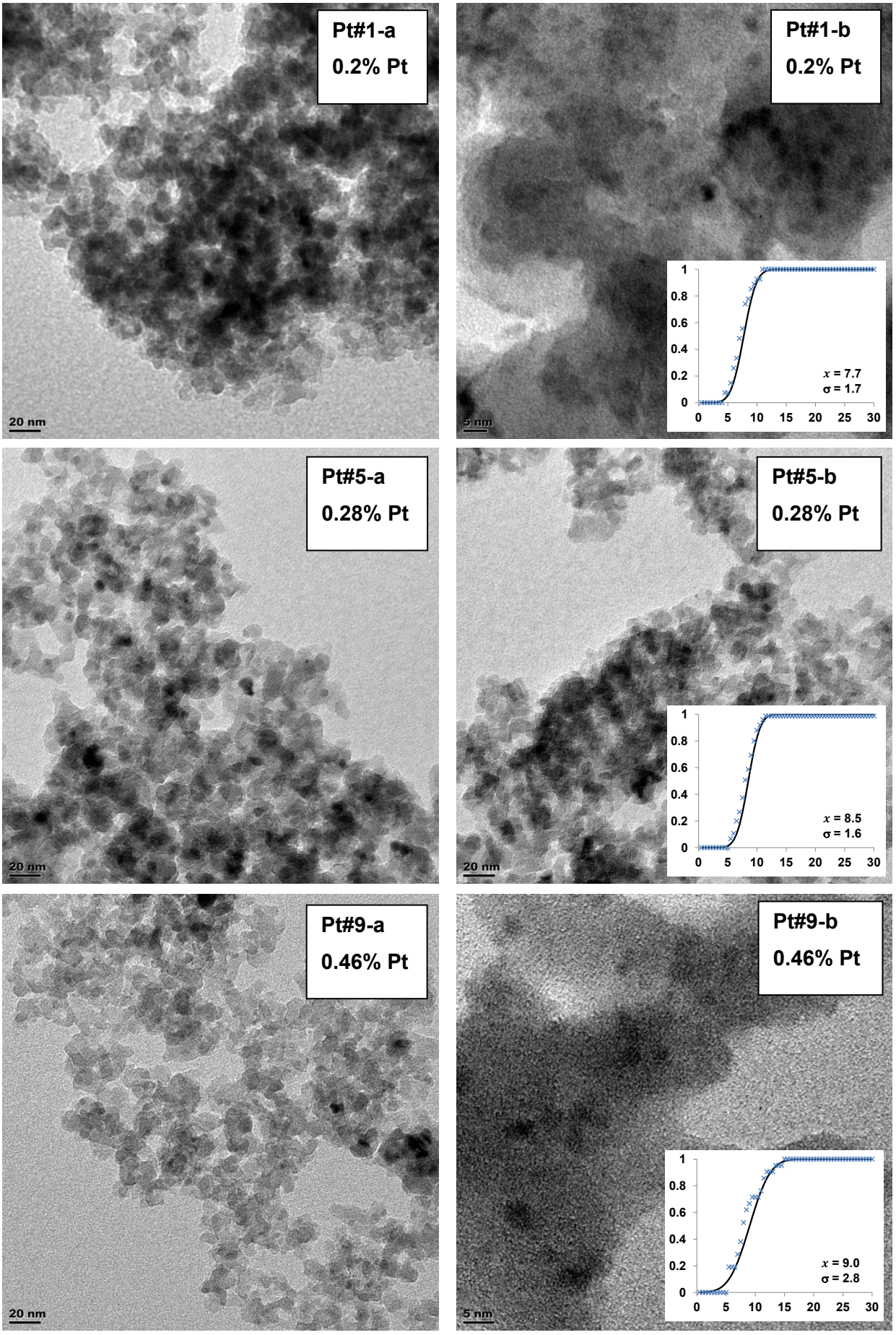

Figure 4.17: TEM micrographs of Pt-promoted catalysts prepared by SEA at different pH values. A plot of the normalised frequency against particle size is given in the bottom right for each catalyst; this has been fitted to a cumulative normal distribution with the mean and standard deviation shown.

4.3.2 Au Promotion

The Au-promoted catalysts prepared by SEA at different pH values are shown in Table 4.8. The pH of the solutions was adjusted using NaOH (aq). NH_4OH (aq)-solutions could not be used since the addition of small amounts of NH_4OH (aq) to the gold solution yields a white precipitate, fulminating gold (or Knallgold) [82]. Although this is a very interesting side reaction, it is not of interest in this investigation. NaOH was used to adjust the pH value to avoid the formation of this fulminating gold. The pH of the gold solution was difficult to adjust and large amounts of NaOH were needed to exact small changes in the pH, for this reason the pH range investigated is not as extensive as that in Pt. The difficulty in adjusting the pH value of the $AuCl_4^-$ upon addition of NaOH is most probably caused by the speciation reactions which the $AuCl_4^-$ complex undergoes in solution:

$$AuCl_4^- + xOH^- \leftrightarrow AuCl_{4-x}OH_x^- + xCl^-$$

As this reaction utilises OH^- ions it will cause a drop in the pH as the forward reaction proceeds causing a "buffering effect" on the solution pH. As such the pH did not vary as significantly during the promotion by SEA (as shown in Figure 4.18)

Table 4.8: Au-promoted catalysts prepared by SEA.

Catalyst	$pH_{initial}$	Au-loading*
Au#1	1.9	0.41
Au#2	2.3	0.8
Au#3	3.1	1.1
Au#4	3.5	1.02
Au#5	3.9	1.22
Au#6	4.4	1.11
Au#7	5.5	1.81
Au#8	6.6	1.71
Au#9	7.4	1.60

* Determined from digestion and ICP-AAS.

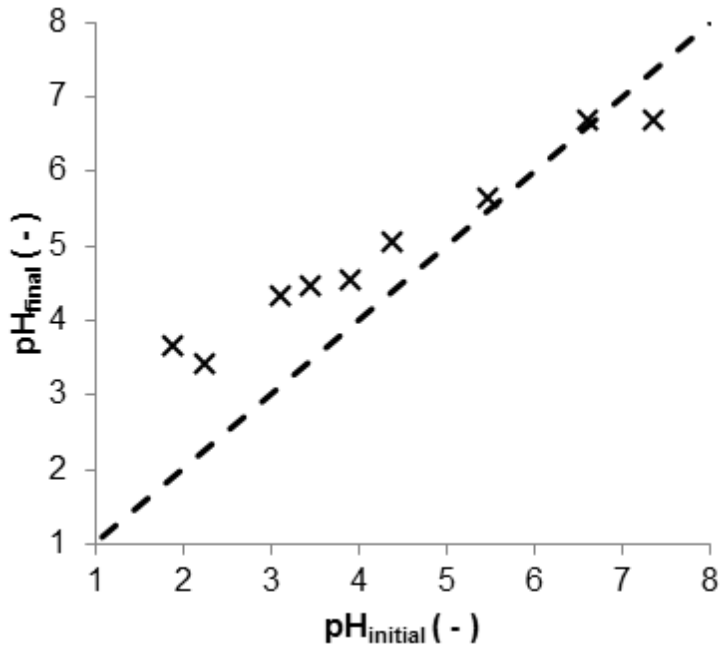

Figure 4.18: $pH_{initial}$ vs. pH_{final} for SEA of Co_3O_4/SiO_2 with $HAuCl_4$ (aq)

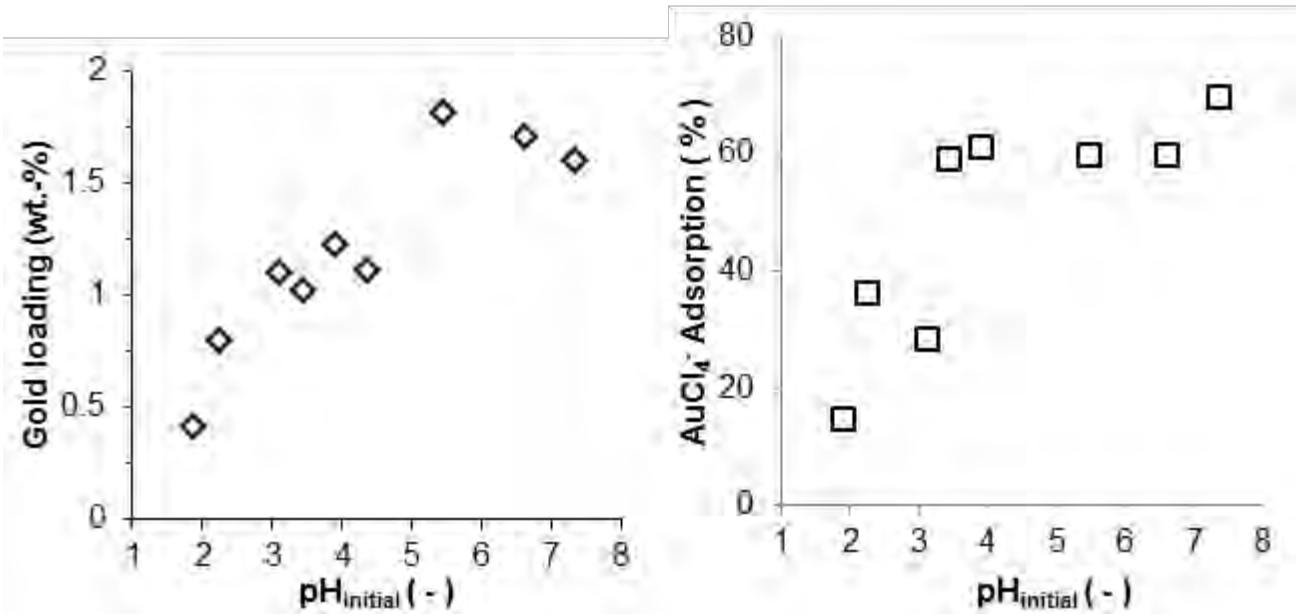

Figure 4.19: **A**u-loading present on gold promoted Co_3O_4/SiO_2 prepared by SEA at different $pH_{initial}$ values (left), $AuCl_4^-$ adsorption from solution (%) for the different Co_3O_4 catalysts prepared by SEA at different $pH_{initial}$ values

X-Ray Diffraction

The average crystallite size of Co3O4 was investigated using XRD in order to determine whether the promotion of Co_3O_4/SiO_2 with Au affected the Co_3O_4 particle size or crystallite phases present. The XRD spectra of selected Au promoted Co_3O_4/SiO_2 catalysts prepared at various pH values are shown in Figure 4.20.

The XRD scans immediately reveal additional peaks to those present in the unpromoted catalyst. These peaks are identified as metallic gold. It has been suggested that the metallic gold arises during calcination at 350°C as a result of the reduction of Au hydroxide [83].

Rietveld refinement was conducted on these catalysts over the range of 2θ=[40:80] to determine the crystallite size of the Au and Co_3O_4 since the Debye-Scherrer equation could not be used as the metallic Au peaks overlap significantly with the Co_3O_4 peaks. The relative amounts of crystalline Au and Co_3O_4 are then also determined.

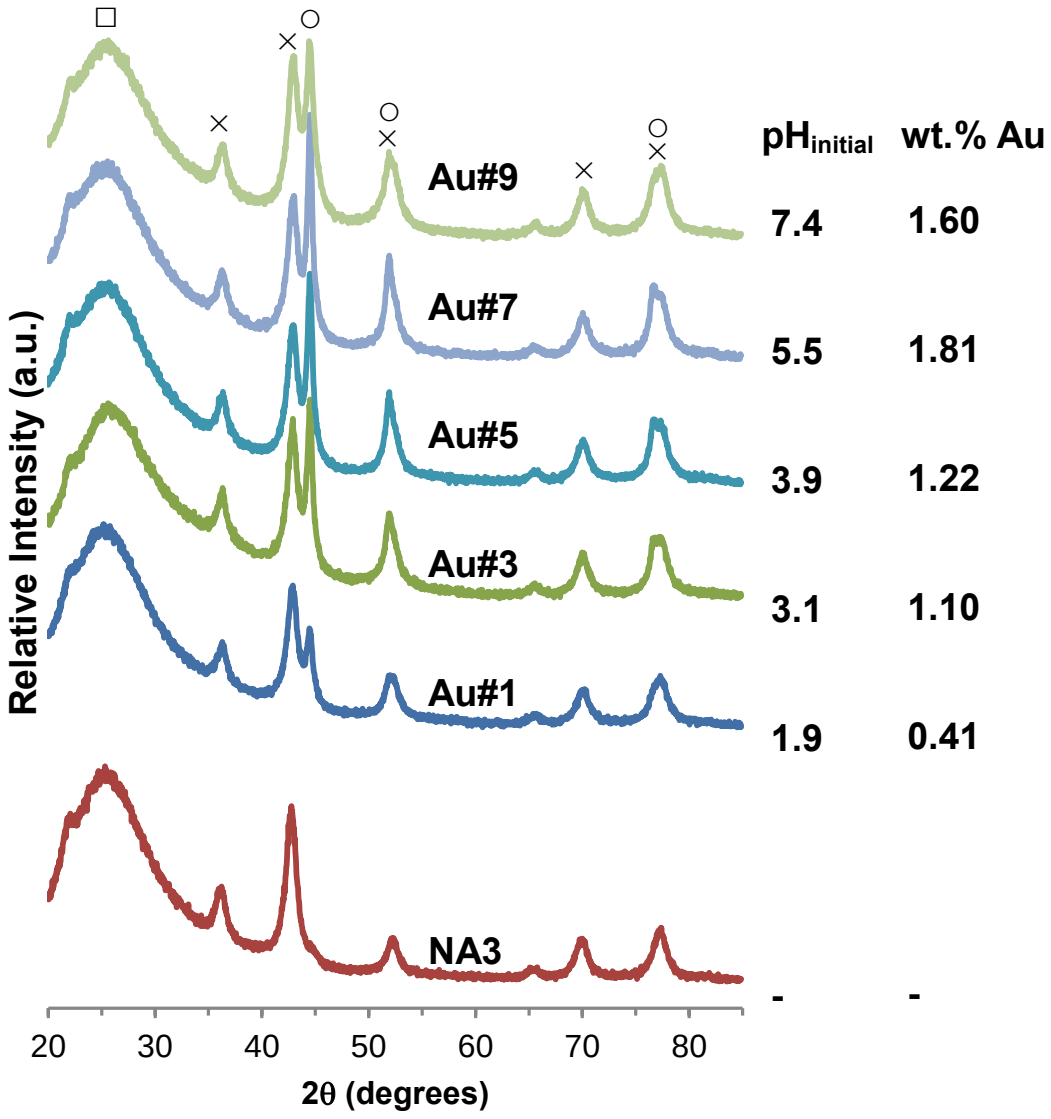

Figure 4.20: XRD Spectra of unpromoted (NA3) and selected Au-promoted Co_3O_4/SiO_2 catalysts. ×- Co_3O_4 ○ - Au

The Co_3O_4 and Au crystallite size are given in Figure 4.21.

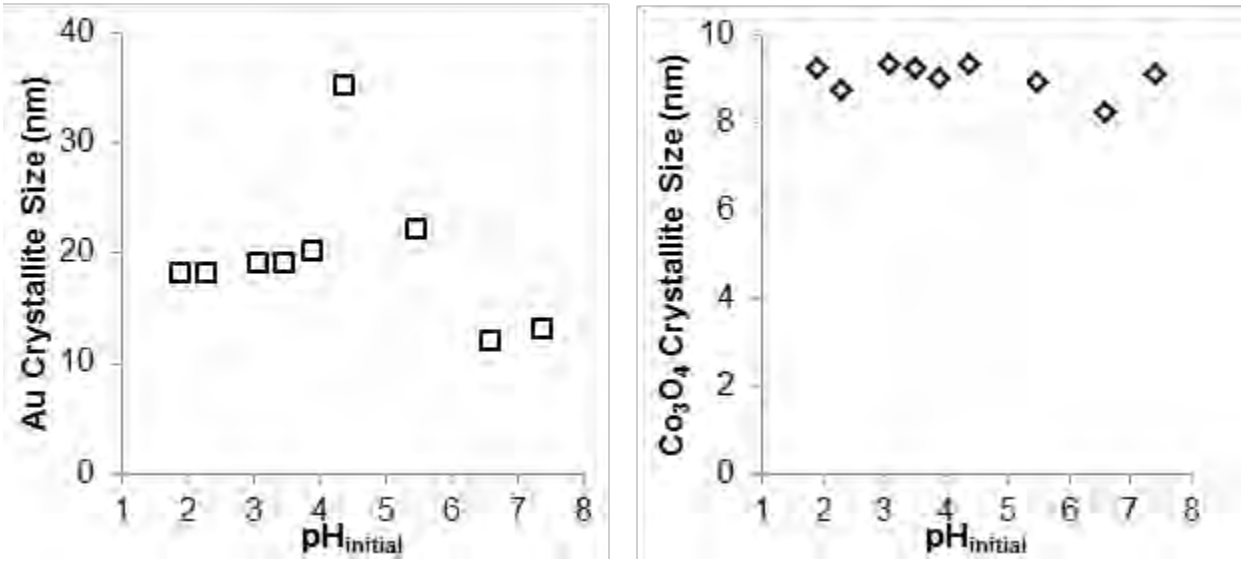

Figure 4.21: Au (left) and Co_3O_4 (right) crystallite size determined from Rietveld refinement on the Au [1 1 1] and Co_3O_4 [3 1 1] peaks

The Au crystallite size increases slightly as the pH of the SEA solution increases, with the exception of the catalysts prepared at pH4.4 and pH>6. It is unclear whether the drop in crystallite size at higher pH is as a result of experimental error or an actual physical phenomenon. These crystallites are very large and probably arise during the second calcination step of the catalyst preparation by migration and agglomeration of reduced Au species.

The Co_3O_4 crystallites are all in the region of 8-10nm indicating the pH of the Au SEA solution does not have any significant effect on the Co_3O_4 crystallite size.

The relative amount of Au:Co_3O_4 is also a result of the Rietveld refinement, these were converted to a mass basis and are plotted against the relative amount of Au:Co_3O_4 determined from AAS in Figure 4.22.

It is important to remember that in any XRD technique it is only crystalline material that is detected. Thus the mass ratio presented in Figure 4.22 is the ratio of crystalline Au to crystalline Co_3O_4. If we assume the amount of crystalline Co_3O_4 is constant in all of the samples (which is a reasonable assumption as all these were prepared from the same batch of Co_3O_4/SiO_2) then it is fair to conclude that the amount of Au present on these catalysts is increasing as the $pH_{initial}$ of the SEA solution is increased.

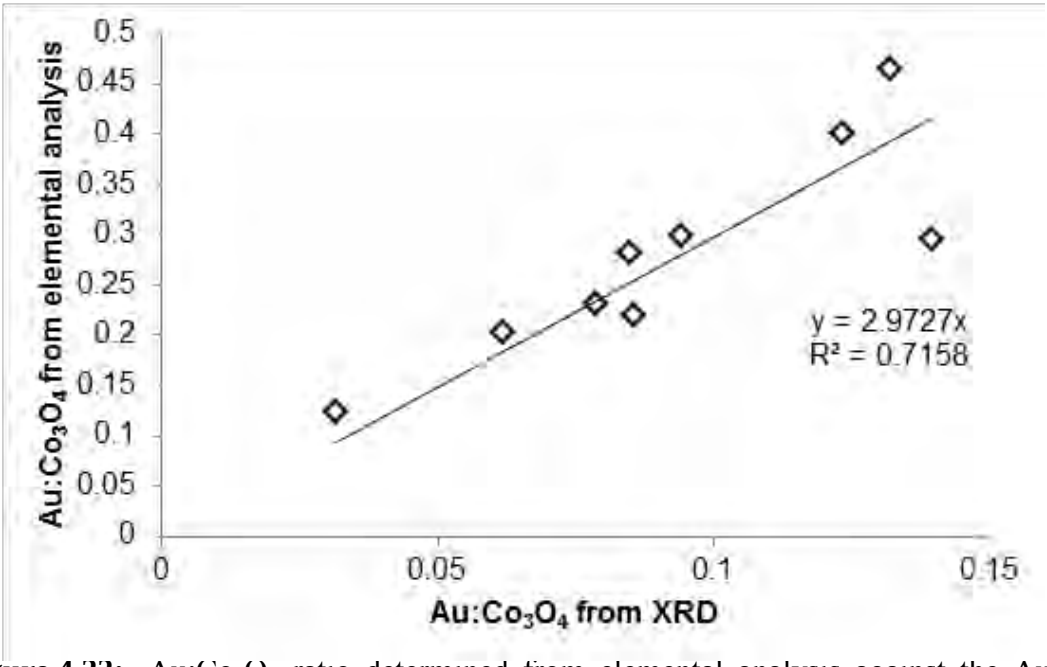

Figure 4.22: Au:Co_3O_4 ratio determined from elemental analysis against the Au:Co_3O_4 ratio observed by TOPAS refinement of the XRD spectrum

Temperature Programmed Reduction

The reduction behaviour of these Au promoted Co_3O_4/SiO_2 catalysts was investigated using TPR. The TPR curves for selected Au promoted catalysts are given in Figure 4.23.

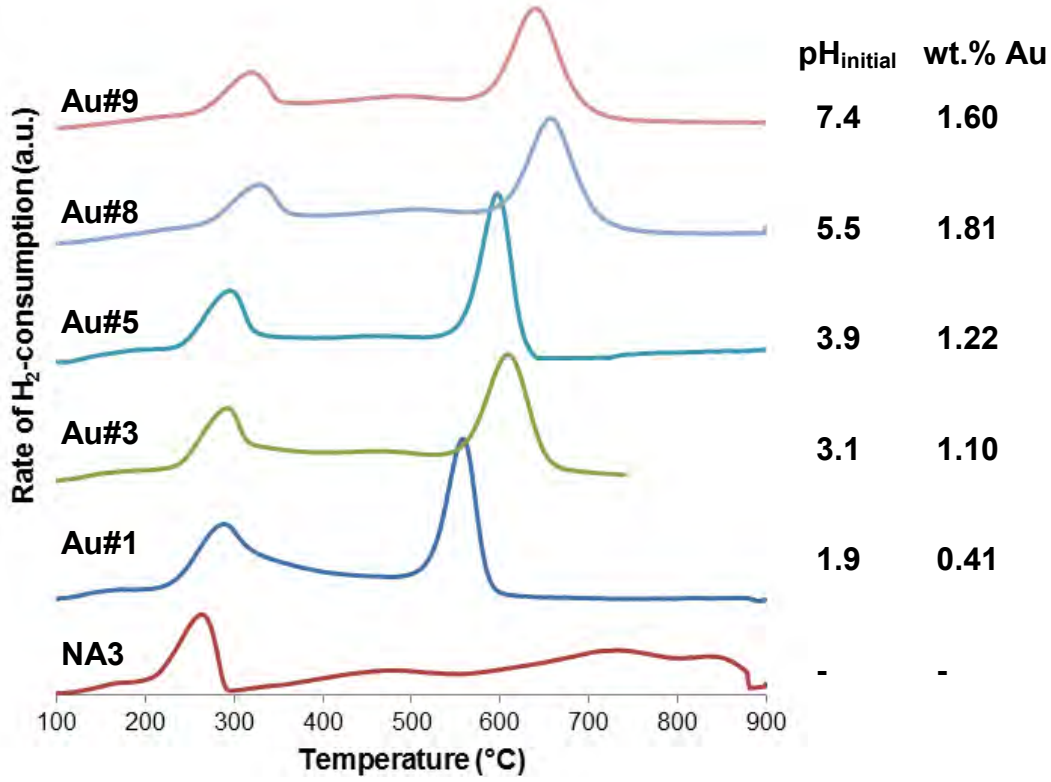

Figure 4.23: TPR profile of unpromoted Co_3O_4/SiO_2 (NA3) and Au-promoted catalysts prepared at a range of pH values

From the TPR profiles we can see that in all the catalysts promotion with gold causes the reduction temperature of the first peak to shift from 280°C to 295-300°C. The broad peaks in the unpromoted catalyst from 500 to 900°C are brought together to form a single peak. The temperature of this peak however appears to increase for the catalysts prepared at increasing pH. Jalama *et al.*[83] investigated the reducibility of Au promoted Co/TiO_2 catalysts and found that the reduction temperature of the first peak shifts slightly to higher temperatures. This was also observed by other authors for Au promoted Co/Al_2O_3 [6, 84]. Jalama *et al*. [83] suggest the promotional effect observed does not come as a result of H_2-spillover but instead as a result of the Au-Co contact.

Thermal Gravimetric Analysis

The degree of reduction (DOR) for the Au-promoted and unpromoted catalysts were determined using thermal gravimetric analysis.

The method used differed from that of the Pt. After reduction in H_2 for 12 hours the gold catalysts were then reoxidised. This was done by first switching to N_2 flow (for safety reasons) and then O_2. Upon changing the flow to N_2 the mass is seen to drop, this is as N_2 is much denser than H_2 and as such the sample will weigh less in a N_2 environment. When the O_2 flow is initiated the mass is seen to increase again. The density difference between O_2 and N_2 is assumed to be negligible in analysis.

A sample calculation is given in Appendix H.

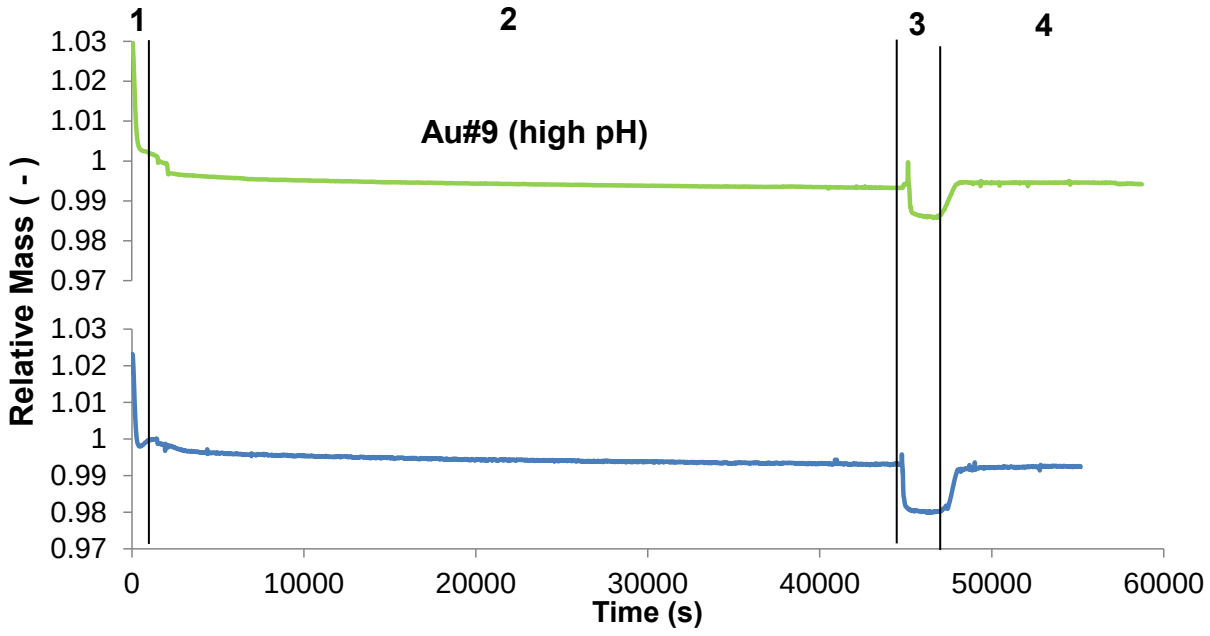

Figure 4.24: TGA profiles for reduction and reoxidation of Au-promoted Co_3O_4/SiO_2 catalysts. 1-Drying in flowing N_2, 2-Reduction in H_2, 3-Flow in N_2, 4-Re-oxidation in O_2

The degree of reductions obtained for the unpromoted and the Pt-promoted catalysts which were tested in the Fischer-Tropsch reaction are given in Table 4.9.

Table 4.9: Degree of reduction for Au-promoted catalysts determined from TGA analysis

Catalyst	Degree of Reduction (%)
NA3	47
Au#1 (low pH)	36
Au#9 (high pH)	26

The degree of reduction has decreased with the addition of Au to the Co_3O_4/SiO_2 solution. It has also decreased more significantly in the catalyst promoted at high pH. This result is surprising since it has been reported in literature that the degree of reduction increases with addition of Au. Jalama *et al*. [41] reported an increase in the degree of reduction from 20.1% to 42.7% with the addition of Au to Co/SiO_2. Jacobs *et al*. [6] reported increases in the degree of reduction from 49.8% to 58.8, 94.3 and 83.2% with the addition of 0.1, 1.5 and 5wt. % Au respectively to Co/Al_2O_3.

Hydrogen Chemisorption

Once again the effect of promotion with Au on the metallic surface area has been investigated by H_2-chemisorption. Note the chemisorption energy on the Au surface is very low [85] and as such the additional metallic surface area due solely to the presence of the added Au is ignored in this analysis. The addition of gold increases the surface area (albeit marginally) of the metallic Co^0 phase, compared with that of the unpromoted catalyst, for all catalysts except the one prepared at pH~7.4. It would appear that as the pH of the SEA solution increases the metallic Co^0 surface area decreases. Reasons for this will be discussed in detail in the discussion section of this report.

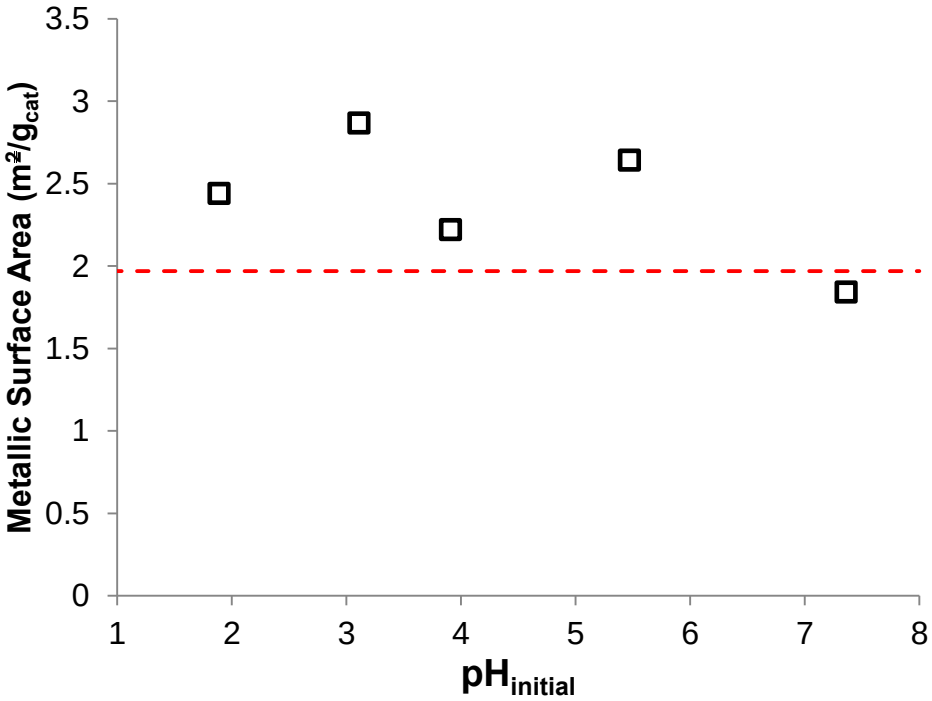

Figure 4.25: Metallic surface area (m^2/g_{cat}) determined from H_2-chemisorption measurements for Au-promoted Co_3O_4/SiO_2 prepared by SEA at different pH values. - - - Unpromoted Co_3O_4/SiO_2 catalyst

Transmission Electron Microscopy

TEM was done to gain insight into the effect of the addition of Au by SEA on the Co_3O_4 particle size as well to investigate the presence of Au crystallites on the surface. The TEM images are shown in Figure 4.26. These images show a large amount of grey material which can be attributed to the silica support which is comprised of small particles (the actual size of these particles is not of interest), the darker regions can be attributed to Co_3O_4 due to the higher density (and hence higher electron density) of Co_3O_4 relative to SiO_2 In certain images (e.g. Au#1b &Au#9a) there is the appearance of large dark particles with very well defined edges. These particles appear to have a higher density than that of Co_3O_4 and may be thus be agglomerated Au particles. A sufficient number of these particles could not be found to conduct a reasonable size analysis for these particles. The particle sizes of a number of Co_3O_4 particles for each sample were averaged and are shown in Table 4.10. From the data in Table 4.10 it can be concluded that the addition of Au to the Co_3O_4/SiO_2 system does not significantly affect the Co_3O_4 particle size.

Table 4.10: Co_3O_4 particle sizes determined from measurement of particles from TEM images

Catalyst	Co_3O_4 Particle Size (nm) {number of particles measured}
NA3	9.2±2.1 {79}
Au#1	9.5±2.6 {49}
Au#5	9.6±3 {71}
Au#9	9.9±2.2 {49}

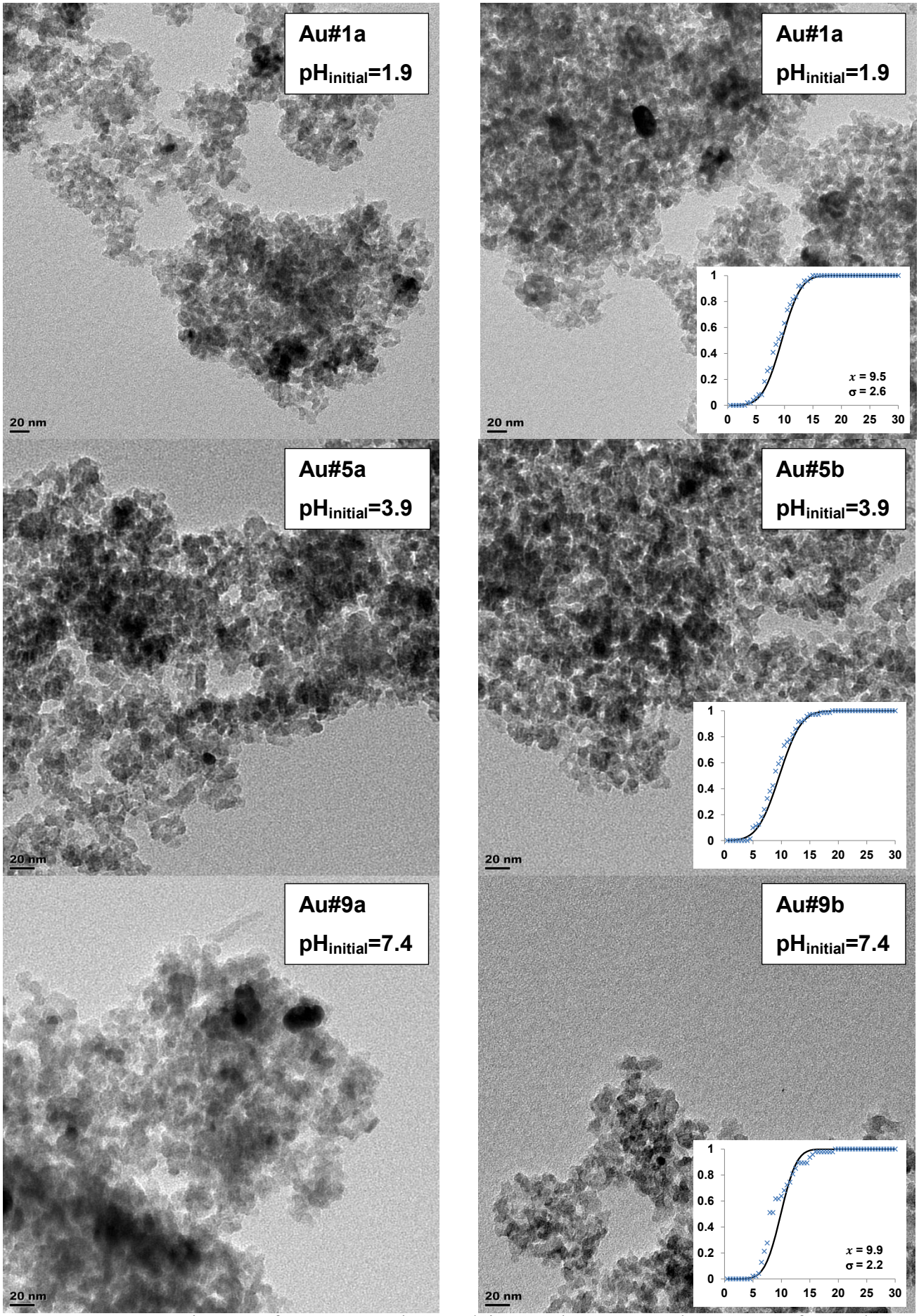

Figure 4.26: TEM images of Au-promoted Co_3O_4/SiO_2 catalysts prepared at a range of pH values

4.4 Catalyst Testing

4.4.1 Rates of CO-conversion for Promoted and Unpromoted Catalysts

The activity of selected catalysts (i.e. NA3, Pt#5, Pt9, Au#1 and Au#9) for the Fischer-Tropsch reaction was investigated. These catalysts were investigated as they are the extremes of the pH range used during SEA. The conversion profiles for these catalysts are given in Figure 4.27. The steady state CO-conversions achieved by these catalysts are summarised in Table 4.11.

The CO-conversion for the unpromoted catalyst was essentially constant at a conversion level of approximately 7.5% over the entire catalyst test. It was assumed that the promoted catalyst would have a much higher activity than the unpromoted catalyst and hence a higher steady state conversion. To avoid operating at significantly higher feed flowrates only half the mass (i.e. 0.5g) of the promoted catalysts were added to the reactor. In the Pt-promoted catalyst the conversion slowly decreases with time on stream. This deactivation, while interesting to note, is not central to this investigation. No significant deactivation is observed in the Au-promoted catalyst over the course of the catalyst test.

Upon promotion with platinum the steady state CO-conversion drastically increased. The catalyst promoted at the low pH having a higher increase in the CO-conversion than that of the one promoted at high pH.

The Au promoted catalyst prepared at low pH had a higher CO-conversion than the unpromoted however the catalyst promoted at high pH had a lower CO-conversion.

When testing the catalysts there is initially a very high conversion observed, this does not occur as a result of a high initial catalyst activity instead it occurs as a result of residual argon being flushed from the reactor. When this H_2/CO-free argon passes through the GC the TCD detects no H_2 or CO and as such will reflect as a 100% conversion. This conversion quickly drops as the system reaches steady state.

In order to compare the catalyst products it is desired to compare the catalysts at a low conversion level (X_{CO}<10%) to minimise the partial pressure of water in the catalyst bed (water has been previously shown to detrimentally affect CO-conversion and enhance deactivation in Pt-promoted Co/Al_2O_3 catalysts [38]) this was done by adjusting the feed gas flowrate (i.e. WHSV). This was only necessary for the Pt-promoted catalysts as the Au catalysts typically had a low conversion without adjusting.

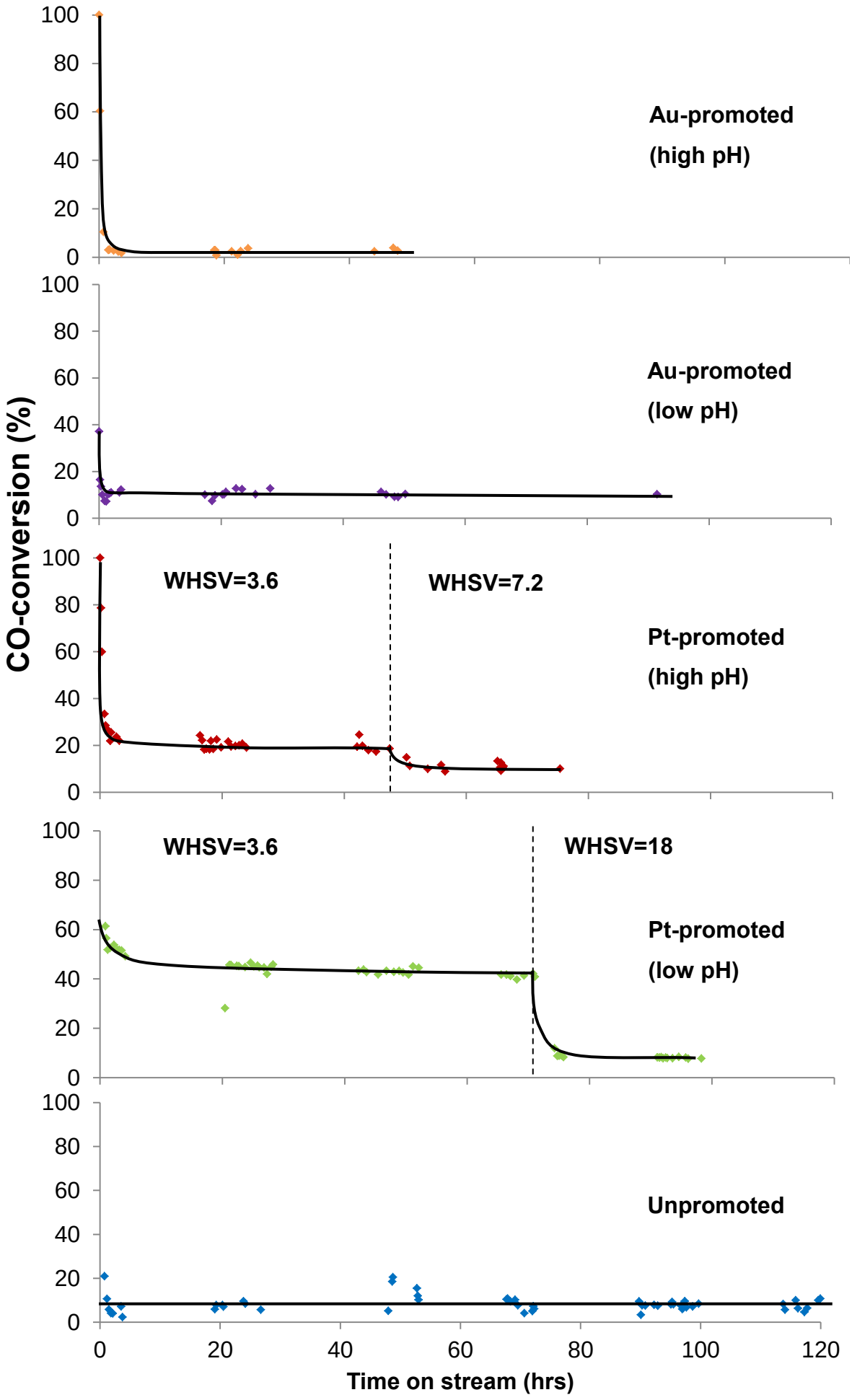

Figure 4.27: Co-conversion (%) as a function of time for the unpromoted Co_3O_4/SiO_2 catalyst and the Au/Pt promoted Co_3O_4/SiO_2 catalysts prepared by SEA at high and low pH. Tubular packed bed reactor, 220°C, 20bar , H_2/CO =2

Table 4.11: Results from Fischer-Tropsch tests in a tubular packed bed reactor, 220°C, 20bar and $H_2/CO=2$

Catalyst	WHSV ($Nml/g_{cat}.s$)	CO-conversion (%)*	$-r_{CO}$ ($\mu mol_{CO}/g_{CO}.s$)**	Cobalt-Time Yield ($\times 10^4\ s^{-1}$)***	TOF†
NA3	1.8	7.4±1.4	5.6	3.20	0.011
Pt#9 (low pH)	3.6	43.8±1.1	65	38.4	0.069
	18	8±0.24	60	35	0.063
Pt#5 (high pH)	3.6	20.3±1.8	30	17.8	0.022
	7.2	10.4±1.0	31	18.2	0.023
Au#1 (low pH)	3.6	10.8±1.6	16	9.64	0.026
Au#9 (high pH)	3.6	2.4±1.0	3.6	2.10	0.0077

*After 24hrs
**Packed bed reactor, 220°C, 20bar , H_2/CO =2
***Cobalt-time yield: moles of CO molecules converted per gram-atom of Co
† CO moleculesconverted/(mol H_{ads}.s)

From Table 4.11 it is can be seen that the both catalysts promoted with platinum have a much higher rate of CO-conversion (and hence a higher cobalt time yield). The turnover frequencies of the platinum promoted catalysts are also higher than that of the unpromoted catalyst. The catalysts promoted with platinum by SEA at low pH have a significantly higher rate of CO-conversion and turnover frequency than those promoted at high pH.

The gold promoted catalyst prepared at low pH shows an increase in the rate of CO-conversion as well as the turnover frequency. The gold promoted catalyst prepared at high pH has a decreased rate of CO-conversion and turnover frequency.

4.4.2 Selectivity for Fischer-Tropsch Products of Unpromoted and Promoted Catalysts

The selectivity of a catalyst is of utmost importance. The selectivity of the unpromoted and Pt/Au promoted catalysts were investigated using GC-FID with a cyclohexane standard. A typical chromatogram obtained is given in Appendix I. This analysis was done at low conversion (X_{CO}<10%) for all catalysts.

The chain growth probability gives a measure of the likelihood an adsorbed molecule will grow in length as opposed to desorbing as a reaction product (see Appendix). Thus a high chain growth probability is desirable as it will indicate the formation of more long chain hydrocarbons (and hence less methane). The chain growth probability is thus an important parameter to consider when analysing FT catalysts. The Anderson-Shultz-Flory (ASF) plots for each of the catalysts tested are given in Figure 4.28. It should be noted for that the catalysts which were less active i.e. NA3 and Au#1 (low pH) it was difficult to quantify product in the C_9+ range due to their low concentration in the product stream. The carbon species in the C_4-C_{12} range were considered when determining the chain growth probability. The results from this analysis are summarised in Table 4.12.

Table 4.12: Chain growth probabilities from GC-FID analysis

Catalyst	α
Au#9 (high pH)	0.63
Au#1 (low pH)	0.79
Pt#5 (high pH)	0.82
Pt#9 (low pH)	0.86
NA3	0.85

The promotion with Pt/Au in general resulted in a decrease in the chain growth probability with the exception of the Pt-promoted catalyst prepared at low pH (i.e. Pt#9) which showed a slight increase. The Au promoted catalysts had a significantly lower chain growth probability than the Pt promoted catalyst. Catalysts prepared at lower pH showed higher chain growth probabilities than those prepared at higher pH. Tsubaki *et al*. [44] reported chain growth probabilities of 0.83 and 0.75 for the Co/SiO_2 and $Pt\text{-}Co/SiO_2$ catalysts.

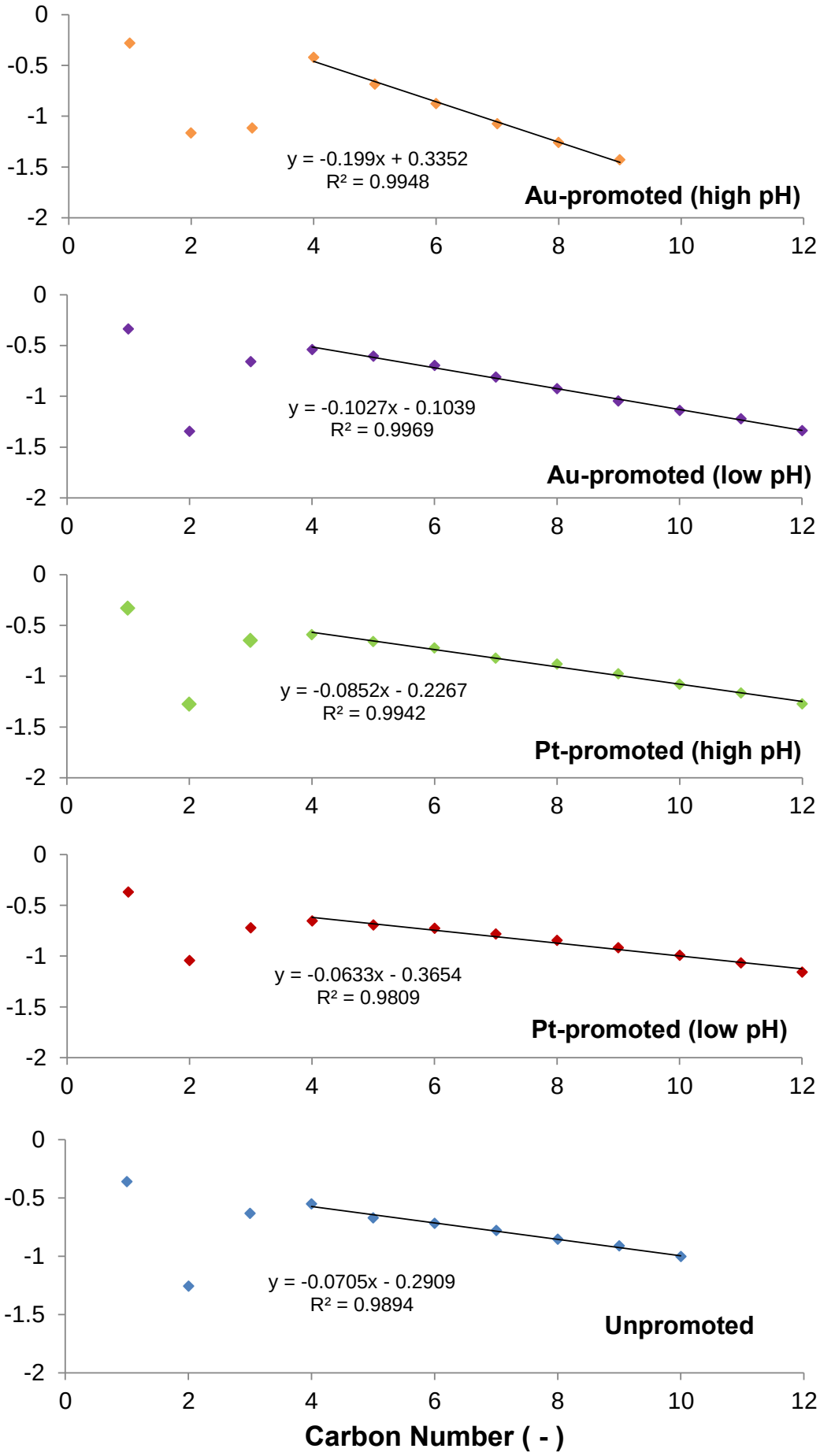

Figure 4.28: ASF plots for unpromoted and Au/Pt promoted Co_3O_4/SiO_2 catalysts determined from GC-FID analysis

The selectivity of the catalyst for olefin formation is also an important factor to consider. Figure 4.29 gives the olefin content as well as the 1-olefin content as a function of carbon number for all the catalysts tested. The 1-olefin content decreases with increasing carbon number for all catalyst. This comes as a result of a higher paraffin content i.e. decreasing olefin to paraffin ratio with increasing carbon number. The gap between the olefin and the 1-olefin content increases with increasing carbon number which means the fraction of cis- and trans- 2-olefins increases with increasing carbon number. It was only possible to determine the olefin content accurately up to the C_9 olefins since the trans-2-olefin joins with the paraffin peak (see Appendix I).

It is interesting to note that the addition of Pt to the catalyst results in an increase in the ethene content. It appears that the promotion of the Co_3O_4/SiO_2 (with the exception of Au at high pH) causes the formation of higher fractions of olefins at higher carbon numbers.

Upon close inspection the olefin to paraffin ratio for the Pt-promoted catalyst can be seen to increase for the C_2 species but decrease slightly for the carbon numbers higher than 2.

The formation of methane in the Fischer-Tropsch synthesis is undesirable and hence the methane selectivity needs to be considered. The fraction of methane in the volatile organic compounds (VOC) gives an indication of the methane selectivity of the catalyst. These are calculated from the GC-FID chromatograms and shown in Table 4.13.

Table 4.13: Hydrocarbon selectivity for unpromoted and Pt/Au promoted catalysts

Catalyst	CH_4 in VOC* (%)	EtOH in VOC* (%)
Au#9 (high pH)	28.8	2.9
Au#1 (low pH)	27.2	0.84
Pt#5 (high pH)	27.2	1.4
Pt#9 (low pH)	24.9	0.91
NA3	25.8	1.23

*VOC – Volatile organic compounds, these are the compounds which are present in the vapour phase at below 200°C and are detected by the GC-FID.

The CH_4 in VOC is observed to increase in all the promoted catalysts with the exception of the Pt-promoted catalyst prepared at low pH. Thus the promoted catalysts have in general higher methane selectivity than the unpromoted catalysts. Since the methane selectivity is related to the chain growth

probability one would expect these results to mirror the results obtained for the chain growth probabilities. This is what is observed (see Table 4.12).
The promotion with either platinum or gold can be seen to have an effect on the amount of ethanol in the VOC and hence the ethanol selectivity. Interestingly the catalysts prepared at low pH (either Pt/ Au) have a lower selectivity to ethanol and the catalysts promoted at high pH having a higher ethanol selectivity than the unpromoted catalyst.

Note that it was desirable to test these catalysts at a low of CO-conversion level (~10%) to reduce the effect of water formed during reaction on the product distribution. Low activity in the Au-promoted catalyst prepared at high pH made it difficult to achieve this level of conversion. The conversion level could not be practically increased within the operating limits of the equipment (it could also not be increased with the use of a higher mass of catalyst due to the mass prepared initially).

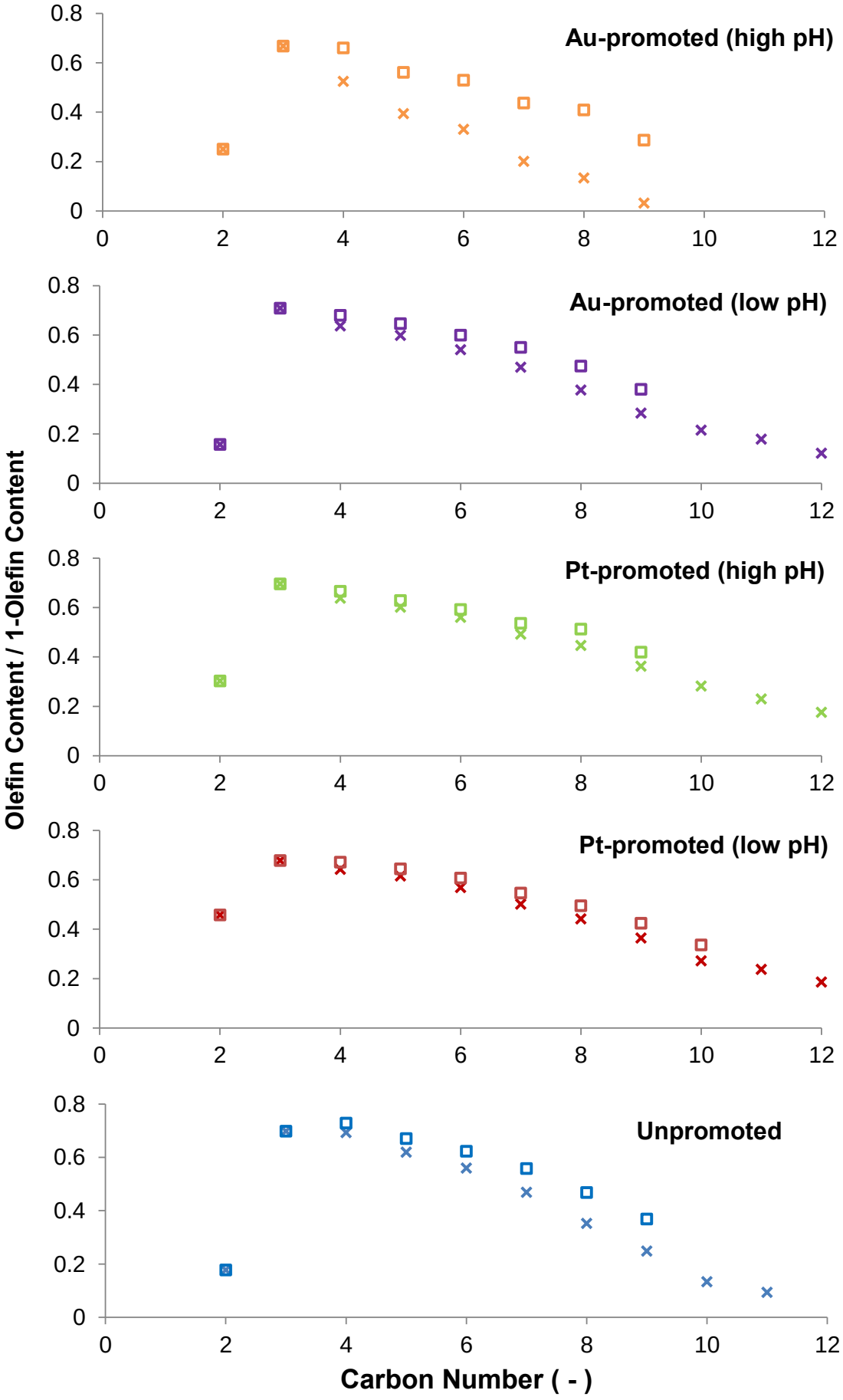

Figure 4.29: Olefin content and 1-Olefin content as a function of carbon number from GC-FID analysis. × - 1-Olefin content □-Olefin content

5. Discussion

5.1 Co/SiO_2 Prepared by Wet Impregnation from $Co(NO_3)_2$ / $Co(Ac)_2$ Mixtures

From XRD and TPR we can see that increasing the fraction of cobalt acetate in catalysts prepared by wet impregnation with mixed cobalt acetate and cobalt nitrate precursors results in catalysts with smaller Co_3O_4 crystallites and increasing amounts of hardly-reducible strongly-interacting cobalt species. Small crystallites will result in a higher surface area per gram but this is outweighed by the increasing amount of hardly reducible species. From H_2-chemisorption we see that the net effect, however, is that the metallic surface area of the catalysts decreases with increasing amounts of acetate.

Based solely on the H_2-chemisorption results it would be desirable to use a pure cobalt nitrate solution in the preparation of cobalt Fischer-Tropsch catalysts. However since small crystallites are desirable it would be justifiable to include some cobalt acetate in the impregnation solution. This comes at the cost of introducing cobalt species (cobalt silicates) which will not reduce to metallic cobalt (although it has been shown that some cobalt silicates are necessary to create highly dispersed Co_3O_4 crystallites [86]). The effect of addition of a reduction promoter (i.e. a noble metal) to catalysts with a significant amount of hardly-reducible species has not been investigated significantly in open literature. It is possible that the addition of a noble metal will enhance the reduction of these species and result in a catalyst with small particles and a high reducibility. It was therefore decided to include a small fraction of acetate (i.e. 0.3) in the impregnation solution of the catalysts to be promoted in the next section of this investigation.

5.2 Pt/Au Adsorption by Co_3O_4/SiO_2

5.2.1 Pt Adsorption

In the strong electrostatic adsorption model (SEA) [87] it is assumed that the adsorption of $PtCl_6^{2-}$ (and its derivative species) is considered to be purely electrostatic in nature. It is justifiable to assume that adsorption will only happen on the $–OH_2^+$ surface sites.

Experimentally it has been observed that pure silica has almost no attraction for $PtCl_6^{2-}$ [51]. Thus considering only the Co_3O_4 sites we can plot, qualitatively, the amount of $–OH_2^+$ sites present on the surface using the following equations (derived in Appendix C):

$$f_{-OH\cdot} = \frac{1}{\left(K_1[H^+] + \frac{K_2}{[H^+]} + 1\right)}$$

$$f_{-OH_2^+} = K_1 . f_{-OH\cdot} . [H^+]$$

$$[H^+] = 10^{-pH}$$

If the Pt complexes are adsorbing predominantly on the $–OH_2^+$ sites this should give an indication of the adsorption capacity of the surface.

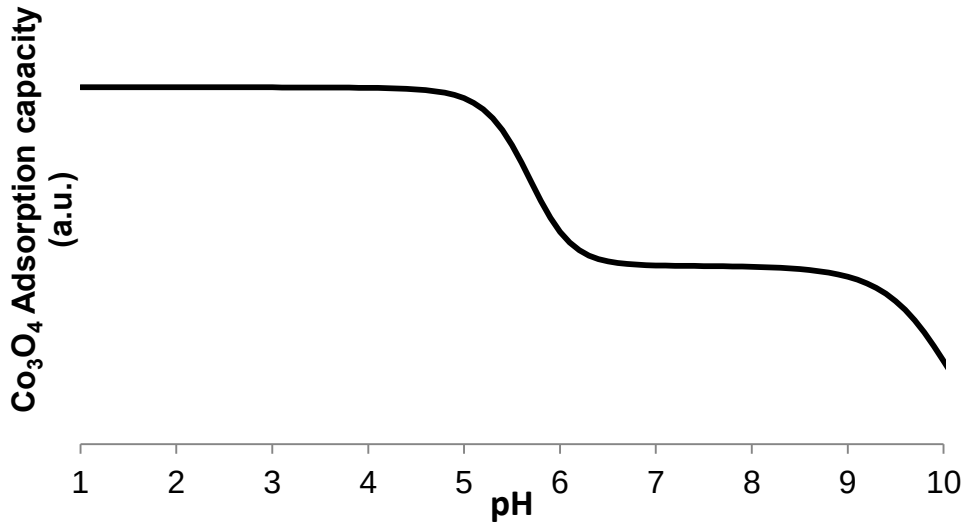

Figure 5.1: Theoretical adsorption capacity for Co_3O_4 surface determined from surface equilibrium relationships

From this plot there is some justification that a higher adsorption of $PtCl_6^{2-}$ will occur at lower pH values. This is what was observed in the Pt-uptake as a function of pH (see Figure 4.10 right) where the platinum uptake is initially high but suddenly drops to a lower value above a pH of approximately 5. This, however, is a cautious statement as the other mechanisms of adsorption of

these species are not taken into account. The adsorption system in question is rather complex. The $PtCl_6^{2-}$ species formed by aquation and hydrolysis may have different adsorption characteristics to the $PtCl_6^{2-}$ species considered here as well as different concentrations across the pH range. Additionally, preferential adsorption of certain species will shift the speciation equilibrium to replace the adsorbed species in the aqueous phase. The effect of the slight variation in the ionic strength caused by addition of acid or base is uncertain at this point. Although it does not affect the value of the IEP it does affect the magnitude of the ζ-potential and will hence affect the strength of adsorption.

5.2.2 $AuCl_4^-$ Adsorption

From Figure 4.20 the adsorption of $AuCl_4^-$ increases as the starting pH of the adsorption increases. In order explain this phenomenon it is required that we first re-evaluate the mechanism of adsorption as well as the gold speciation in solution.

It is proposed that adsorption of certain hydroxychloro gold species is not purely electrostatic and that the predominant mechanism for adsorption is the reaction of gold species with the –OH groups on the surface to form a covalently bonded surface species [65]. Since in this pH range the SiO_2 surface contains the vast majority of –OH sites as a result of the 90 wt.% SiO_2 as well as the shape of the ζ-potential curve (Figure 4.1) we will consider that adsorption only occurs on these sites in our analysis. The surface –OH groups for the silica are calculated from the constants obtained in the ζ-potential analysis of the SiO_2 and Co_3O_4 (see Table 4.1) using the following equations:

$$f_{-OH\cdot} = \frac{1}{\left(K_1[H^+] + \frac{K_2}{[H^+]} + 1\right)}$$

$$[H^+] = 10^{-pH}$$

Figure 5.2 (left) shows the fraction of SiO_2 surface groups which are present as –OH. The amount of strongly adsorbing gold species ($AuCl_2OH_2^-$ and $AuClOH_3^-$) is known to increase as the pH increases [61, 63, 64]. In order to demonstrate this trend this is represented very simply as a straight line (Figure 5.2 (centre)). Note it is understood this will most likely not be a straight line this is strictly for demonstrative purposes.

It is then assumed that the adsorption is some function which depends on the fraction of sites and the fraction of strongly adsorption species i.e. $Ads = f_{-OH} \times f_{adsorbing\ species}$

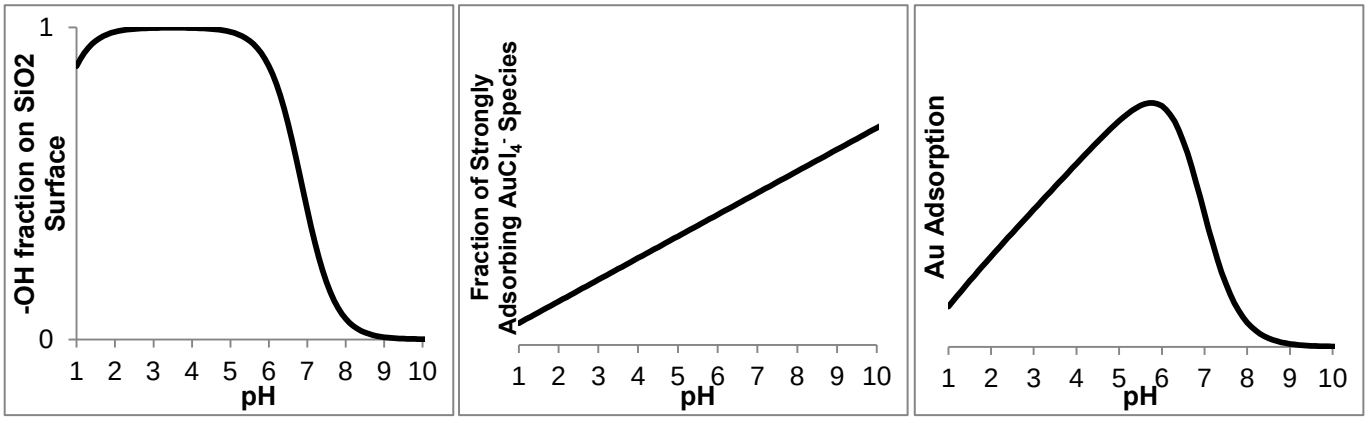

Figure 5.2: Plot illustrating the fraction of –OH groups on the silica surface (left) and the amount of strongly adsorbing gold species present in the aqueous phase (center) and the theorised Au adsorption capacity (right) as a function of pH

From Figure 5.2 it can be seen that while the fraction of available sites for adsorption remains approximately constant in the pH range 1 – 6 the amount of strongly adsorbing gold species increases. This offers a possible explanation for the observed increase in gold adsorption with increasing pH as shown in Figure 4.20. Note that this explanation does not take into account the adsorption which occurs on the Co_3O_4 –OH sites as well as the electrostatic adsorption which may (and most likely will) be taking place.

It is important to note that the PZC of the Co_3O_4 phase present in the Co_3O_4/SiO_2 system may have a different value than that of pure Co_3O_4 as a result of electronic interaction with SiO_2. Hao *et al*. [51] were able to vary the PZC of silica (from 4 to a value as high as 8.8) by doping with potassium. Similarly introducing Co_3O_4 onto the SiO_2 surface we may have inadvertently altered the local PZC of certain SiO_2 sites (i.e. those closely associated with Co_3O_4). On a macroscopic scale this may propagate into an observable difference in the PZC for the SiO_2 (and Co_3O_4 as well).

The role of sodium (from the NaOH used to basify the solution) cannot be ignored. It may be fair however to assume this role to be negligible. The reason for this is that the quantity added to basify the solution was typically less than 2ml of 0.1M which will result in a maximum Na loading of 0.3% if all sodium goes onto the surface.

5.3 Pt/Au Promotion of Co_3O_4/SiO_2

5.3.1 Pt-promoted Co_3O_4/SiO_2: Characterisation and Reaction Testing

Promotion of the Co_3O_4/SiO_2 catalyst with Pt by SEA resulted in Pt particles on the surface of the catalyst which could not be detected by XRD (Figure 4.11), indicating the presence of small platinum Pt crystallites or crystalline domains. The TEM images (Figure 4.17) also indicate the possibility of very small Pt particles. The Co_3O_4 particle size determined from XRD analysis seemed to be affected by the promotion with Pt at higher pH values (i.e. pH>5) however this could not be confirmed by analysis of Co_3O_4 particles in the TEM images.

From TPR we can see these Pt-particles facilitate the reduction of Co_3O_4 at lower temperature, which results in an enhanced degree of reduction observed in thermal gravimetric analysis measurements. This occurs with a decrease in the activation energy of the first reduction peak (from 192 kJ/mol in the unpromoted to 114 kJ/mol in the promoted) which implies a different pathway for reduction. This could possibly be evidence of H_2-spillover. It seems the presence of Pt enables the reduction of the hardly reducible cobalt species (tentatively attributed to cobalt silicates). The increase in the degree of reduction observed in the TGA experiments on these catalysts is most likely due to the enabling of the reduction of these species.

The effect of decreasing the pH of promotion resulted in a low temperature peak in the TPR profile (T_{max}=120°C) which increased in size as the pH decreased. Due to the low Pt-loading (i.e. Co/Pt = 25) this peak cannot be ascribed to the reduction of a platinum species (e.g. PtO_2) in addition to this no peaks were observed in the catalysts prepared at higher pH which would also contain PtO_2 if this were the case. When one considers that the catalysts prepared at $pH_{initial}$ <5 have essentially constant loading of Pt (Figure 4.10 (left)) it is reasonable to state that the change in magnitude of this peak is not as a result of a Pt-loading effect. If this peak occurs as a result of some direct Pt-Co interaction (which results in a cobalt species which reduces at a much lower temperature) then the presence of higher amounts of this species at low pH indicate there to be some directing effect on the surface chemistry by the pH during promotion.

From H_2-chemisorption it could be seen that the addition of Pt resulted an increase in the metallic Co^0 surface area after reduction. Since the catalysts prepared at higher pH values had, in general, slightly higher metal surface areas than those prepared at lower pH values it would be expected that the catalyst prepared at higher pH would have a higher mass specific activity than those prepared at low pH. However, upon reaction testing of these catalysts it was observed that the catalyst prepared

at the lowest pH in fact had a much higher conversion and rate of CO-conversion under the same conditions. As the activity generally follows the same trend as the active surface area this result was unexpected. This may be tentatively ascribed to the presence of some highly active Pt-Co bimetallic clusters which are present in the reduced catalyst (possibly the cause of the low temperature peak observed in the TPR profiles).

The literature available for Pt-promoted Co/SiO_2 Fischer-Tropsch catalysts is very limited and literature which is available has not been conducted under the same conditions as the present study. As such the empirical rate expression proposed by Yates & Satterfield [88]was used to adjust for the different conditions used in literature:

$$-R_{CO} = \frac{aP_{CO}P_{H_2}}{(1+bP_{CO})^2}$$

Where $-R_{CO}$ is the rate of carbon monoxide conversion in mmol/(min.g_{cat}), a and b are temperature dependent constants with units mmol/(min.g_{cat}.MPa^2) and 1/MPa respectively. P_{CO} and P_{H_2} are the partial pressure of CO and H_2 respectively in MPa.

Using this method the turnover frequency and cobalt-time yield reported by Schanke *et al* [37] and Tsubaki *et al*. [44] were adjusted for differences in the temperature, pressure and partial pressures of H_2 and CO (i.e. H_2/CO ratio) for comparison with the results obtained in the present study. It is important to remember that this approach assumes that the same rate law applies for all catalysts (i.e. promoted and unpromoted catalysts) and that this rate law is applicable across the conditions of operation. Table 5.1 compares the results in the present study with those values found in literature.

Table 5.1: Reaction performance of current and literature catalysts

Catalyst		Turnover Frequency (TOF)*		Cobalt-time Yield (CTY) ($\times 10^4$)**	
		Current Study	Schanke *et al*.	Current Study	Tsubaki *et al*.
10%Co/SiO_2		0.011	0.043 (0.0063)†	3.20	1.00 (1.86)‡
Pt-10%Co/SiO_2	Low pH	0.069	0.095 (0.0140) †	38.4	1.49 (2.75)‡
	High pH	0.022		17.8	

*TOF: moles CO converted per moles surface Co atoms per second
**Cobalt time-yield: moles of CO converted per moles Co per second
†Values in parentheses show original result at 210°C, 1bar, H_2/CO=7.3, 44% inert (Ar), 10-20% CO conversion
‡ Values in parentheses show original result at 240°C, 10bar, CO/H_2=1/2, W/F=5g_{cat}.h.mol^{-1}

The catalysts prepared in this study seem to perform very poorly compared with those of Schanke *et al*. [37] in terms of turnover however the magnitude of the TOFs obtained by Schanke *et al*. [37]

these values suspiciously high. This may be as a result of a scaling error or an error in reporting the value by Schanke *et al*. [37]. Note that it was impossible to re-calculate the TOFs provided by Schanke *et al*. [37] due to poor reporting of the catalyst testing method.
The work by Tsubaki *et al*. [44] reported their results as a cobalt-time yield (which can be calculated as follows: $CTY = TOF \times Dispersion$). Both the unpromoted and promoted catalysts prepared by Tsubaki *et al*. [44] have a much lower site time yield than those prepared in the current study.
The increases in the turnover frequency and cobalt time yield reported in literature by Schanke *et al*. [37] and Tsubaki *et al*. [44] are similar in magnitude to the increase observed in the Pt-promoted catalyst prepared at high pH in the current study. However a significantly larger increase i.e. a six fold increase was observed in the catalyst prepared at low pH.

The Pt-promoted catalysts showed differing effects on the chain growth probability and methane selectivity depending on the pH of promotion. The catalyst promoted at low pH had a similar chain growth probability to the unpromoted catalyst and hence a similar methane selectivity. The catalyst promoted at high pH showed a lower chain growth probability as well as higher methane selectivity.
The Pt-promoted catalysts had a lower olefin to paraffin ratio for all carbon numbers except C_2 than their unpromoted counterpart. There is little reported literature on the olefin-paraffin ratio for the Co/SiO_2 and Pt-promoted Co/SiO_2 system. Ma *et al*. [3] studied the selectivity of $25\%Co/Al_2O_3$ when promoted with Pt, they observed a decrease in the olefin to paraffin ratio however this was found to be dependent on the time on stream.
Higher methane selectivity and lower olefin to paraffin ratio is indicative of higher hydrogenation activity in these catalysts. Assuming H_2-spillover on these catalysts is significant, which by the lowering of the activation energy of the reduction peaks appears to be the case, it is possible that the presence of Pt causes a higher amount of dissociated hydrogen to be present on the catalyst surface. This larger presence of dissociated hydrogen would favour the desorption of the growing chains as saturated hydrocarbons i.e. paraffins and methane.

The ethanol selectivity on the promoted catalysts appears to be some function of the pH. The catalysts promoted at low pH had lower ethanol selectivity whereas those promoted at high pH had higher ethanol selectivity. Ma *et al*. [3] observed an increase in the oxygenate selectivity in Pt-Co/Al_2O_3 over unpromoted Co/Al_2O_3.

5.3.2 Au-promoted Co_3O_4/SiO_2: Characterisation and Reaction Testing

Promotion of the Co_3O_4/SiO_2 catalyst with Au by strong electrostatic adsorption (SEA) in the pH range 2-8 resulted in catalysts with very large XRD visible gold crystallites (in the size range 10-30nm). It is very unlikely that crystallites of this size are formed at the adsorption stage of the preparation of these catalysts. The gold crystallites are most probably formed as a result of sintering during the calcination step. The addition of Au to the Co_3O_4/SiO_2 had no detectable effect on the average Co_3O_4 crystallite size measured by XRD or TEM over the entire pH range.

The TPR profiles show the presence of Au has some effect on the reduction process in these catalysts with the broad reduction peak of the hardly reducible cobalt species being condensed into a single peak at around 500-700°C and the low temperature reduction peak in fact shifting to slightly higher temperatures. While the temperature of the first reduction peak was essentially constant across the entire pH preparation range the temperature of the second peak shifted to higher temperatures as the pH of promotion increased. It seems unlikely that this effect of gold on the reduction behaviour of Co_3O_4/SiO_2 will translate to a higher degree of reduction in an isothermal reduction at 350°C. From TGA analysis it was found that indeed lower degrees of reduction were achieved on the Au-promoted catalysts with the catalyst prepared at high pH having a lower degree of reduction than that prepared at low pH.

The H_2-chemisorption of these catalysts showed only slight increase in the metallic surface area in the catalysts prepared at low pH and a decrease in the catalyst prepared at the highest pH. The increase in the metallic surface area observed at low pH is difficult to explain in light of the lower degree of reduction observed in these catalysts. The lower metallic surface area at high pH may be due to the lower reducibility observed in these catalysts or as a result of Au effectively blocking the Co and as Au does not adsorb H_2 this will result in a reduction of surface area. Note that adsorption of Au onto the Co_3O_4 is possible at higher pH values due to a higher presence of –OH groups on the Co_3O_4 surface at high pH.

The reaction performance of the Au-promoted catalyst is interesting however since the catalyst promoted at low pH experiences an increase in the TOF whereas the catalyst promoted at high pH shows a decrease. Jalama *et al.*[83] observed an increase in the CO-conversion and rate of CO-conversion when promoting Co/SiO_2 with Au for loadings up to 5 wt. %. In previous studies by Jalama *et al*. [42] and Jacobs *et al*. [6] showed in promoted Co/TiO_2 and Co/Al_2O_3 that the addition of small amounts Au to these catalysts had a beneficial effect on the conversion but the addition of

high amounts of Au (typically around 5wt. %) had a detrimental effect. Jacobs *et al*. [6] attributed this decrease to site blocking by the Au particles.

The rate of CO-conversion for the Au-promoted catalysts in the present study are compared to those obtained by Jalama *et al* [41]. It is necessary to compare the rate data as turnover frequencies for the catalysts prepared by Jalama *et al*. [41] could not be calculated. These are shown in Table 5.2.

Table 5.2: Comparison of CO-conversion rate for catalysts tested in current study with those reported by Jalama *et al*. [41]

Catalyst	CO-conversion rate ($\mu mol_{CO}/(g_{cat}.s)$)	
	Current Study	Jalama *et al*. [41]
10%Co/SiO_2 (NA3)	0.54	0.18
0.5%Au/10%Co/SiO_2 (Au#1)*	1.64	0.49
1% Au/10%Co/SiO_2	-	0.60
1.5%Au/10%Co/SiO_2 (Au#9)*	0.54	0.65
2%Au/10%Co/SiO_2	-	0.66
5%Au/10%Co/SiO_2	-	0.68

* From ICP Au#1 has 0.41wt. %Au and Au#9 has 1.60wt. %Au

The CO-conversion rate for the unpromoted Co/SiO_2 and Au-promoted catalyst prepared at low pH, which resulted in a low loading, are much higher than the catalysts prepared by Jalama *et al*. [41], however the CO-conversion rate for the catalysts prepared at high pH, which had a higher loading, was much lower than observed by Jalama *et al*. [41]. Jalama *et al*. [41] also did not observe any drop in the CO-conversion rate at higher loadings of Au.

The Au-promoted catalysts showed lower chain growth probability than the unpromoted catalyst with the Au-promoted catalyst promoted at high pH demonstrating a significantly lower chain growth probability than the catalyst promoted at low pH. An increase in the CH_4-selectivity was also observed in the Au-promoted catalyst this would be expected considering the lower chain growth probabilities.

In the Au-promoted catalysts decreases in the chain growth probability and subsequently higher methane selectivities were observed when compared with the unpromoted Co/SiO_2. The Au-promoted catalyst prepared at high pH has a significantly lower chain growth probability and higher

methane selectivity than the catalyst prepared at low pH. It is known that the methane selectivity increases with a decreasing CO-conversion [34]. As the catalyst promoted at high pH has a very low steady state conversion it is difficult to conclude whether the elevated methane selectivity observed occurs as a result of a promotional effect or simply as a result of the lower conversion achieved by this catalyst.

In addition to the increased methane selectivity the Au-promoted catalysts showed slightly lower olefin to paraffin ratios for the C_{2-5} range. The FT reaction results obtained by Jalama *et al*. [41]or the comparable Au promoted catalysts are shown in Table 5.3. In contrast to the Pt-promoted catalyst an increase in the amount of dissociated hydrogen present on the surface of the catalyst is unlikely as gold is known to have a very low chemisorption energy [85]. The observed decrease in the olefin to paraffin ratio is therefore more difficult to explain.

Table 5.3: FT reaction performance of Au promoted and unpromoted Co/SiO_2 in the current study and that reported by Jalama *et al*. [41]

Catalyst	CO conv. (%)	CH_4-selectivity (%)*	EtOH selectivity (%)	Olefin to Paraffin Ratio			
				C_2	C_3	C_4	C_5
Unpromoted Co/SiO_2	7.8	1.5	0.05	0.34	2.8	2.9	2.1
Au-Co/SiO_2 (low pH)	10.8	3.8	0.71	0.27	2.9	2.3	2.0
Au-Co/SiO_2 (high pH)	2.4	3.5	0.28	0.59	2.5	2.4	1.5
Co/SiO_2	1.6	7.8	-	0.63	0.76	0.88	0.49
0.5%Au-Co/SiO_2	4.4	17.2	1.1	0.4	2.76	1.30	0.54
1.5%Au-Co/SiO_2	5.8	16.3	1.2	0.13	1.89	0.73	0.28

*Based on moles CO converted

It is difficult to compare the selectivities obtained in the current study with those obtained by Jalama *et al*. [41] as these catalysts were tested at varying CO-conversions. Jalama *et al*. [41] reported a decrease in the C_2 and increases in the C_3-C_5 olefin to paraffin ratio for the Au promoted catalyst with 0.5%Au. The catalyst with higher Au loading (i.e. 1.5% Au) only showed an increase in the C_2 olefin to paraffin ratio.

Jalama *et al*. [41] ascribed the changes in the product selectivity to two factors: (i) increase in the water-gas shift activity of the catalyst upon addition of gold, and (ii) modification of some surface Co sites by the presence of Au. We, however, did not observe any significant WGS as no CO_2 was observed during analysis.

6. Conclusions

The ζ-potential as a function of pH for Co_3O_4 and SiO_2 was successfully determined and hence the PZC of these oxides found i.e. 3.5 for SiO_2 and 9.6 for Co_3O_4 which were in good agreement with literature. A semi empirical model was developed from a thermodynamic understanding of the metal oxide surface chemistry when in contact with an aqueous media. It was postulated that there exists two distinct cobalt adsorbing sites on the Co_3O_4 surface. This was justified by the presence of surface oxides bonded to Co^{2+} and Co^{3+} sites.

The effect of preparing Co/SiO_2 Fischer-Tropsch catalysts from wet impregnation with mixtures of cobalt nitrate and cobalt acetate was investigated. It was found that the use of higher fractions of acetate in the impregnating mixture resulted in smaller Co_3O_4 crystallites but a higher amount of irreducible cobalt species which would result in a lower reducibility. It was observed from H_2-chemisorption that the resulting effect of these two competing factors is that catalysts prepared with a higher acetate fraction have lower metallic Co^0 surface area per gram after isothermal reduction at 350°C. Thus cobalt catalysts prepared from cobalt nitrate should result in the most active Fischer-Tropsch catalyst when no noble metal promoter is added.

It was found that $PtCl_6^{2-}$ will readily adsorb onto Co_3O_4/SiO_2 at all pH values with a higher adsorption (and hence higher loading) observed in the lower pH range. The Pt-promoted catalysts showed no presence of Pt in XRD due to the very small size of the Pt particles. The addition of Pt caused a lowering in the temperature of reduction for the entire Co_3O_4 reduction process. It seems that the reduction of hardly reducible cobalt species are facilitated by Pt but no mechanism of this process can be suggested from this work. These effects resulted in a higher degree of reduction in the platinum-promoted catalyst. The Pt-promoted catalysts had a higher metallic surface area than the unpromoted catalyst, with higher metallic surface area being observed on the catalysts prepared at higher pH. The FT activity of the promoted catalysts was drastically improved. This was contradictory to the Fischer-Tropsch activity observed on these catalysts where the catalysts prepared at lower pH showed significantly higher FT activity. This was possibly due to a Pt-Co phase which is highly active for FT being formed at low pH. Higher methane selectivity was observed in the promoted catalyst as well as a decrease in the olefin to paraffin ratio. This was attributed to a higher surface hydrogen concentration causing an increase in the hydrogenation activity of these catalysts.

The adsorption of $AuCl_4^-$ by Co_3O_4/SiO_2 was found to increase with increasing pH. This was opposite to what was observed in the $PtCl_6^{2-}$ adsorption system. The reason for this was a difference in the adsorption mechanism. The resulting gold particles present on the promoted catalysts were very large and the reason for this was most probably as a result of the calcination conditions. The addition of gold caused an increase in the reduction temperature for the first reduction peak (Co_3O_4 to CoO) and seemed to facilitate the reduction of the hardly reducible cobalt species however only at a much higher temperature. This didn't translate to an increase in the degree of reduction in the promoted catalyst. Higher degrees of reduction were observed in the catalysts prepared at low pH than that at high pH, but these were both not higher than the unpromoted catalyst. The Co^0 metallic cobalt surface area was found to decrease with increasing pH with the surface area of the catalyst promoted at the highest pH having a metallic surface area lower than the unpromoted. The activity of the gold-promoted catalysts was a mixed bag with those promoted at low pH showing an increase in the activity whereas those promoted at high pH had lower activity. It is unclear whether this is strictly a gold loading effect or in combination with a positional effect. These promoted catalysts also showed higher methane selectivity, lower chain growth probability and also a higher selectivity for ethanol than the unpromoted catalyst.

7. Recommendations for Future Work

- The ζ-potential determined in this study was for isolated Co_3O_4 and SiO_2. Since a chemical mixture of Co_3O_4 and SiO_2 is used in the adsorption experiments it is possible that the point of zero charge of one or both phases has changed. I would recommend looking at the PZC evolution as a function of pH of the calcined Co_3O_4/SiO_2.
- The observation that the reduction of these hardly reducible cobalt species appears to be facilitated when promoted with Pt is quite interesting. It is therefore possible that catalysts prepared with higher fractions of cobalt acetate (and hence have a higher amounts of cobalt silicates but smaller Co_3O_4 particles) and promoted with Pt may in fact have very high activity for the FT reaction.
- A fundamental understanding of the adsorption system could not be gained in this investigation due to the presence of an inseparable Co_3O_4 and SiO_2 phase. To gain a better understanding an investigation needs to be done where Co_3O_4 and SiO_2 are physically separated (possibly Co_3O_4 and SiO_2 on opposite sides of double sided tape or separated by a fine wire mesh) and exposed to similar adsorption conditions as were used in this experiment. Separate analysis of the amount of Au / Pt on the SiO_2 or Co_3O_4 phase will give insight into the adsorption selectivity for these ions and give insight into position of these ions in the mixed Co_3O_4/SiO_2 catalyst.
- The Pt-promoted catalyst prepared at low pH is very promising however it contains a significant loading of Pt. If this Pt-loading could be decreased without affecting the performance of the catalyst, the resulting catalyst would be very attractive. Thus an investigation needs to be done with SEA solutions of lower concentrations than the ones used in this investigation which will hopefully result in a lower Pt-loading on the catalyst. These catalysts should then be characterised and tested for their Fischer-Tropsch activity.
- The Au-promoted catalyst prepared in this investigation performed very poorly when compared alongside the Pt-promoted catalyst. It may be possible that the Au-loading is too high and as such is affecting the performance of the catalyst. It may be beneficial to investigate lower loadings of Au to see if this is the case before completely dismissing Au-promotion as a possible method of promotion for FT catalysts. Also the calcination conditions used in this investigation weren't suited to maintain small Au crystallites. A better method of transforming the $AuCl_4^-$ into metallic Au needs to be found.

8. References

[1] R. L. Espinoza, a. P. Steynberg, B. Jager, and a. C. Vosloo, "Low temperature Fischer–Tropsch synthesis from a Sasol perspective," *Appl. Catal. A Gen.*, vol. 186, no. 1–2, pp. 13–26, Oct. 1999.

[2] F. Diehl and A. Y. Khodakov, "Promotion of cobalt Fischer-Tropsch catalysts with noble metals: A review," *Oil Gas Sci. Technol.*, vol. 64, no. 1, pp. 11–24, 2009.

[3] W. Ma, G. Jacobs, R. a. Keogh, D. B. Bukur, and B. H. Davis, "Fischer–Tropsch synthesis: Effect of Pd, Pt, Re, and Ru noble metal promoters on the activity and selectivity of a 25%Co/Al_2O_3 catalyst," *Appl. Catal. A Gen.*, vol. 437–438, pp. 1–9, Sep. 2012.

[4] W. Chu, P. Chernavskii, L. Gengembre, G. Pankina, P. Fongarland, and a Khodakov, "Cobalt species in promoted cobalt alumina-supported Fischer–Tropsch catalysts," *J. Catal.*, vol. 252, no. 2, pp. 215–230, Dec. 2007.

[5] G. Jacobs, T. K. Das, Y. Zhang, J. Li, G. Racoillet, and B. H. Davis, "Fischer–Tropsch synthesis: support, loading, and promoter effects on the reducibility of cobalt catalysts," *Appl. Catal. A Gen.*, vol. 233, no. 1–2, pp. 263–281, Jul. 2002.

[6] G. Jacobs, M. C. Ribeiro, W. Ma, Y. Ji, S. Khalid, P. T. a. Sumodjo, and B. H. Davis, "Group 11 (Cu, Ag, Au) promotion of 15%Co/Al_2O_3 Fischer–Tropsch synthesis catalysts," *Appl. Catal. A Gen.*, vol. 361, no. 1–2, pp. 137–151, Jun. 2009.

[7] H. Schulz, "Short history and present trends of Fischer–Tropsch synthesis," *Appl. Catal. A Gen.*, vol. 186, no. 1–2, pp. 3–12, Oct. 1999.

[8] M. E. Dry, "The Fischer–Tropsch process: 1950–2000," *Catal. Today*, vol. 71, no. 3–4, pp. 227–241, Jan. 2002.

[9] A. Y. Khodakov, W. Chu, and P. Fongarland, "Advances in the development of novel cobalt Fischer-Tropsch catalysts for synthesis of long-chain hydrocarbons and clean fuels.," *Chem. Rev.*, vol. 107, no. 5, pp. 1692–744, May 2007.

[10] Y. Traa, "Is a renaissance of coal imminent?--challenges for catalysis.," *Chem. Commun. (Camb).*, vol. 46, no. 13, pp. 2175–87, Apr. 2010.

[11] R. A. van Santen, I. M. Ciobica, E. van Steen, and M. M. Ghouri, "Mechanistic Issues in Fischer-Tropsch Catalysis," *Adv. Catal.*, vol. 54, pp. 127–187, 2011.

[12] M. Ojeda, R. Nabar, A. U. Nilekar, A. Ishikawa, M. Mavrikakis, and E. Iglesia, "CO activation pathways and the mechanism of Fischer–Tropsch synthesis," *J. Catal.*, vol. 272, no. 2, pp. 287–297, Jun. 2010.

[13] S. Shetty, A. P. J. Jansen, and R. a van Santen, "Direct versus hydrogen-assisted CO dissociation.," *J. Am. Chem. Soc.*, vol. 131, no. 36, pp. 12874–5, Sep. 2009.

[14] O. R. Inderwildi, S. J. Jenkins, and D. A. King, "Fischer - Tropsch Mechanism Revisited : Alternative Pathways for the Production of Higher Hydrocarbons from Synthesis Gas," pp. 1305–1307, 2008.

[15] M. Claeys and E. van Steen, "Fischer-Tropsch synthesis: Basic studies," *Stud. Surf. Sci. Catal.*, vol. 152, pp. 601–680, 2004.

[16] H. Schulz, B. R. Rao, and M. Elstner, "14C-Studien zum Reaktionsmechanismus der Fischer-Tropsch Synthese," *Erdoel und Kohle*, vol. 23, p. 651, 1970.

[17] H. Schulz, E. Erich, H. Gorre, and E. van Steen, "Regularities of Selectivity as a Key for Discriminating FT Surface Reactions and Formation of the Dynamic System," *Catal. Letters*, vol. 7, p. 157, 1990.

[18] R. Ferrando, J. Jellinek, and R. L. Johnston, "Nanoalloys: from theory to applications of alloy clusters and nanoparticles.," *Chem. Rev.*, vol. 108, no. 3, pp. 845–910, Mar. 2008.

[19] M. De Beer, A. Kunene, D. Nabaho, M. Claeys, and E. Van Steen, “Technical and economic aspects of promotion of cobalt-based Fischer-Tropsch catalysts by noble metals – a review,” vol. 114, no. October 2013, pp. 14–16, 2014.
[20] M. A. Vannice, “The Catalytic Synthesis of Hydrocarbons from H_2/CO Mixtures over the Group VIII Metals,” *J. Catal.*, vol. 50, pp. 228–236, 1977.
[21] B. Jager, “Developments in Fischer-Tropsch Technology,” *Stud. Surf. Sci. Catal.*, vol. 119, 1998.
[22] S. Bessell, “Support effects in cobalt-based fischer-tropsch catalysis,” *Appl. Catal. A Gen.*, vol. 96, no. 2, pp. 253–268, Mar. 1993.
[23] R. Oukaci, A. H. Singleton, and J. G. Goodwin, “Comparison of patented Co F–T catalysts using fixed-bed and slurry bubble column reactors,” *Appl. Catal. A Gen.*, vol. 186, no. 1–2, pp. 129–144, Oct. 1999.
[24] B. Y. F. Morales and B. M. Weckhuysen, “Promotion Effects in Co-based Fischer – Tropsch Catalysis,” vol. 19, no. i, 2006.
[25] G. Jacobs, Y. Ji, B. H. Davis, D. Cronauer, a. J. Kropf, and C. L. Marshall, “Fischer–Tropsch synthesis: Temperature programmed EXAFS/XANES investigation of the influence of support type, cobalt loading, and noble metal promoter addition to the reduction behavior of cobalt oxide particles,” *Appl. Catal. A Gen.*, vol. 333, no. 2, pp. 177–191, Dec. 2007.
[26] E. Iglesia, “Design, synthesis, and use of cobalt-based Fischer-Tropsch synthesis catalysts,” *Appl. Catal. A Gen.*, vol. 161, no. 1–2, pp. 59–78, Nov. 1997.
[27] a Barbier, “Characterization and Catalytic Behavior of Co/SiO_2 Catalysts: Influence of Dispersion in the Fischer–Tropsch Reaction,” *J. Catal.*, vol. 200, no. 1, pp. 106–116, May 2001.
[28] G. L. Bezemer, J. H. Bitter, H. P. C. E. Kuipers, H. Oosterbeek, J. E. Holewijn, X. Xu, F. Kapteijn, A. J. Van Dillen, and K. P. De Jong, “Cobalt Particle Size Effects in the Fischer-Tropsch Reaction Studied with Carbon Nanofiber Supported Catalysts,” no. 6, pp. 11568–11569, 2006.
[29] a Martinez and G. Prieto, “Breaking the dispersion-reducibility dependence in oxide-supported cobalt nanoparticles,” *J. Catal.*, vol. 245, no. 2, pp. 470–476, Jan. 2007.
[30] N. Fischer, E. van Steen, and M. Claeys, “Structure sensitivity of the Fischer–Tropsch activity and selectivity on alumina supported cobalt catalysts,” *J. Catal.*, vol. 299, pp. 67–80, Mar. 2013.
[31] J. P. den Breejen, J. R. a. Sietsma, H. Friedrich, J. H. Bitter, and K. P. de Jong, “Design of supported cobalt catalysts with maximum activity for the Fischer–Tropsch synthesis,” *J. Catal.*, vol. 270, no. 1, pp. 146–152, Mar. 2010.
[32] A. Y. Khodakov, “Fischer-Tropsch synthesis: Relations between structure of cobalt catalysts and their catalytic performance,” *Catal. Today*, vol. 144, no. 3–4, pp. 251–257, Jun. 2009.
[33] G. Jacobs, J. a Chaney, P. M. Patterson, T. K. Das, J. C. Maillot, and B. H. Davis, “Fischer-Tropsch synthesis: study of the promotion of Pt on the reduction property of Co/Al_2O_3 catalysts by in situ EXAFS of Co K and Pt LIII edges and XPS.,” *J. Synchrotron Radiat.*, vol. 11, no. Pt 5, pp. 414–22, Sep. 2004.
[34] J. Yang, W. Ma, D. Chen, A. Holmen, and B. H. Davis, “Applied Catalysis A : General Fischer – Tropsch synthesis : A review of the effect of CO conversion on methane selectivity,” *"Applied Catal. A, Gen.*, vol. 470, pp. 250–260, 2014.
[35] E. van Steen, G. S. Sewell, R. A. Makhothe, C. Micklethwaite, H. Manstein, M. de Lange, and C. T. O’Connor, “TPR Study on the Preparation of Impregnated Co/SiO_2 Catalysts,” *J. Catal.*, no. 162, pp. 220–229, 1996.
[36] S. Rane, Ø. Borg, J. Yang, E. Rytter, and A. Holmen, “Effect of alumina phases on hydrocarbon selectivity in Fischer–Tropsch synthesis,” *Appl. Catal. A Gen.*, vol. 388, no. 1–2, pp. 160–167, Nov. 2010.

[37] D. Schanke, S. Vada, E. A. Blekkan, A. M. Hilmen, A. Hoff, and A. Holmen, "Study of Pt-Promoted Cobalt CO Hydrogenation Catalysts," *J. Catal.*, vol. 156, pp. 85–95, 1995.
[38] J. Li, X. Zhan, Y. Zhang, G. Jacobs, T. Das, and B. H. Davis, "Fischer – Tropsch synthesis : effect of water on the deactivation of Pt promoted Co / Al_2O_3 catalysts," vol. 228, pp. 203–212, 2002.
[39] D. Xu, W. Li, H. Duan, Q. Ge, and H. Xu, "Reaction performance and characterization of Co/Al_2O_3 Fischer–Tropsch catalysts promoted with Pt, Pd and Ru," *Catal. Letters*, vol. 102, no. 3–4, pp. 229–235, Aug. 2005.
[40] G. E. Batley, A. Ekstrom, and D. A. Johnson, "Studies of Topochemical Heterogeneous Catalysis of the Reduction of Metal Oxides by Hydrogen," *J. Catal.*, vol. 34, pp. 368–375, 1974.
[41] K. Jalama, N. J. Coville, H. Xiong, D. Hildebrandt, D. Glasser, S. Taylor, A. Carley, J. a. Anderson, and G. J. Hutchings, "A comparison of Au/Co/Al2O3 and $Au/Co/SiO_2$ catalysts in the Fischer–Tropsch reaction," *Appl. Catal. A Gen.*, vol. 395, no. 1–2, pp. 1–9, Mar. 2011.
[42] K. Jalama, N. J. Coville, D. Hildebrandt, D. Glasser, L. L. Jewell, J. a. Anderson, S. Taylor, D. Enache, and G. J. Hutchings, "Effect of the addition of Au on Co/TiO_2 catalyst for the Fischer–Tropsch reaction," *Top. Catal.*, vol. 44, no. 1–2, pp. 129–136, Jun. 2007.
[43] A. M. Hilmen, D. Schanke, and A. Holmen, "TPR Study of the Mechanism of Rhenium Promotion of Alumina Supported Cobalt Fischer-Tropsch Catalysts," *Catal. Lett.*, vol. 38, pp. 143–147, 1996.
[44] N. Tsubaki, S. Sun, and K. Fujimoto, "Different Functions of the Noble Metals Added to Cobalt Catalysts for Fischer–Tropsch Synthesis," *J. Catal.*, vol. 199, no. 2, pp. 236–246, Apr. 2001.
[45] S. Vada, A. Hoff, D. Adnanes, D. Schanke, and A. Holmen, "Fischer-Tropsch Synthesis on Supported Cobalt Catalysts Promoted by Platinum and Rhenium," *Top. Catal.*, vol. 2, pp. 155–162, 1995.
[46] G. Jacobs, P. M. Patterson, Y. Zhang, T. Das, J. Li, and B. H. Davis, "Fischer – Tropsch synthesis : deactivation of noble metal-promoted Co /Al_2O_3 catalysts," vol. 233, pp. 215–226, 2002.
[47] J. Miller, "A fundamental study of platinum tetraammine impregnation of silica2. The effect of method of preparation, loading, and calcination temperature on (reduced) particle size," *J. Catal.*, vol. 225, no. 1, pp. 203–212, Jul. 2004.
[48] S. Sun, N. Tsubaki, and K. Fujimoto, "The reaction performances and characterization of Fischer – Tropsch synthesis Co / SiO 2 catalysts prepared from mixed cobalt salts," vol. 202, pp. 121–131, 2000.
[49] S. Lambert, N. Job, L. Dsouza, M. Pereira, R. Pirard, B. Heinrichs, J. Figueiredo, J. Pirard, and J. Regalbuto, "Synthesis of very highly dispersed platinum catalysts supported on carbon xerogels by the strong electrostatic adsorption method," *J. Catal.*, vol. 261, no. 1, pp. 23–33, Jan. 2009.
[50] L. Dsouza, J. Regalbuto, and J. Miller, "Preparation of carbon supported cobalt by electrostatic adsorption of $[Co(NH_3)_6]Cl_3$," *J. Catal.*, vol. 254, no. 2, pp. 157–169, Mar. 2008.
[51] X. Hao, L. Quach, J. Korah, W. . Spieker, and J. R. Regalbuto, "The control of platinum impregnation by PZC alteration of oxides and carbon," *J. Mol. Catal. A Chem.*, vol. 219, no. 1, pp. 97–107, Sep. 2004.
[52] J. P. Brunelle, "Preparation of catalysts by metallic complex adsorption on mineral oxides," *Pure Appl. Chem.*, vol. 50, no. 9–10, pp. 1211–1229, 1978.
[53] H. Butt, K. Graf, and M. Kappl, *Physics and Chemistry of Interfaces*, 1st ed. Weinheim: Wiley, 2003.

[54] a. V. Delgado, F. González-Caballero, R. J. Hunter, L. K. Koopal, and J. Lyklema, "Measurement and Interpretation of Electrokinetic Phenomena (IUPAC Technical Report)," *Pure Appl. Chem.*, vol. 77, no. 10, pp. 1753–1805, 2005.
[55] D. J. . Shaw, *Introduction to colloid and surface chemistry*, 3rd ed. London: Butterwoths, 1980, pp. 149–162.
[56] L. Jiao and J. R. Regalbuto, "The synthesis of highly dispersed noble and base metals on silica via strong electrostatic adsorption: I. Amorphous silica," *J. Catal.*, vol. 260, no. 2, pp. 329–341, Dec. 2008.
[57] F. Chemistry and M. C. Sq, "A Thermodynamic Analysis of Ion Adsorption in the Metal Oxide / Electrolyte Systems in which PZC and CIP do not Coincide," pp. 327–338, 2002.
[58] P. H. Tewari and A. B. Campbell, "Temperature dependence of point of zero charge of cobalt and nickel oxides and hydroxides," *J. Colloid Interface Sci.*, vol. 55, no. 3, pp. 531–539, Jun. 1976.
[59] S. Ardizzone, G. Spinolo, and S. Trasatti, "The Point of Zero Charge of Co_3O_4 Prepared by Thermal Decomposition of Basic Cobalt Carbonate," *Electrochem. Acta*, vol. 40, no. 16, pp. 2683–2686, 1995.
[60] R. O. James and T. W. Healy, "Adsorption of Hydrolyzable Metal Ions at the Oxide-Water Interface," *J. Colloid Interface Sci.*, vol. 40, no. 1, 1972.
[61] P. J. Murphy and M. S. LaGrange, "Raman spectroscopy of gold chloro-hydroxy speciation in fluids at ambient temperature and pressure : A re-evaluation of the effects of pH and chloride concentration," *Geochim. Cosmochim. Acta*, vol. 62, no. 21, pp. 3515–3526, 1998.
[62] A. Corma and H. Garcia, "Supported gold nanoparticles as catalysts for organic reactions.," *Chem. Soc. Rev.*, vol. 37, no. 9, pp. 2096–126, Sep. 2008.
[63] S. Ivanova, C. Petit, and V. Pitchon, "A new preparation method for the formation of gold nanoparticles on an oxide support," *Appl. Catal. A Gen.*, vol. 267, no. 1–2, pp. 191–201, 2004.
[64] J. A. Peck, C. Drew Tait, B. I. Swanson, and G. E. Brown Jr., "Speciation of aqueous gold(III) chlorides from ultraviolet/visible absorption and Raman/resonance Raman spectroscopies," *Geochim. Cosmochim. Acta*, vol. 55, no. 3, pp. 671–676, 1991.
[65] R. Zanella, S. Giorgio, C. R. Henry, C. Louis, M. Curie, P. Cedex, C. Cnrs, and C. De Luminy, "Alternative Methods for the Preparation of Gold Nanoparticles Supported on TiO 2," pp. 7634–7642, 2002.
[66] S.-J. Lee and A. Gavriilidis, "Supported Au Catalysts for Low-Temperature CO Oxidation Prepared by Impregnation," *J. Catal.*, vol. 206, no. 2, pp. 305–313, Mar. 2002.
[67] Y. A. Nechayev and N. V. Nikolenko, "Effects of surface charge on the adsorption of gold (III) chloride complexes on oxides," *Geochemical Int.*, vol. 23, no. 9, pp. 142–146, 1986.
[68] B. . Shelimov, J.-F. Lambert, M. Che, and B. Didillon, "Molecular-level studies of transition metal–support interactions during the first steps of catalysts preparation: platinum speciation in the hexachloroplatinate/alumina system," *J. Mol. Catal. A Chem.*, vol. 158, no. 1, pp. 91–99, Sep. 2000.
[69] J. Kramer and K. R. Koch, "^{195}Pt NMR study of the speciation and preferential extraction of Pt(IV)-mixed halide complexes by diethylenetriamine-modified silica-based anion exchangers.," *Inorg. Chem.*, vol. 45, no. 19, pp. 7843–55, Sep. 2006.
[70] W. A. Spieker, J. Liu, J. T. Miller, A. J. Kropf, and J. R. Regalbuto, "An EXAFS study of the co-ordination chemistry of hydrogen hexachloroplatinate (IV) 1 . Speciation in aqueous solution," vol. 232, pp. 219–235, 2002.
[71] W. A. Spieker, J. Liu, X. Hao, J. T. Miller, A. J. Kropf, and J. R. Regalbuto, "An EXAFS study of the coordination chemistry of hydrogen hexachloroplatinate(IV) 2 . Speciation of complexes adsorbed onto alumina," vol. 243, pp. 53–66, 2003.

[72] T. Mang, B. Breitscheidel, P. Polanek, and H. Knözinger, “Adsorption of platinum complexes on silica and alumina: Preparation of non-uniform metal distributions within support pellets,” *Appl. Catal. A Gen.*, vol. 106, no. 2, pp. 239–258, Dec. 1993.
[73] H. E. Kissinger, “Variation of peak temperature with heating rate in differential thermal analysis,” *J. Res. Natl. Bur. Stand.*, vol. 57, no. 4, p. 217, Oct. 1956.
[74] R. Kaiser, “Precision and Accuracy in quantitative gas chromatography,” *Methods Phys. Anal.*, vol. 5, pp. 357–69, 1969.
[75] E. I. Mabaso, “Nanosized Iron Crystallites for Fischer-Tropsch Synthesis,” University of Cape Town, 2005.
[76] J. Chen and A. Selloni, “Water Adsorption and Oxidation at the Co_3O_4 (110) Surface,” *J. Phys. Chem. Lett.*, vol. 3, no. 19, pp. 2808–2814, Oct. 2012.
[77] M. L. Hair and W. Hertl, “Acidity of surface hydroxyl groups,” *J. Phys. Chem.*, vol. 74, no. 1, pp. 91–94, Jan. 1970.
[78] J. M. Jablonski, M. Wolcyrz, and L. Krajczyk, “On Cobalt Silicate Formation during High-Temperature Calcination of Impregnated Cobalt / Silica Catalysts,” *J. Catal.*, vol. 173, pp. 530–534, 1998.
[79] J. Park and J. R. Regalbuto, “A Simple, Accurate Determination of Oxide PZC and the Strong Buffering Effect of Oxide Surfaces at Incipient Wetness,” *J. Colloid Interface Sci.*, vol. 175, pp. 239–252, 1995.
[80] L. Jiao and J. R. Regalbuto, “The synthesis of highly dispersed noble and base metals on silica via strong electrostatic adsorption: II. Mesoporous silica SBA-15,” *J. Catal.*, vol. 260, no. 2, pp. 342–350, Dec. 2008.
[81] J. Girardon, E. Quinet, a Gribovalconstant, P. Chernavskii, L. Gengembre, and a Khodakov, “Cobalt dispersion, reducibility, and surface sites in promoted silica-supported Fischer–Tropsch catalysts,” *J. Catal.*, vol. 248, no. 2, pp. 143–157, Jun. 2007.
[82] G. Steinhauser, J. Evers, S. Jakob, T. M. Klapötke, and G. Oehlinger, “A review on fulminating gold (Knallgold),” *Gold Bull.*, vol. 41, no. 4, pp. 305–317, 2008.
[83] K. Jalama, N. J. Coville, D. Hildebrandt, D. Glasser, L. L. Jewell, J. a. Anderson, S. Taylor, D. Enache, and G. J. Hutchings, “Effect of the addition of Au on Co/TiO_2 catalyst for the Fischer–Tropsch reaction,” *Top. Catal.*, vol. 44, no. 1–2, pp. 129–136, Jun. 2007.
[84] A. J. McCue, J. Aponaviciute, R. P. K. Wells, and J. a. Anderson, “Gold modified cobalt-based Fischer-Tropsch catalysts for conversion of synthesis gas to liquid fuels,” *Front. Chem. Sci. Eng.*, pp. 1–8, Jul. 2013.
[85] B. Hammer and J. K. Norskov, “Why gold is the noblest of all the metals,” *Nature*, vol. 376, no. 6537. pp. 238–240, 1995.
[86] K. E. Coulter and A. G. Sault, “Effects of Activation on the Surface Properties of Silica-Supported Cobalt Catalysts,” *J. Catal.*, vol. 154, pp. 56–64, 1995.
[87] L. D’Souza, L. Jiao, J. Regalbuto, J. Miller, and A. Kropf, “Preparation of silica- and carbon-supported cobalt by electrostatic adsorption of Co(III) hexaammines,” *J. Catal.*, vol. 248, no. 2, pp. 165–174, Jun. 2007.
[88] I. C. Yates and C. N. Satterfield, “Intrinsic Kinetics of the Fischer-Tropsch Synthesis on a Cobalt Catalyst,” no. 10, pp. 168–173, 1991.
[89] S. I. Sandler, *Chemical & Engineering Thermodynamics*, 3rd ed. John Wiley & Sons, 1999.
[90] L. G. Sillen, A. E. Martell, and J. Bjerrum, *Stability constants of metal-ion complexes*, 2nd ed. London: Chemical Society, 1964.
[91] T. C. Watling, A. F. Gusovius, R. Prins, "Synthesis of Methanol from CO over Ca-Promoted Pt/SiO_2", *J. Catal.*, vol. 188, pp. 233-236, 1999
[92] Y. Yang, L. Jia, Y. Meng, B. Hou, D. Li and Y. Sun, "Fischer-Tropsch Synthesis over Ordered Mesoporous Carbon Supported Cobalt Catalysts: The Role of Amount of Carbon Precurosr in Catalytic Performance", *Catal. Lett,* vol. 142, pp. 195-204, 2012

9. Appendices

Appendix A: Heat of Reaction in the Fischer-Tropsch Synthesis

The heat of reaction for selected Fischer-Tropsch products were calculated using a thermodynamic equilibrium program supplied by Sandler [89]. The heat of reaction for the formation of n-paraffins, a-olefins, primary alcohols and aldehydes for a range of chain lengths were determined according to the following stoichiometric equations:

Formation of paraffins:

$$(2n+1)H_2 + nCO \rightarrow C_nH_{2n+2} + nH_2O$$

Formation of olefins:

$$2nH_2 + nCO \rightarrow C_nH_{2n} + nH_2O$$

Formation of primary alcohols:

$$2nH_2 + nCO \rightarrow C_nH_{2n+2}O + (n-1)H_2O$$

Formations of aldehydes:

$$(2n-1)H_2 + nCO \rightarrow C_nH_{2n}O + (n-1)H_2O$$

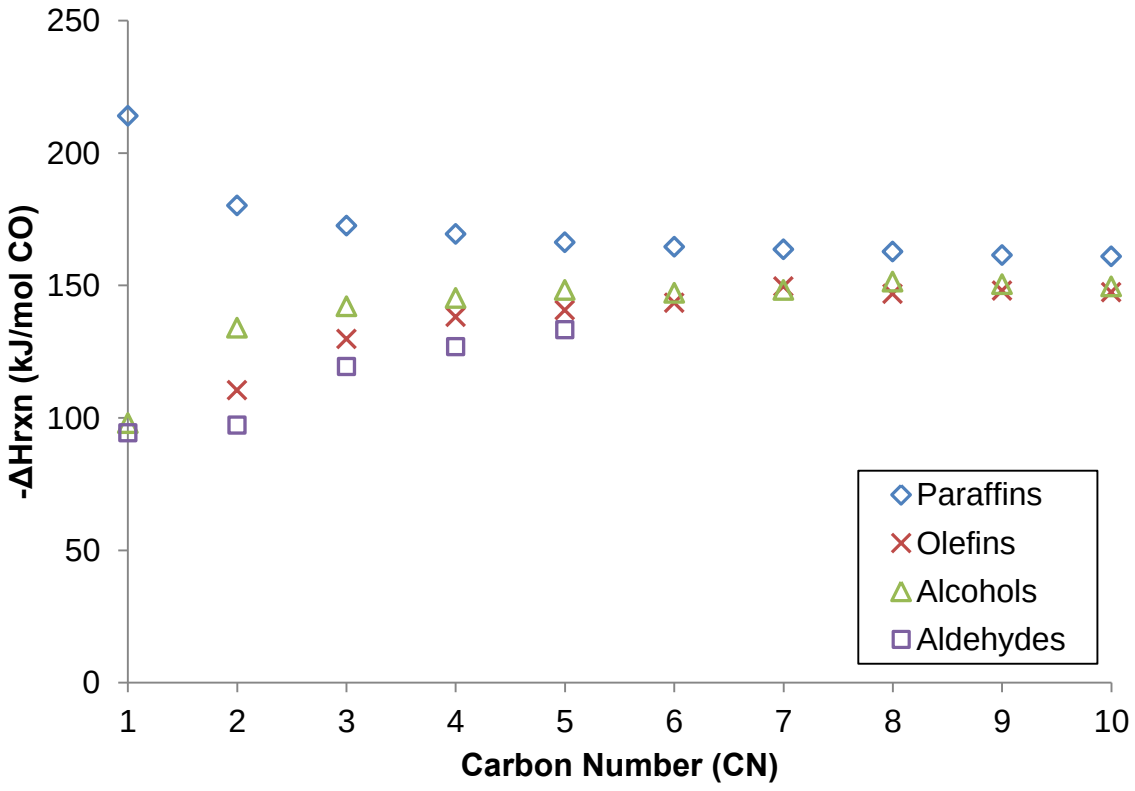

Figure A.1: Heat of reaction (kJ/mol$_{CO}$) for various Fischer-Tropsch products at a number of different chain lengths

Appendix B: Historical Metal Prices for Active Fischer-Tropsh Metals

The prices relative to iron for the metals with the most significant Fischer-Tropsch catalytic activity since 2000 are given in Figure B.1.

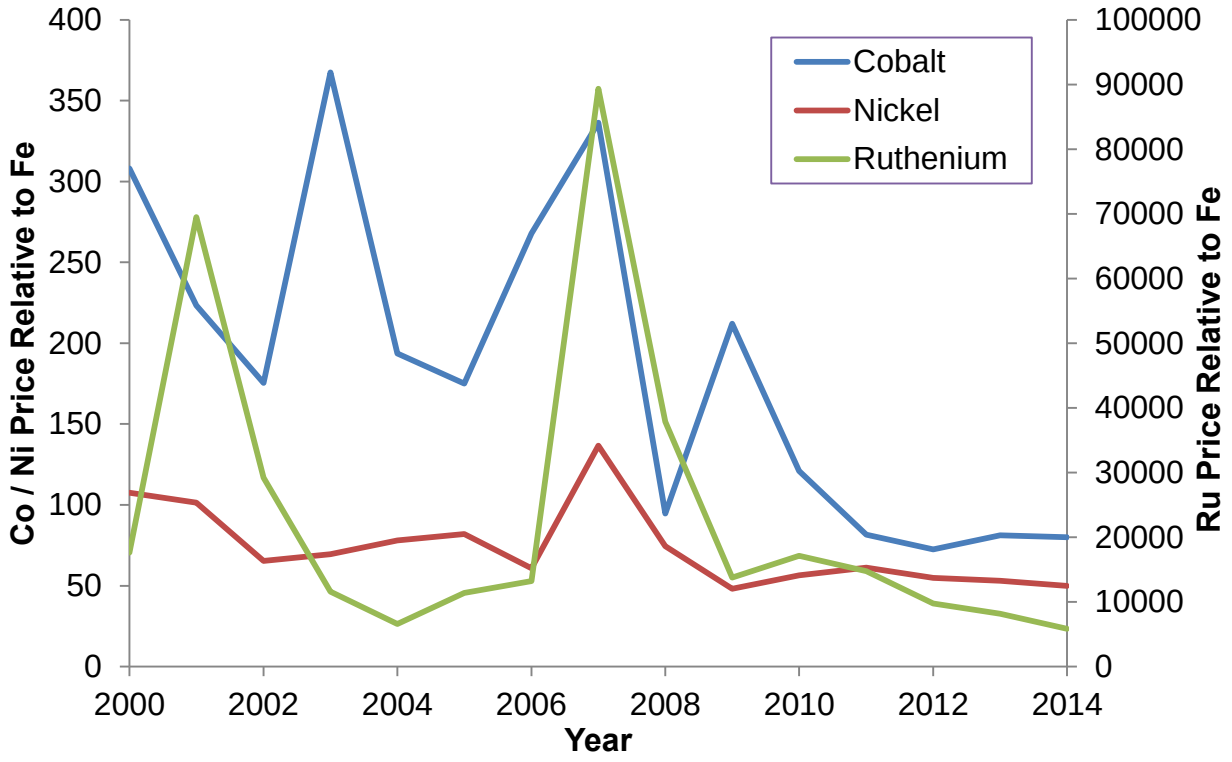

Figure B.1: Historical Co, Ni and Ru metal prices relative to that of scrap iron since 2000

Sources:

Nickel - http://www.tradingeconomics.com/commodity/nickel

Cobalt - http://www.sfp-cobalt.co.uk/cobalt/cobalt-price-chart.asp

Ruthenium - http://www.platinum.matthey.com/prices/price-tables?metalTab=Ru

Iron - http://minerals.usgs.gov/minerals/pubs/commodity/iron_&_steel_scrap/

Appendix C: Derivation of Surface Equilibrium Model for SiO_2

Surface Reactions:

$$-OH + H^+ \leftrightarrow -OH_2^+ \qquad K_1 = \frac{[-OH_2^+]}{[-OH][H^+]}$$

$$-OH \leftrightarrow -O^- + H^+ \qquad K_2 = \frac{[-O^-][H^+]}{[-OH]}$$

Rearranging:

$$[-OH_2^+] = K_1[-OH][H^+]$$

$$[-O^-] = \frac{K_2[-OH]}{[H^+]}$$

Dividing though by the total concentration of sites yields a site fraction:

$$f_{-OH_2^+} = K_1 . f_{-OH} . [H^+]$$

$$f_{-O^-} = \frac{K_2 . f_{-OH}}{[H^+]}$$

Site balance:

$$f_{-OH_2^+} + f_{-O^-} + f_{-OH} = 1$$

Substituting and rearranging:

$$K_1 . f_{-OH} . [H^+] + \frac{K_2 . f_{-OH}}{[H^+]} + f_{-OH} = 1$$

$$f_{-OH} . = \frac{1}{\left(K_1[H^+] + \frac{K_2}{[H^+]} + 1\right)}$$

The charge on the surface can be given by the difference between the positively charged and negatively charged species:

$$Charge = [-OH_2^+] - [-O^-]$$

Substituting and rearranging:

$$Charge = K_1 . f_{-OH} . [H^+] - \frac{K_2 . f_{-OH}}{[H^+]}$$

$$Charge = f_{-OH}\left(K_1[H^+] - \frac{K_2}{[H^+]}\right)$$

$$Charge = \frac{\left(K_1[H^+] - \frac{K_2}{[H^+]}\right)}{\left(K_1[H^+] + \frac{K_2}{[H^+]} + 1\right)}$$

$$[H^+] = 10^{-pH}$$

$$Charge = \frac{\left(K_1 10^{-pH} - \frac{K_2}{10^{-pH}}\right)}{\left(K_1 10^{-pH} + \frac{K_2}{10^{-pH}} + 1\right)}$$

If it assumed that the ζ-potential is some constant multiplied by the charge:

$$\zeta - potential = \frac{\alpha\left(K_1 10^{-pH} - \frac{K_2}{10^{-pH}}\right)}{\left(K_1 10^{-pH} + \frac{K_2}{10^{-pH}} + 1\right)}$$

Appendix D: Derivation of Surface Equilibrium Model for Co_3O_4

The derivation is the same as in Appendix A, however two sets of reactions are considered:

$1 - OH + H^+ \leftrightarrow 1 - OH_2^+$ $\qquad K_{11} = \frac{[1-OH_2^+]}{[1-OH][H^+]}$

$1 - OH \leftrightarrow\ 1 - O^- + H^+$ $\qquad K_{12} = \frac{[1-O^-][H^+]}{[1-OH]}$

$$2-OH+H^{+} \leftrightarrow 2-OH_2^{+} \qquad K_{21}=\frac{[2-OH_2^{+}]}{[2-OH][H^{+}]}$$

$$2-OH \leftrightarrow\ 2-O^{-}+H^{+} \qquad K_{22}=\frac{[2-O^{-}][H^{+}]}{[2-OH]}$$

Each type of site is considered to be distinct and the overall surface charge comes from a linear summation of the charges of each fraction:

$$Charge=\frac{f_1\left(K_{11}10^{-pH}-\frac{K_{12}}{10^{-pH}}\right)}{\left(K_{11}10^{-pH}+\frac{K_{12}}{10^{-pH}}+1\right)}+\frac{f_2\left(K_{21}10^{-pH}-\frac{K_{22}}{10^{-pH}}\right)}{\left(K_{21}10^{-pH}+\frac{K_{22}}{10^{-pH}}+1\right)}$$

The ζ-potential is then given by a constant multiplied by the charge.

$$\zeta-potential=\frac{\alpha_1\left(K_{11}10^{-pH}-\frac{K_{12}}{10^{-pH}}\right)}{\left(K_{11}10^{-pH}+\frac{K_{12}}{10^{-pH}}+1\right)}+\frac{\alpha_2\left(K_{21}10^{-pH}-\frac{K_{22}}{10^{-pH}}\right)}{\left(K_{21}10^{-pH}+\frac{K_{22}}{10^{-pH}}+1\right)}$$

Appendix E: Calculation of IWI Volumes for Different Nitrate fractions

AAS-ICP the concentration of the cobalt nitrate and acetate solutions:

Table E.1: Concentrations measured with ICP-AAS

	AAS-ICP measurements concentration (mol/l)	Concentration [mol/l]
Cobalt acetate	0.9193	0.9234±0.0083
	0.9180	
	0.9329	
Cobalt nitrate	0.9710	0.9828±0.0127
	0.9963	
	0.9811	

From the concentration of the nitrate and acetate solutions (determined from AAS-ICP), $[Co(NO_3)_2]$=0.9828 mol/L and $[Co(Ac)_2]$=0.923 mol/L and the desired mass of catalyst to be prepared we can calculate the volume to be added:

$$C_{Co}=f_{Ac}\times[Ac]+f_N\times[N]$$

$$V_{WI}=\frac{L.m_c}{100.C_{Co}.M_{Co}}$$

$$V_N=f_N\times V_{WI} \qquad V_{Ac}=f_{Ac}\times V_{WI}$$

f_{Ac} and f_N are the fractions of acetate and nitrate in the impregnation solution and $[Ac]$ and $[N]$ and the concentrations of acetate and nitrate determined from ICP. V_{WI} is the volume to be added in ml, L is the desired metal loading on the catalyst in percent, C_{Co} is the concentration of the cobalt solution in mol/ml and M_{Co} is the molar mass of cobalt in g/mol. V_N and V_{Ac} are the volumes of the nitrate and acetate solution to be added in ml.

Example:

For 1g of 10wt. % cobalt catalyst with 0.15 nitrate with from cobalt nitrate and cobalt acetate solutions with concentrations of $[Co(NO_3)_2]$=0.9828 mol/L and $[Co(Ac)_2]$=0.923 mol/L respectively.

$$C_{Co} = f_{Ac} \times [Ac] + f_N \times [N]$$

$$C_{Co} = 0.85 \times 0.923 + 0.15 \times 0.9828$$

$$C_{Co} = 0.93197 \times 10^{-3}\ mol/ml$$

$$V_{WI} = \frac{L \times m_c}{100 \times C_{Co} \times M_{Co}}$$

$$V_{WI} = \frac{10 \times 1}{100 \times 0.93197 \times 10^{-3} \times 58.9883} = 2.02ml$$

$$V_N = f_N \times V_{WI} \quad V_{Ac} = f_{Ac} \times V_{WI}$$

$$V_N = 0.15 \times 2.02 \quad V_{Ac} = 0.85 \times 2.02$$

$$V_N = 0.30 \quad V_{Ac} = 1.72$$

Appendix F: Calculation of $[PtCl_6^{2-}]$ / $[AuCl_4^{2-}]$ for SEA

Using a Co_3O_4 crystallite size of 8.9nm (from XRD), one can calculate the volume of one particle assuming spherical particles:

$$V_p = \frac{4}{3}\pi r_p^3$$

$$V_p = \frac{4}{3}\pi\left(\frac{8.9}{2}\right)^3 = 369.12nm^3$$

The mass of a single particle can then be calculated using a density of 6.11g/cm^3 for Co_3O_4

$$m_p = \mathrm{V_p} \times \rho_{Co_3O_4};$$

$$m_p = 369.12nm^3 \times 6.11 \times 10^{-21} g/nm^3 = 2.26 \times 10^{-18}\mathrm{g};$$

The mass of Co_3O_4 on the catalyst can be calculated knowing the mass of Co on the surface which is assumed to be 9wt. %.

$$m_{Co_3O_4} = m_{Co} \times \frac{M_{Co_3O_4}}{3M_{Co}}$$

$$m_{Co_3O_4} = \frac{0.09\mathrm{g_{Co}}}{\mathrm{g_{cat}}} \times \frac{\frac{240.8 g_{Co_3O_4}}{mol_{Co_3O_4}}}{\frac{3\mathrm{mol_{Co}}}{\mathrm{mol_{Co_3O_4}}} \times \frac{58.9883\mathrm{g_{Co}}}{mol_{Co}}} = 0.123 g_{Co_3O_4}/g_{cat}$$

The number of particles can then be calculated:

$$n_p = \frac{m_{Co_3O_4}}{m_p}$$

$$n_p = \frac{0.123}{2.26 \times 10^{-18}} = 5.44 \times 10^{16}\text{particles}$$

And hence the total surface area of the Co_3O_4:

$$SA_p = 4\pi r_p^2 = 4\pi \times \left(\frac{8.9}{2}\right)^2 = 248.9 nm^2$$

$$SA_{Co_3O_4} = n_p \times SA_p$$

$$SA_{Co_3O_4} = 5.44 \times 10^{16} \times 248.9 nm^2 = 1.383 \times 10^{19} nm^2$$

If we use the diameter of the $PtCl_6^{2-}$ ion as 0.83nm (from molecular modelling) we can calculate the cross-sectional area of the $PtCl_6^{2-}$ ion.

$$A_{PtCl_6^{2-}} = 4\pi r_{PtCl_6^{2-}}$$

$$A_{PtCl_6^{2-}} = 4\pi \left(\frac{0.83}{2}\right)^2 = 0.541 nm^2$$

If we assume monolayer coverage the maximum possible number of $PtCl_6^{2-}$ that can adsorb on the Co_3O_4 surface will be:

$$N_{PtCl_6^{2-}} = \frac{\mathrm{SA_{Co_3O_4}}}{A_{PtCl_6^{2-}}} = 2.556 \times 10^{19} ions/g_{cat}$$

$$m_{PtCl_6^{2-}} = \frac{2.556 \times 10^{19} \times 408}{6.022 \times 10^{23}} = 0.0173 g/g_{cat}$$

$$\mathrm{m_{Pt}} = m_{PtCl_6^{2-}} \times \frac{M_{Pt}}{M_{PtCl_6^{2-}}} = 0.008277 g/g_{cat}$$

Thus we arrive at a maximum possible mass of Pt-loading value of 0.8 wt% as the. To have an excess of Pt in our system we will continue with a total platinum amount in our system which would result in 1 wt% on the catalyst.

Thus if we use 1.5g of Co_3O_4/SiO_2 we will need to add 0.01515g of Pt to this system which equates to 0.04g of $H_2PtCl_6.6H_2O$. If this mass of $H_2PtCl_6.6H_2O$ is being delivered by a 50ml solution the concentration will have to be approximately 0.8g/l.

Appendix G: Kissinger Analysis

The Kissinger equation relates the temperature ramp rate and peak maximum temperature to the activation energy of the process:

$$\ln\frac{\beta}{T_{max}^2} = -\ln\frac{Ea}{A\cdot R\cdot p_{H_2}^q} - \frac{Ea}{R}\cdot\frac{1}{T_{max}}$$

Example:

For the unpromoted Co_3O_4/SiO_2 catalyst we tested three different ramp rates:

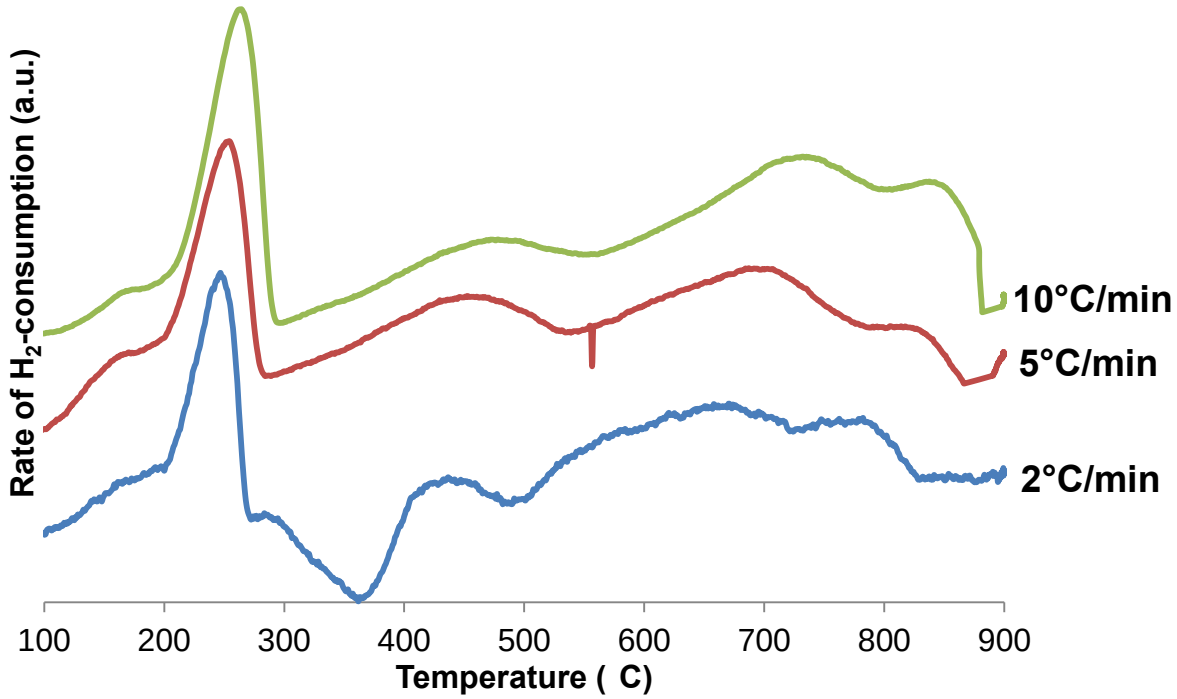

Figure G.1: TPR profiles for the unpromoted Co_3O_4/SiO_2 catalyst (NA3) at three different temperature ramp rates

The peak maximum temperatures for the first peak for each of these ramp rates are shown in Table G.1:

Table G.1: Table of ramp rates and peak maximum temperatures used in Kissinger analysis of unpromoted Co/SiO_2 catalyst

β (°C/min)	T_{max} (K)
2	537.5
5	527.3
10	519

If we then plot ln $\left(\frac{\beta}{T_{max}^2}\right)$ against $\frac{-1}{R \times T_{max}}$ it should yield a straight line with the gradient equal to $-\frac{E_a}{R}$.

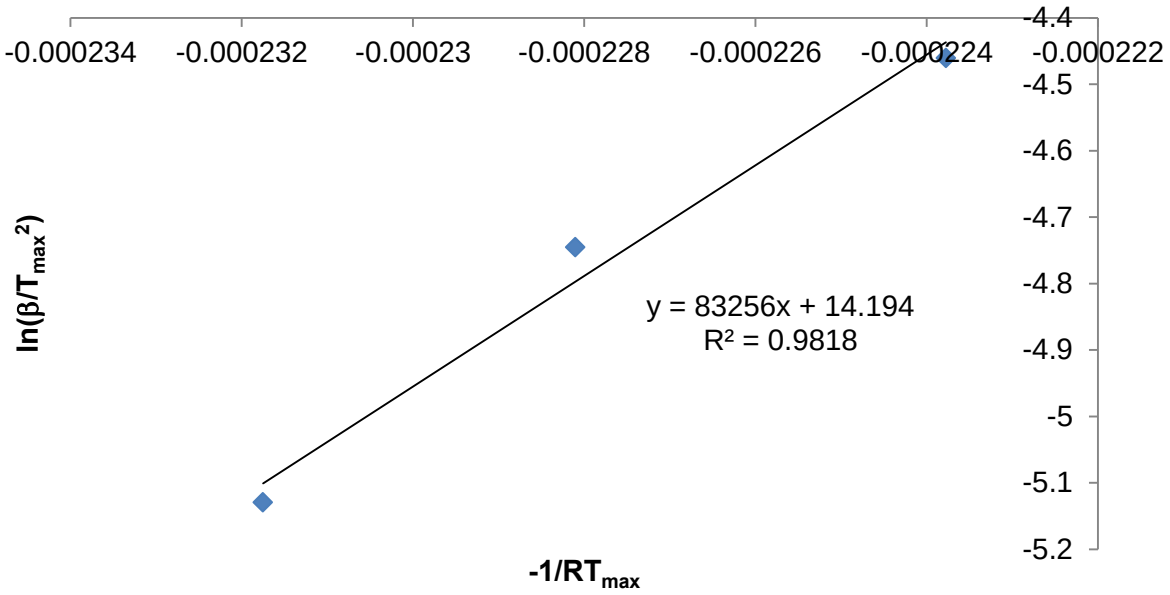

Figure G.2: Kissinger plot for the first reduction peak for the unpromoted Co_3O_4/SiO_2 (NA3)

From the gradient of this curve we can see the activation energy for this process is 83256 J/mol or 83.256 kJ/mol.

This analysis was also conducted for the promoted catalyst using the ramp rates and peak maximum temperatures shown in Table G.2:

Table G.2: Ramp rates and peak maximum temperatures used in Kissinger analysis of the Pt-promoted Co/SiO_2 catalyst

β (°C/min)	T_{max}(K)		
	Peak 1	Peak 2	Peak 3
2	469	518	623
10	446	496	574

Note that peak 1 and 3 correspond to the reduction of Co_3O_4 to CoO and CoO to Co^0 respectively. Peak 2 corresponds to a peak which was attributed to the reduction of Co_3O_4 which was unaffected by the promoter.

Appendix H: Degree of reduction calculation from TGA data

If we have 1g of Co_3O_4/SiO_2 then there is approximately 10 wt.% metallic cobalt present i.e. 0.1g. Then if we assume that all this exists as Co_3O_4 in the calcined catalyst there will be $0.1 \times \frac{M_{Co_3O_4}}{3M_{Co}} = 0.136g$ of Co_3O_4 present. Thus the complete reduction of Co_3O_4 to metallic Co^0 will result in a mass loss of $0.136 - 0.1 = 0.036g$.

For the Pt-promoted catalyst prepared by SEA at low pH we have the following weight loss curve:

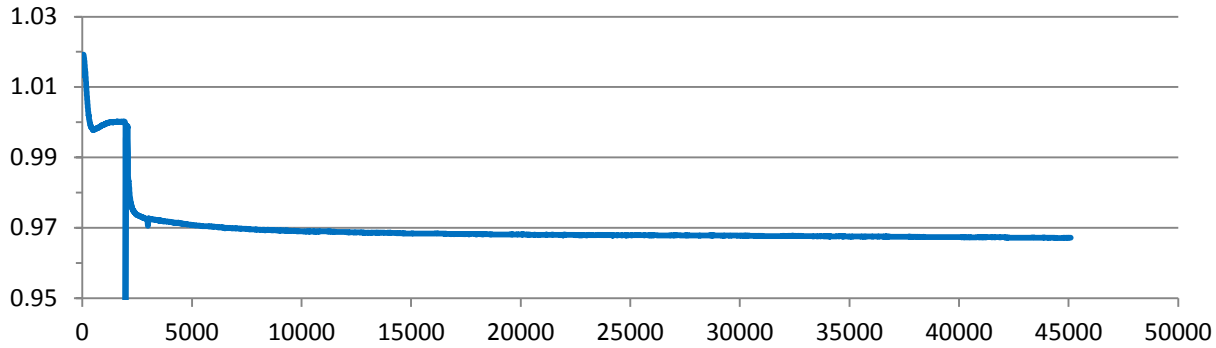

Figure H.1: TGA weight loss curve for reduction of Pt-promoted Co_3O_4 prepared by SEA at low pH

The relative mass at the end of the reduction is found to be 0.967 and since the mass is calculated relative to the mass when H_2 flow begins this will have a value of 1.

Thus the mass loss is calculated:

$$Mass\ loss = 1 - 0.967 = 0.033$$

The degree of reduction can then be calculated:

$$DOR = \frac{Mass\ loss}{Mass\ loss\ for\ complete\ reduction} = \frac{0.033}{0.036} = 0.92 = 92\%$$

Appendix I: GC-FID Method and Peak Assignment

Table I.1: Varian 3400 GC-FID Analysis conditions used

Detector	Flame ionization detector (FID), $T_{detector}$=250°C
Column	Column RT-X-1 (Resket) Fused Silica capillary column, 60mm x 0.25mm Stationary phase: 0.5mm dimethyl siloxane (cross linked)
Carrier gas	H_2
Introduction Gas	N_2
Injector	Split Injector, T=250°C Split ratio 1:20
Temperature programme	-55 °C, 1.5 min, Isothermal raised to 0°C at 12 °C/min, 0 min isothermal raised to 100°C at 9 °C/min, 0 min, isothermal raised at to 280°C at 7°C/min, thereafter isothermal at 280°C

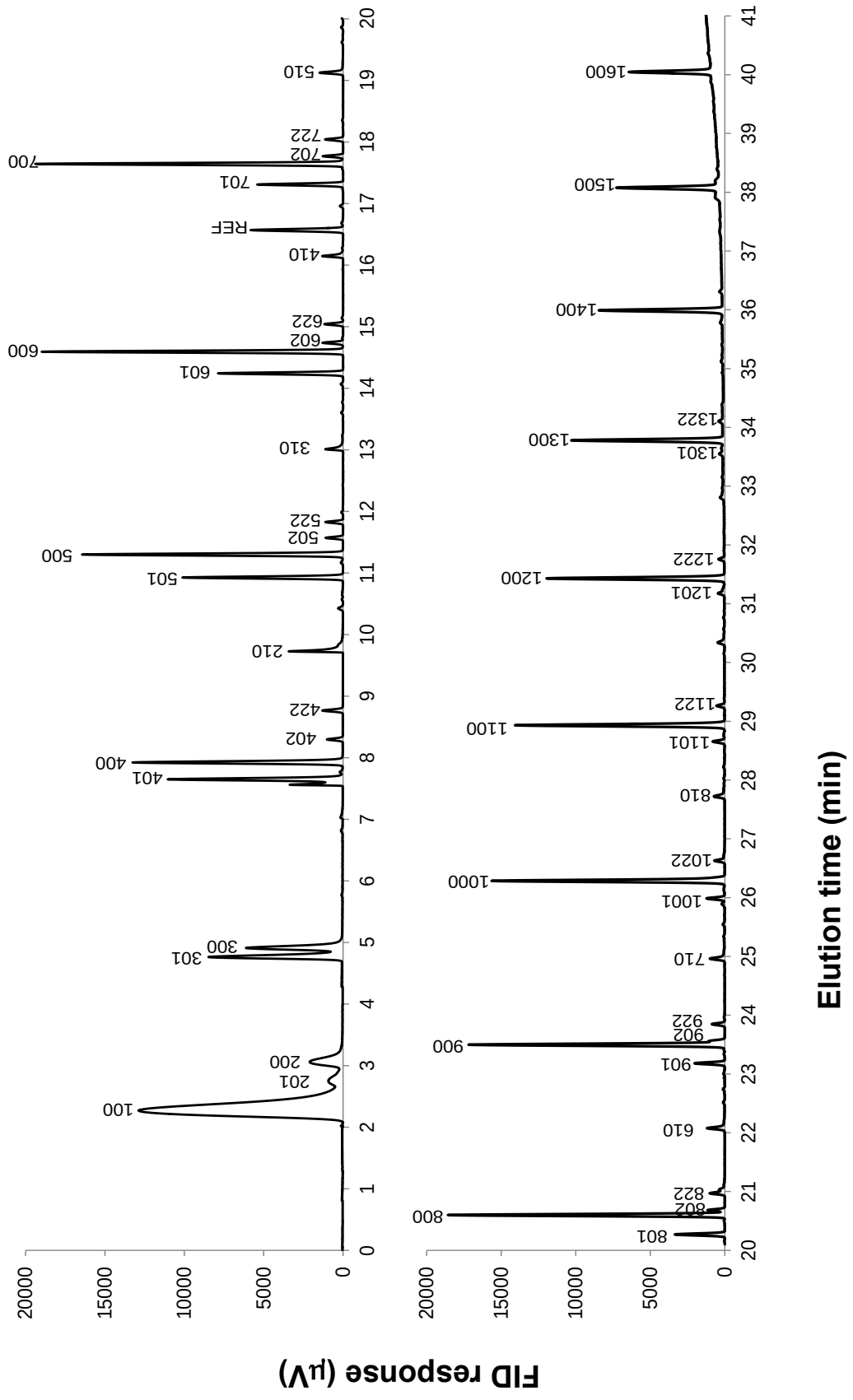

Figure I.1: Typical chromatogram obtained from GC-FID analysis, compounds labelled according to their compound code (see Table I.1)

Table I.2: Compounds codes from GC-FID analysis

Compound	Code
Methane	100
Ethane	200
Ethene	201
Ethanol	210
Propane	300
Propene	301
1-Butene	401
Butane	400
trans-2-Butene	402
cis-2-Butene	422
1-Pentene	501
Pentane	500
trans-2-Pentene	502
cis-2-Pentene	522
Propanol	310
1-Hexene	601
Hexane	600
trans-2-Hexene	602
cis-2-Hexene	622
Butanol	410
Cyclohexane	REF
1-Heptene	701
Heptane	700
trans-2-Heptene	702
cis-2-Heptene	722
Pentanol	510

Compound	Code
1-Octene	801
Octane	800
trans-2-Octene	802
cis-2-Octene	822
Hexanol	610
1-Nonene	901
Nonane	900
trans-2-Nonene	902
cis-2-Nonene	922
Heptanol	710
1-Decene	1001
Decane	1000
cis-2-Decene	1022
Octanol	810
1-Undecene	1101
Undecane	1100
cis-2-Undecene	1122
Nonanol	910
1-Dodecene	1201
Dodecane	1200
Decanol	1010
1-Tridecene	1301
Tridecane	1300
cis-2-Tridecene	1322
Tetradecane	1400
Pentadecane	1500
Hexadecane	1600